

BlackboxBench: A Comprehensive Benchmark of Black-box Adversarial Attacks

Meixi Zheng*, Xuanchen Yan*, Zihao Zhu, Hongrui Chen, Baoyuan Wu†

Abstract—Adversarial examples are well-known tools to evaluate the vulnerability of deep neural networks (DNNs). Although lots of adversarial attack algorithms have been developed, it is still challenging in the practical scenario that the model’s parameters and architectures are inaccessible to the attacker/evaluator, *i.e.*, black-box adversarial attacks. Due to the practical importance, there has been rapid progress from recent algorithms, reflected by the quick increase in attack success rate and the quick decrease in query numbers to the target model. However, there is a lack of thorough evaluations and comparisons among these algorithms, causing difficulties of tracking the real progress, analyzing advantages and disadvantages of different technical routes, as well as designing future development roadmap of this field. Thus, in this work, we aim at building a comprehensive benchmark of black-box adversarial attacks, called *BlackboxBench*. It mainly provides: 1) a unified, extensible and modular-based codebase, implementing 25 query-based attack algorithms and 30 transfer-based attack algorithms; 2) comprehensive evaluations: we evaluate the implemented algorithms against several mainstreaming model architectures on 2 widely used datasets (CIFAR-10 and a subset of ImageNet), leading to 14,106 evaluations in total; 3) thorough analysis and new insights, as well analytical tools. The website and source codes of *BlackboxBench* are available at <https://blackboxbench.github.io/> and <https://github.com/SCLBD/BlackboxBench/>, respectively.

Index Terms—Black-box adversarial attacks, benchmark, query-based adversarial attacks, transfer-based adversarial attacks.

I. INTRODUCTION

DEEP neural networks (DNNs) have been densely applied to safety-critical applications such as autonomous driving and face recognition due to their remarkable success. Worryingly, adversarial examples, which add human-imperceptible noises to benign inputs, capable of deceiving well-trained models, pose a significant threat to DNNs. In real-world scenarios, attackers typically have limited access to information about the target classifier, making them black-box adversaries.

Machine learning (ML) security has witnessed a rapid evolution of black-box adversarial attacks. Numerous researchers strive to enhance the state-of-the-art (SOTA) attack performance against vulnerable DNNs [132]–[134]. These endeavors are also inherently double as robustness assessments to develop stronger defenses and more resilient models [135]–[138]. They are like the spear and the shield, mutually reinforcing each other. However, the proliferation of diverse works, varying in experimental settings and code styles, perplexes researchers

regarding the actual utility and security efficacy of attacks and defenses. As a result, there is a growing demand for building a comprehensive platform for black-box adversarial attacks to facilitate fair comparisons within the community. Moreover, the identification of factors contributing to adversarial vulnerabilities remains unclear, perpetuating a vicious cycle in the study of neural network robustness. Such a platform not only addresses these challenges but also empowers a more profound exploration of this topic through an analysis of its intrinsic properties.

Contributions We build a comprehensive benchmark of black-box adversarial attacks, called **BlackboxBench**. It provides the following key contributions:

- **Modular&unified codebase** *BlackboxBench* takes a modular and unified implementation. As the core part of *BlackboxBench*, *i.e.*, the attack module, is implemented based on a unified pipeline composed of several functional blocks (see Fig. 4), *BlackboxBench* could be easily extended to cover more latest methods, and could also facilitate the involvement of new contributors. To date, we have included 25 query-based attacks and 30 transfer-based attacks, the largest collection of black-box adversarial attacks to our best knowledge.
- **Comprehensive evaluations** Using *BlackboxBench*, we conduct evaluations of 25 query-based attacks and 30 transfer-based attacks on comprehensive attack scenarios, leading to 14,106 evaluations in total. These standardized evaluations establish a leaderboard to identify the most effective methods and track actual progress of this field.
- **Thorough analysis** The comprehensive evaluations enable us to delve deeper into black-box adversarial attacks. We further present 13 types of analysis to reveal the mechanisms of black-box attacks and the effects of various factors to attack performance, with the assistance of ten analytical tools. The insights from our evaluations, as well as the provided analytical tools, could not only broaden and deepen our understanding of the inherent characteristics of black-box attacks, but also facilitate researchers to develop more advanced attack and defense methods.

The remaining parts of this manuscript are organized as follows. Section 2 introduces the related benchmarks and the uniqueness of *BlackboxBench*. Section 3 provides the preliminary, introduction to implemented algorithms, an overview of *BlackboxBench* architecture and library modules. Section 4 provides the evaluation results, systematic analyses and our new insights.

All authors are with the School of Data Science, The Chinese University of Hong Kong, Shenzhen, China, email: meixizheng@link.cuhk.edu.cn, xuanchenyan@link.cuhk.edu.cn, zihaozhu@link.cuhk.edu.cn, hongruichen@link.cuhk.edu.cn, wubaoyuan@cuhk.edu.cn.

*These two authors contribute equally.

† Corresponding author: Baoyuan Wu (wubaoyuan@cuhk.edu.cn).

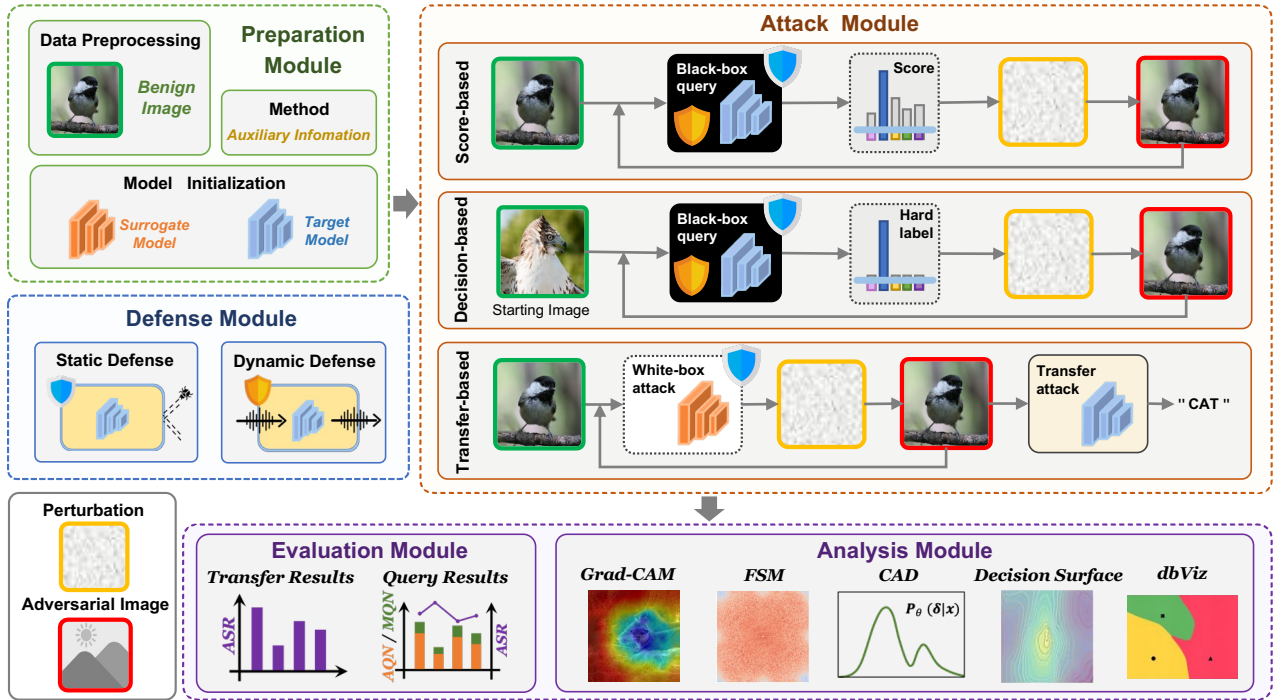


Fig. 1. The general structure of the modular-based codebase of BlackboxBench.

II. RELATED WORK

ML models have demonstrated vulnerability to imperceptible deliberate perturbations. Some researchers identify these vulnerabilities by designing new attacks, others pay ongoing efforts toward new defenses against such perturbations [140]. These perturbations encompass various types (*e.g.*, patch-based, norm-bounded) to fool models in different ML tasks (*e.g.*, computer vision, natural language understanding). Within this research community, many benchmarks have emerged for standardized evaluations. GRB [125] evaluates the adversarial robustness of graph machine learning. SmartBox [123] benchmarks the performance of adversarial attack detection and mitigation algorithms against face recognition. REAP [124] is a benchmark for security against patch attacks. AdvGLUE [126] evaluates the vulnerabilities of modern large-scale language models. CARBEN [127] and MultiRobustBench [128] are unified frameworks for considering multiple attacks against ML models.

BlackboxBench is designed for vision tasks, currently the most extensively studied ML setting. Moreover, unlike some excellent benchmarks specialized in defenses (*e.g.*, RobustBench, [42], RobustML), our aim is to track the real progress in black-box adversarial attacks. Various libraries including CleverHans [82], FoolBox [81], ART [85], DEEPSEC [130] AdverTorch [83], SecML [86], RealSafe [131], AdvBox [84], DeepRobust [87], and TransferAttackEval [129] have all provided evaluation for popular adversarial attacks. Nevertheless, BlackboxBench sets itself apart from existing benchmarks from five key perspectives, as detailed in Tab. I.

- **Programming characteristic** Most libraries employ the object-oriented programming (OOP) language. However, we notice that all the attack algorithms within query-

based category or transfer-based category share highly similar procedures. In essence, all the methods can be implemented through specific modules (see Fig. 1). Particularly, their modules for generating perturbations (*i.e.*, attack module) can be consolidated into a unified pipeline, comprising multiple functional blocks (see Fig. 4). By building a modular and unified procedural programming structure, BlackboxBench can easily switch from one method to another by just modifying a single functional block, without redefining the whole optimization process like OOP-style benchmarks. Note that while DEEPSEC and SecML also feature a modular architecture, they lack an unified attack module compared to BlackboxBench.

- **Code framework** BlackboxBench is implemented in PyTorch, a widely used framework within the deep learning research community.
- **Algorithms coverage** The number and published years of white-box (WA) and black-box (BA) adversarial attacks¹ that each library covers is listed in the fifth and sixth column of Tab. I, respectively. BlackboxBench stands out by supporting 55 black-box attack methods from 2017 to 2023, diverging from other benchmarks that mainly encompass white-box or early black-box techniques.
- **Leaderboard** BlackboxBench is the first to provide an up-to-date leaderboard to track the progress in black-box adversarial attacks.
- **Analysis & tools** Besides analyzing quantitative results like DEEPSEC, RealSafe and TransferAttackEval, BlackboxBench also offers several analysis tools to elucidate

¹White-box attacks can tackle black-box tasks owing to the transferability of adversarial examples. Without specifications in original papers, we categorize white-box attacks evaluated within a black-box setting as black-box attacks.

TABLE I
COMPARISON BETWEEN BLACKBOXBENCH AND OTHER BENCHMARKS.

	Description	Programming characteristic	Code framework	IWA / IBA	Years	Leaderboard	Analysis & tools
CleverHans [82]	A library provides standardized implementations of attacks and adversarial training.	All attacks are independent of each other.	JAX, PyTorch, Tensorflow	12 / 1	2013-2020	\	\
FoolBox [81]	A collection of gradient-based and decision-based adversarial attacks.	Object-oriented programming.	PyTorch, Tensorflow, JAX	8 / 11	2015-2021	\	\
ART [85]	ART provides tools to defend and evaluate ML models against the Evasion, Poisoning, Extraction, and Inference attacks.	Object-oriented programming.	All popular ML frameworks	26 / 10	2013-2022	\	\
DEEPSEC [130]	DEEPSEC incorporates attacks, defenses, and multiple utility metrics.	All modules are independent of each other, but multiple modules can also work together.	PyTorch	0 / 16	2014-2018	\	Draw a set of key findings from their systematically evaluations.
AdverTorch [83]	AdverTorch contains modules for attacks and defenses, also scripts for robust training	Object-oriented programming.	PyTorch	18 / 6	2014-2020	\	\
SecML [86]	SecML implements: (i) evasion attacks and poisoning attacks; and (ii) explainable methods to understand attacks.	SecML has a modular architecture oriented to code reuse. Each module owns an interface.	PyTorch	Attacks in CleverHans and Foolbox	\	\	Provide four explainability methods from two perspective
RealSafe [131]	RealSafe benchmarks the adversarial robustness of image classification and object detection models, and introduces robust training.	Object-oriented programming.	PyTorch	5 / 10	2015-2019	\	Give some important findings by analyzing the quantitative results.
AdvBox [84]	AdvBox supports black box attacks on Machine-Learning-as-a-service, as well as more attack scenarios, such as Face Recognition Attack.	Object-oriented programming.	PaddlePaddle, Keras, PyTorch, TensorFlow, Caffe2, MxNet	8 / 2	2014-2017	\	\
DeepRobust [87]	DeepRobust contains attacks and defenses in image domain and graph domain.	Object-oriented programming.	PyTorch	8 / 2	2013-2019	\	\
TransferAttackEval [129]	The first large-scale evaluation of transferable adversarial examples.	All attacks are independent of each other.	PyTorch	0 / 23	2018-2022	\	The evaluation leads to a number of new insights.
BlackboxBench	A comprehensive benchmark of black-box adversarial attacks, including query-based attacks and transfer-based attacks.	Modular, unified procedural programming.	PyTorch	0 / 55	2017-2023	BlackboxBench LeaderBoard	Provide 13 analyses and new insights via 10 analytical tools from 4 perspectives.

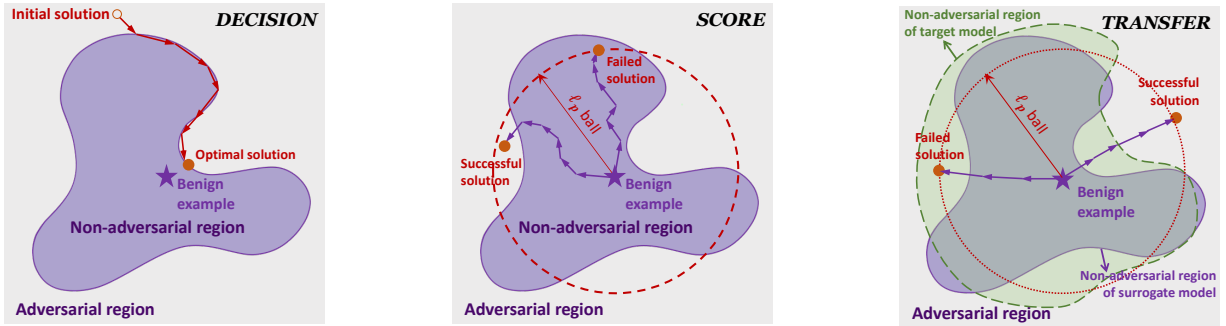


Fig. 2. Graphical illustrations of score-base attack (**left**), decision-based attack (**middle**) and transfer-based attack (**right**), under the untargeted attack setting.

the underlying mechanisms of generating adversarial samples in black-box scenarios, striving to provide fresh perspectives for future research in this domain. Note that although SecML provide tools, only partial tools are involved in the analysis presented in its paper.

III. OUR BENCHMARK

A. Preliminary

BlackboxBench focuses on black-box adversarial attacks against deep learning models. This section seeks to provide the novice reader with a complete grasp of black-box adversarial attacks.

Given the victim neural network $f : \mathbb{R}^n \rightarrow \mathcal{P}(\mathcal{Y})$, parameterized by θ , where $\mathcal{P}(\mathcal{Y})$ is the K -dimensional probability simplex. For a benign example x whose ground truth label is y , adversarial attacks aim at misleading, with imperceptible perturbation δ_x , the prediction of x from f , which lead to the adversarial example $x^* = x + \delta_x$. Formally, x^* satisfies two properties:

- To make sure x^* is perceptually similar to x , x^* is generated within a ℓ_p norm ball centered at x with radius ϵ ,

i.e., $\|x^* - x\|_p \leq \epsilon$. ℓ_∞ and ℓ_2 are the most commonly used norms. The perturbation norm budget ϵ is small enough so as to remain undetectability.

- x^* can be untargeted, in which case the goal of the adversary is to classify x^* as an arbitrary class than the correct one, *i.e.*, $f(x^*) \neq y$. x^* also can be targeted, the targeted x^* is similar but is required to induce a prediction for the target class t , *i.e.*, $f(x^*) = t$.

Depending on the full access to the f or not, adversarial attacks can be divided into *white-box attacks* and *black-box attacks*. The former is deemed easier but less realistic because attackers could access parameters of the victim models. The latter is more practical and challenging because no information is known about the victim, and is the focus of BlackboxBench. As background, we introduce different types of black-box attacks: *query-based attacks*, which query the target model repeatedly and can be further categorized into score-based and decision-based according to the model feedback, and *transfer-based attacks*, which work offline without interacting with the target model².

1) *Decision-based query attacks*: Decision-based query attacks primarily work with only the final decision of a model (e.g., the classification output) without access to the model’s gradients, logits, or any other internal states. Their general formulation is:

$$\min_{\mathbf{x}^*} \mathcal{D}(\mathbf{x}, \mathbf{x}^*) + \xi(\Omega(f(\mathbf{x}^*), y) = 1). \quad (1)$$

The perturbation aims to be as imperceptible as possible (corresponding to minimizing the distance, represented by \mathcal{D} , between the initial input \mathbf{x} and its perturbed counterpart \mathbf{x}^*) while keep misleading the model into incorrect classifications. The term ξ introduces this hard constraint to decision-based optimization process. $\xi(u) = 0$ if u is true. If not, $\xi(u) = \infty$. Within its scope, Ω symbolizes the adversarial criteria, which essentially forces the perturbed input to meet the attack goal. Depending on the type of attack, this criterion varies:

$$\begin{cases} \text{Untargeted:} & \Omega(f(\mathbf{x}^*), y) = \mathbb{I}(f(\mathbf{x}^*) \neq y); \\ \text{Targeted:} & \Omega(f(\mathbf{x}^*), y) = \mathbb{I}(f(\mathbf{x}^*) = t), \end{cases} \quad (2)$$

where \mathbb{I} is the indicator function. In essence, attackers are navigating the adversarial space, defined by the constraints of the model and the criteria. Their goal is to find a point that is both adversarial (misclassified) and as close as possible to the original input. The graphical illustration of untargeted decision-based attacks is shown in Fig. 2(a).

2) *Score-based query attacks*: Score-based query attacks primarily exploit the confidence scores outputted by models, rather than relying solely on the final decision, to create adversarial examples. Their general formulation can be viewed from the perspective of margin maximization.

$$\min_{\mathbf{x}^*} \xi(\mathbf{x}^* \in \mathbb{B}_{\mathbf{x}, \epsilon}) + \max(0, \Delta). \quad (3)$$

The term $\mathbb{B}_{\mathbf{x}, \epsilon}$ denotes a ℓ_p norm ball centered at \mathbf{x} with radius ϵ . ξ denotes the distance function which returns 0 if \mathbf{x}^* locates in the ball $\mathbb{B}_{\mathbf{x}, \epsilon}$ otherwise returns ∞ . It ensures the imperceptibility of adversarial perturbations. The variable Δ differentiates based on the type of attack:

$$\begin{cases} \text{Untargeted:} & \Delta = f(\mathbf{x}^*, y) - \max_{j \neq y} f(\mathbf{x}^*, j); \\ \text{Targeted:} & \Delta = \max_{j \neq t} f(\mathbf{x}^*, j) - f(\mathbf{x}^*, t). \end{cases} \quad (4)$$

The margin loss, captured by the value of Δ , should always be non-negative. A value of 0 for this loss means the attack successfully found its adversarial example, suggesting that the attack process terminates. The primary objective of the attack is to find successful adversarial perturbations while maintaining them within the ℓ_p norm ball $\mathbb{B}_{\mathbf{x}, \epsilon}$. The graphical illustration of untargeted score-based attacks is shown in Fig. 2(b).

3) *Transfer-based attacks*: Unlike query-based attacks that demand repeated queries, transfer-based attacks are inspired by the phenomenon that adversarial samples produced to mislead a surrogate model f' can mislead target models f , even if their architectures are significantly different [66], as long as f and

f' solve the same tasks. Let \mathcal{L} be the loss function (e.g. cross entropy). To fool the classifier f , transfer-based attacks use gradient-based methods to craft ℓ_p norm bounded adversarial perturbation $\delta_{\mathbf{x}}$ against the white-box models f' ,

$$\mathbf{x}^* = \mathbf{x} + \delta_{\mathbf{x}}(f'), \text{ where } \delta_{\mathbf{x}}(f') = \arg \max_{\|\mathbf{z}\|_p \leq \epsilon} \mathcal{L}(f'(\mathbf{x} + \mathbf{z}), y), \quad (5)$$

and then directly utilize the transferability $\mathcal{T}_{\mathbf{x}}(f', f)$ of the adversarial examples to attack the black-box model f ,

$$\mathcal{T}_{\mathbf{x}}(f', f) = |\{f(\mathbf{x}) \neq f(\mathbf{x} + \delta_{\mathbf{x}}(f'))\}|. \quad (6)$$

The graphical illustration of untargeted transfer-based attacks is shown in Fig. 2(c).

B. Implemented Algorithms

We present an elaborate taxonomy of black-box adversarial attacks in Fig. 3. The first level of our taxonomy distinguishes three types of black-box adversarial attacks: decision-based query attacks, score-based query attacks, and transfer-based attacks. At the second level, we subdivide the existing literature within each type based on their technical routes. At the third level, we list the implemented attacks in our BlackboxBench. Given the division of the first level introduced in Sec. III-A, in this section, we introduce our categorization at the second level and the algorithms incorporated into BlackboxBench for each category at the third level. Regarding the method selection, we include classical techniques as baselines and advanced methods to underscore recent advancements in this field.

1) Categorization of implemented decision-based attacks:

In the realm of this research, the focus primarily lies on formulating effective strategies that progressively move the adversarial point toward the decision boundary in each iteration. Regarding the methodologies employed for decision-based attacks, they predominantly bifurcate into two core categories for acquiring the gradient to update the current adversarial examples:

- **Random search methods** These methods involve random direction updates and heuristic parameter adjustments. They include diverse strategies to acquire updating directions, such as sampling from normal distributions, using evolutionary algorithms, gradient-free iterative techniques, and discrete optimization. (e.g., Boundary attack [92], Evolutionary attack [93], GeoDA [94], SFA [95] and Rays [96]).
- **Gradient-estimation-based methods** These methods rely more on the information from the model feedback to guide the search direction. They transform decision-based attacks into optimization problems and incorporate gradient estimation, step size calculation, and binary searching as a framework. Subsequent methods enhance gradient estimation within this framework, and others introduce geometric patterns for improved adversarial detection. (e.g., OPT [97], Sign-OPT [98], HSJA [100], QEBA [4], NonLinear-BA [5], PSBA [6] and Triangle attack [99]).

2) Categorization of implemented score-based attacks:

Score-based attacks typically initiate from a point within the ℓ_p ball and progressively move the sample closer to the decision

² [122] categorize adversarial attacks as white-box, black-box (specifically referring to query-based attacks) and transfer-based attacks. Here we incorporate transfer-based attacks into black-box category to emphasize the importance of adversarial transferability in enhancing black-box attack power.

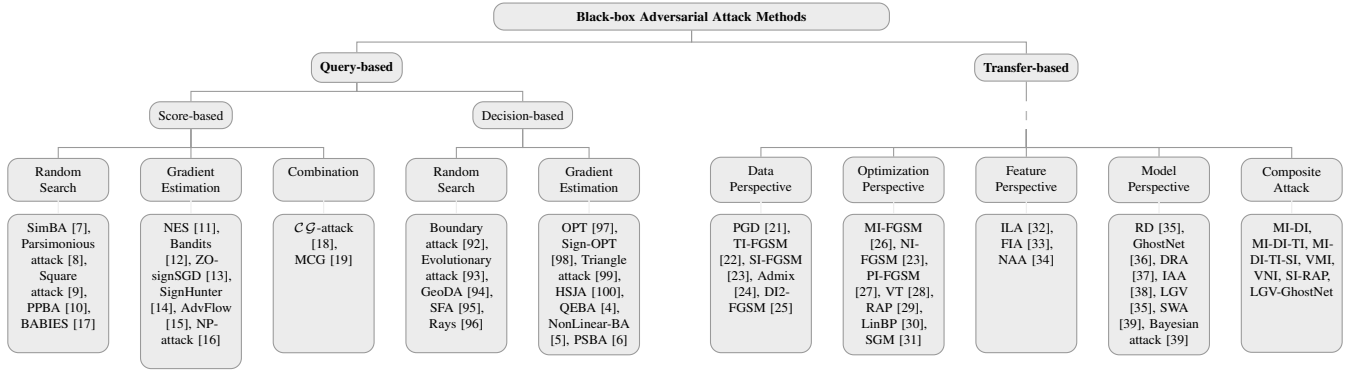


Fig. 3. Taxonomy of black-box adversarial attacks, and implemented methods in each category.

boundary. The objective of the attack is to generate adversarial samples that reside as close as possible to the decision boundary, allowing minimal input perturbations to mislead the model’s classification. Attackers utilize the predicted scores of the target model to guide the movement direction. These methods are usually classified into three categories:

- **Random search methods** These methods usually use stochastic strategies (*e.g.*, sampling) to iteratively modify adversarial perturbations (*e.g.*, SimBA [7], Parsimonious attack [8], Square attack [9], PPBA [10] and BABIES [17]).
- **Gradient-estimation-based methods** These methods utilize model feedback or prior knowledge to approximate gradients for adversarial example creation. (*e.g.*, NES [11], Bandits [12], ZO-signSGD [13], SignHunter [14], AdvFlow [15] and NP-attack [16]).
- **Combination-based methods** These methods enhance adversarial example generation efficiency by integrating extra information from surrogate models, resulting in fewer queries. (*e.g.*, CG-Attack [18], MCG [19]).

As a result, we implemented 25 query-based black-box attack methods in total, covering two types of query feedback, decision and score, returned by the attacked model. 13 decision-based attacks in BlackboxBench are summarized as two categories. 12 score-based attacks in BlackboxBench are summarized as three categories. The general idea of each method will be presented in Appendix D-B and D-A.

3) *Categorization of implemented transfer-based attacks:* Amongst the earliest transfer-based attacks was the Iterative Fast Gradient Sign Method (I-FGSM) [20] which optimizes Eq. 5 iteratively, serving as a stronger adversary for white-box models compared to the single-step attack—Fast Gradient Sign Method (FGSM) [107]. However, iterative attacks tend to overfit the surrogate model and thus cannot transfer across models. *So can we achieve better trade-off between attack ability and transferability?* According to a general formulation:

$$\arg \max_{\mathbf{x}^*} \mathcal{L}(f''(\mathcal{T}(\mathbf{x}_i^*); \theta''), y; \mathbf{I}), \text{ s.t. } \|\mathbf{x}^* - \mathbf{x}\|_p \leq \epsilon, \quad (7)$$

various efforts have been made to enhance the transferability of iterative attacks on the top of I-FGSM, stemming from four distinct perspectives:

- **Data perspective** Methods from this perspective use input transformation $\mathcal{T}(\cdot)$ on the benign sample to alleviate

the overfitting to the surrogate model. (*e.g.*, PGD [21], TI-FGSM [22], SI-FGSM [23], Admix [24], DI2-FGSM [25]).

- **Optimization perspective** Methods from this perspective introduce gradient-based optimization algorithms to escape from poor local maxima or modify the gradients to facilitate transferability. (*e.g.*, MI-FGSM [26], NI-FGSM [23], PI-FGSM [27], VT [28], RAP [29], LinBP [30], SGM [31]).
- **Feature perspective** Methods from this perspective distort intermediate layer features by designing a new adversarial loss function $\mathcal{L}(\cdot; \mathbf{I})$ with the aid of auxiliary information \mathbf{I} (*e.g.*, ILA [32], FIA [33], NAA [34]).
- **Model perspective** Methods from this perspective adjust the basic surrogate model f' to f'' (parameterized by θ'') to improve transferability (*e.g.*, RD [35], GhostNet [36], DRA [37], IAA [38], LGV [35], SWA [39], Bayesian attack [39]).

As shown in Fig. 3, apart from I-FGSM, BlackboxBench incorporates 22 additional transfer-based attacks falling into these four categories. Note that the category *Composed attack* in Fig. 3 indicates compositions of aforementioned individual transfer methods, aimed at harnessing the strengths of each approach for maximum benefit. 7 composite attacks are designed officially in BlackboxBench but more composites could be customized easily by flexibly combining existing functional blocks to constitute the attack pipeline. More detailed descriptions of transfer-based attacks are presented in the Appendix D-C.

4) *Categorization of implemented defenses:* Existing defenses aiming at mitigating adversarial examples can be broadly categorized into [139]:

- **Training-time-based approaches** These defenses focus on enhancing the robustness of the classifier itself. It requires significant data augmentation during training, which can be costly and typically isn’t easily adjustable during inference. The most prominent training-time defense is Adversarial Training (AT) [1], [2], [58]–[60], [65], [91], which is a defense strategy designed to bolster the robustness of machine learning models against adversarial attacks by incorporating adversarial examples during training. While this method enhances resilience, it demands more computational resources and may compromise accuracy on

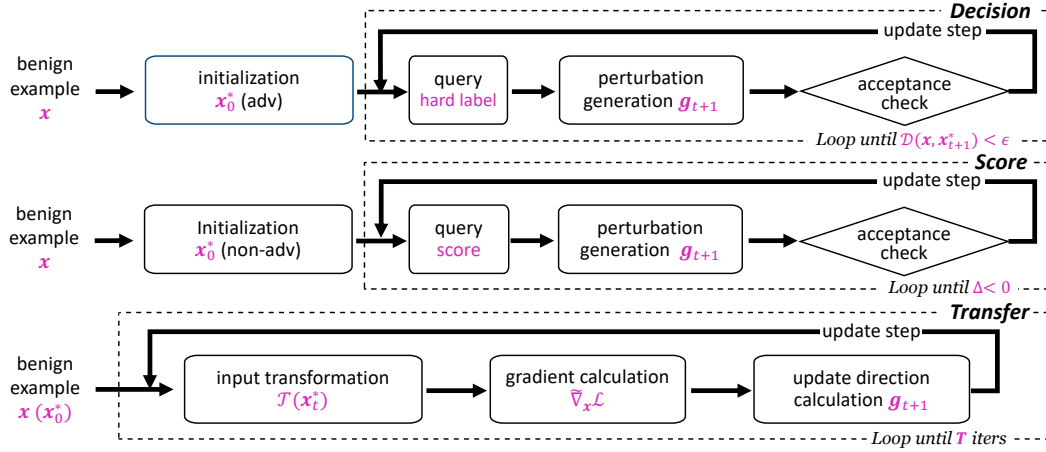


Fig. 4. Unified pipelines of attack modules in decision-based attack methods (**top**), score-based attack methods (**middle**), and transfer-based attack methods (**bottom**).

clean data. Typically, adversarial examples are generated using gradient-based techniques, and the training not only aids in generalizing against diverse attack methods but also offers resistance to transfer attacks. Despite its effectiveness, there’s a trade-off between robustness and clean data accuracy, and various adaptations of adversarial training, like ensemble versions, have emerged to optimize its performance. Essentially, adversarial training proactively modifies model parameters for increased robustness, distinguishing it from static defenses that focus on input or data alterations without changing the model itself. AT is implemented in BlackboxBench and deployed against both query-based attacks and transfer-based attacks.

- **Inference-time-based approaches** These defenses are generally more lightweight since they are applied only during the inference of the classification. Compared to traditional AT, lightweight defenses like Random Noise Defense (RND) [64] and Attack Against Adversarial [108] (AAA) offer several distinct advantages. They are computationally efficient as they deploy defense during inference, eliminating the need for adversarial training across the entire dataset. This makes the defense easier to deploy on existing models without retraining, offering practical convenience. Furthermore, the flexibility of inference-time-based approaches also allow them to be combined with other defense strategies, such as adversarial training, harnessing the strengths of both. RND and AAA are implemented in BlackboxBench and mainly against query-based attacks. More detailed descriptions of AT, RND, AAA can be found in Appendix E.

C. Codebase

We build a unified, extensible, modular-based codebase as the basis of BlackboxBench. As shown in Fig. 1, it consists of five modules, including the preparation module (preparing clean data, pretrained model and auxiliary information), attack module, defense module, evaluation module and analysis module.

1) *Attack module*: The attack module takes preprocessed benign examples, pretrained models and auxiliary information from the preparation module to generate adversarial images. Illustrated in Fig. 4, BlackboxBench summarizes the generation process of various algorithms in decision-based, score-based and transfer-based attacks into three common pipelines, unifying existing methods and illuminate the development of novel attacks. See more details of the unified algorithms in Appendix C. As the pipeline consists of several functional blocks, this attack module is highly extensible to new methods by just modifying individual block functions, without redefining the whole optimization problem. Information regarding how each attack is adapted to this common pipeline is provided in our handbook.

Query-based attack module In the domain of query-based attacks, both score-based and decision-based attack flows can be made up of following four blocks. Nevertheless, they differ significantly inside each block, leading to two independent sub-modules.

- **Initialization block** The decision-based (score-based) attack initiation phase begins with choosing a starting point x_0^* within the adversarial (non-adversarial) region.
- **Query block** In this phase, the adversarial example x_t^* queries the target model and receives feedback—a label for the decision-based or a posterior probability for the score-based.
- **Perturbation-generation block** In the decision-based attack sub-module, this block computes a perturbation g_{t+1} based on hard-label feedback to narrow the distance between x_t^* and x . In the score-based attack sub-module, it finds a perturbation g_{t+1} based on the probability feedback, aiming to cross the decision boundary within an ℓ_p norm ball. The employed perturbation generation function is user-optional.
- **Acceptance-check block** This part checks whether the perturbation from last step is acceptable. Upon a true check, the perturbation is added to x_t^* through an update step.

The latter three blocks are iterated until the objective of

decision-based attacks or score-based attacks is achieved.

Transfer-based attack module According to the basic structure constituted by I-FGSM, BlackboxBench proposes a unified transfer-based attack pipeline, consisting of the input-transformation block, gradient-calculation block, update-direction-calculation block and update step. Other methods developed on the top of I-FGSM from different perspectives are implemented by modifying corresponding blocks along this pipeline, as follows:

- **Input-transformation block** This block contains several image transformation implementations. Methods from data perspective conducted different transformations $\mathcal{T}(\cdot)$ on adversarial samples x_i^* in this block.
- **Gradient-calculation block** Gradient-calculation block takes transformed samples $\mathcal{T}(x_i^*)$ and outputs the gradients $\tilde{\nabla}_x \mathcal{L}$ w.r.t. the adversarial loss \mathcal{L} . Here, methods from feature perspective defined novel loss functions $\mathcal{L}(\cdot)$ based on the intermediate layer features to generate more transferable adversarial examples. Also part of the methods from optimization perspective modifies the way to calculate the gradient in this block.
- **Update-direction-calculation block** In this block, based on the gradients $\tilde{\nabla}_x \mathcal{L}$, methods from optimization perspective derived effective update direction g_{t+1} , i.e., adversarial perturbation.
- **Update step** Passing through the above three blocks, all methods generate adversarial examples x_{i+1}^* by a one-step update—moving x_i^* in the direction of g_{t+1} .

The above procedure will be iterated T times. Note that methods from model perspective refine surrogate models to improve adversarial transferability during the preparation stage rather than in the iterative attack module.

2) *Defense module*: While our primary focus when building the BlackboxBench lies in implementing black-box attack algorithms, we also offer defense options for users to employ attacks with defense strategies. By integrating this module into the evaluation process, we aim to create a holistic understanding of both the robustness of defensive measures and the potency of attack strategies. This module is designed to rigorously assess the effectiveness of black-box attack algorithms when targeting neural network models equipped with defensive methods. As we mentioned above, we mainly provide 2 types of defense strategies including static defense and dynamic defense in BlackboxBench. Note that the involvement of Adversarial Training defenses is accomplished through the utilization of adversarially trained target models, which is static defense. The defense module exclusively provides three dynamic defense methods: RND [64], AAA-Linear [108], and AAA-Sine [108]. These dynamic defense methods are designed to be lightweight algorithms. Our defense module offers a standardized testing environment, ensuring that evaluations are both consistent and replicable.

3) *Evaluation module*: The evaluation module includes three crucial metrics: average query number (AQN), median query number (MQN), and attack success rate (ASR). AQN signifies the average query number over all images made during successful query-based black-box attacks. Similarly, MQN captures the middle value among all query numbers of

successfully crafted adversarial examples. ASR measures the percent of adversarial samples classified as a different class in untargeted attacks or the target class in targeted attacks. For AQN and MQN, a lower value indicates a better attack performance, while for ASR, a higher value indicates a better attack performance. By employing these three metrics, our module provides a comprehensive evaluation to assess and comprehend black-box adversarial attacks. To best align our evaluation with the process of victim models' being attacked, we apply an official pre-processing pipeline on adversarial examples to obtain inputs of specific sizes as models may require different sizes of inputs. We note that most prior works didn't consider transformations during the evaluation.

4) *Analysis module*: We provide ten analytical tools from four analytical aspects to facilitate our comprehension of black-box adversarial attacks, the details of each tool are presented in Appendix F.

Attack-component effect visualization tools An adversarial attack scenario comprises four fundamental components: the method, attack setting, classification model, and dataset. Nevertheless, the influence of each of these components remains unclear. To unravel the effect of each component, we fix other components, expand the one's scope, and summarize the results via five plot tools (line charts, scatter charts, bar charts, bubble charts and heatmaps) to explore the underlying patterns.

Model attention visualization tools As adversarial examples are deliberately designed to deceive classification models, comprehending how proposed methods defocus the model in the pixel domain holds substantial importance. We achieve this by leveraging Full-Gradient Saliency Maps (FullGrad) [118] to visualize the discriminative regions that models capture. Additionally, as the Frequency Saliency Map (FSM) [117] allows us to visually interpret the contributions of frequency components to classification, we also adopt FSM to gain insights into model behavior from a frequency perspective.

Adversarial divergence measurement tools BlackboxBench aims to qualitatively interpret the adversarial transferability and establish a quantitative metric for evaluating transferability between white-box surrogate models and the target model. A high transferability implies that the perturbation crafted by the surrogate resembles that crafted by the target. To gain this resemblance, we adopt the Conditional Adversarial Distribution (CAD) modeling technique [18], which models the distribution of perturbations conditioned on clean examples. Based on the CAD, we design a transferability evaluation metric—Adversarial Divergence—to quantify the difference between models from the adversarial standpoint by calculating the normalized Kullback-Leibler divergence between two CADs.

Decision boundary visualization tools To visualize the proximity of benign images to the decision boundary, we employ Decision Surface [120]. We also utilize dbViz [121] to visualize the information of decision boundary around benign images, aiding in understanding the difficulty for attackers trying to misclassify a benign image into other categories than its ground truth.

TABLE II

A SUMMARY OF ANALYSES IN SEC. IV. ● DENOTES THE ANALYZED QUESTION IS PROPERLY EXAMINED IN THIS ATTACK, WHILE ○ INDICATES IT’S NOT APPLICABLE TO THIS ATTACK. *Used tool* INDICATES THE EMPLOYED TOOL FROM ANALYSIS MODULE TO FACILITATE THIS ANALYSIS.

Analysis object	Analysis content	Query-based		Transfer-based	Used tool ¹
		Score-based	Decision-based		
Result overview	1) How has this research community developed?	●	●	●	AEV
	2) Which attack category exhibits superiority over the others?	●	●	●	AEV
	3) Which task is more challenging, targeted or untargeted?	●	●	●	AEV
Attack procedure analysis	1) How does the attacker traverse from the benign example to its perturbed counterpart?	●	●	●	MAV-A
Effect of data	1) Whether there are samples harder to be attacked by all attack methods?	●	●	○	AEV+DBV-B
	2) How does the dimensionality the adversary restricted to affect its performance?	●	●	●	AEV+DBV-A
Effect of model architecture	1) Which model architecture is most resistant to malicious queries?	●	●	○	AEV
	2) How about the transferability between different model architectures?	○	○	●	AEV+ADM
Effect of attack budget	1) How about the methods’ reliance on the perturbation norm budget?	●	●	●	AEV+MAV-A
	2) How about the methods’ reliance on the query number budget?	●	●	●	AEV
Effect of defense	1) How different attacks perform against various defenses?	●	●	○	AEV
	2) How different is training-time-based defense versus inference-time-based defense?	●	●	○	AEV
	3) Are adversarial images transferable between normally trained models and adversarially trained models?	○	○	●	AEV+MAV-B

¹ AEV → attack-component effect visualization; MAV-A → model attention visualization - FullGrad; MAV-B → model attention visualization - FSM; DBV-A → decision boundary visualization - Decision Surface; DBV-B → decision boundary visualization - dbViz; ADM → adversarial divergence measurement.

TABLE III

CLEAN ACCURACIES OF THE MODELS ADOPTED IN BLACKBOXBENCH. MODELS IN BLUE ARE TREATED AS SURROGATE MODELS. AT INDICATES ADVERSARIALLY TRAINED MODELS. PYRAMIDNET[†] INDICATES PYRAMIDNET [53] + SHAKEDROP [61] + AUTOAUGMENT [62]. VGG-19[†] INDICATES VGG-19 WITH BATCH NORMALIZATION.

	ResNet-50 [43]	VGG-19 [†] [44]	Inception-V3 [45]	DenseNet-121 [46]	WRN-28-10 (AT w/ DDPM) [65]	WRN-28-10 (AT w/ optimization trick) [2]				
Query	CIFAR-10	93.65%	93.95%	93.74%	94.06%	60.75%	62.80%			
	ImageNet	76.13%	74.22%	77.29%	83.62%	81.07%	62.83%	ResNet-50 (AT- ℓ_2) [1]	ResNet-50 (AT- ℓ_∞) [1]	
								54.53%	43.46%	
Transfer	CIFAR-10	ResNet-50 [43]	VGG-19 [†] [44]	Inception-V3 [45]	DenseNet-BC [46]	ResNeXt-29 [49]	WRN-28-10 [50]	PyramidNet [†] [30]	GDAS [54]	WRN-28-10 (AT) [60]
		95.30%	93.34%	94.77%	96.68%	96.31%	96.21%	98.44%	97.19%	89.69%
	ImageNet	ResNet-50 [43]	VGG-19 [†] [44]	Inception-V3 [45]	DenseNet-121 [46]	VIT-B/16 [55]	ResNet-152 [43]	MobileNet-V2 [47]	SENet-154 [48]	ResNeXt-101 [49]
		76.15%	74.24%	77.29%	74.65%	81.07%	78.31%	71.88%	81.32%	79.31%
	WRN-101 [50]	PNASNet [51]	MNASNet [52]	Swin-B [56]	ConvNeXt-B [57]	ResNet-50 (AT) [58]	Swin-B (AT) [59]	ConvNeXt-B (AT) [59]		
	78.84%	82.90%	73.46%	85.20%	83.80%	64.02%	76.16%	76.02%		

IV. EVALUATION AND ANALYSIS

Based on the benchmark shown in Sec. III, we further provide thorough evaluations and detailed analyses of implemented black-box adversarial attacks. We first analyze the overview results and attack procedure, then study the effects of data, model architecture, attack budget and defense respectively. Our analyses are broken into several related questions and summarized in Tab. II.

A. Experimental Setup

Datasets We evaluate our benchmark on CIFAR-10 [40] and ImageNet [41]. For CIFAR-10, the test set with 10,000 images is evaluated. For ImageNet, considering the popularity in different fields, query-based attacks use randomly chosen 1000 images belonging to the 1,000 categories (1 image in 1 class) from ILSVRC 2012 validation set, transfer-based attacks use the ImageNet-compatible dataset³ in the NIPS 2017 adversarial competition, which contains 1,000 images with a resolution of $299 \times 299 \times 3$.

³https://github.com/tensorflow/cleverhans/tree/master/examples/nips17_adversarial_competition/dataset

Models In query-based attacks, we attack 4(5) normally trained target models and 2(3) adversarially trained target models on CIFAR-10(ImageNet) dataset. In transfer-based attacks, following prior works [29], [30], [35], [39], [42], we choose 4(5) surrogate models, evaluate 8(14) normally trained target models and 1(3) adversarially trained target models on CIFAR-10(ImageNet) dataset. The model architectures are diverse and belong to different families to study the transferability. All the adopted models and their clean accuracies on benign test sets are shown in Tab. III. On CIFAR-10, they are evaluated on 10,000 test set. On ImageNet, they are evaluated on the 50,000 validation set. The download links of checkpoints are provided in Appendix A-A.

B. Result Overview

We first exhibit the attack results of various attacks. Each method is evaluated under four attack settings. An attack setting \mathcal{A} is defined by a combination of attack targets $t \in \{\text{targeted, untargeted}\}$ and norms $p \in \{2, \infty\}$, i.e., $\mathcal{A} = t \times p$.

In query-based attacks, we evaluate 25 methods outlined in Sec. III-B using datasets and models detailed in Sec. IV-A across all four attack settings. ℓ_2 and ℓ_∞ are implemented for most attacks, even though some attacks are explicitly

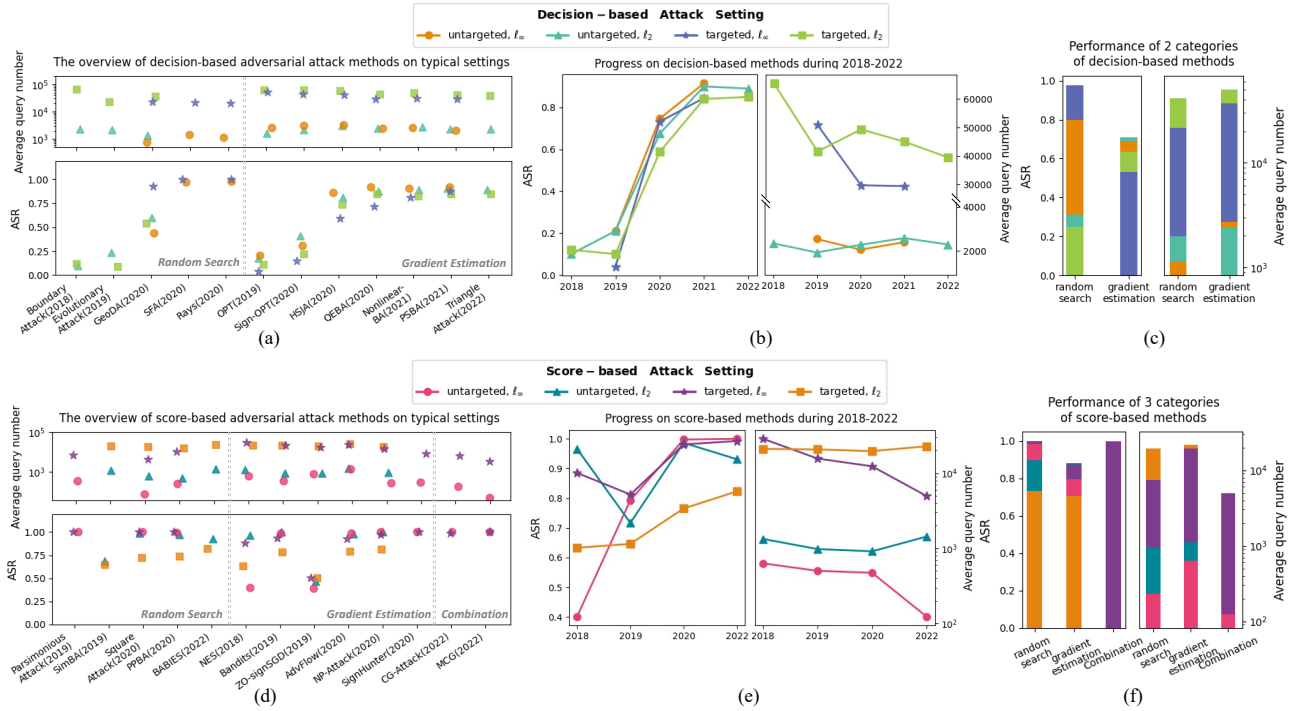


Fig. 5. **Result overview of query-based attacks.** The overviews of various decision-based (**top row**) and score-based (**bottom row**) black-box adversarial attacks implemented in BlackboxBench. The first column shows attack performances, measured using ASR and AQN metrics. The second and third columns present performance summaries *w.r.t.* years and attack categories, respectively. Each color-mark pattern denotes an attack setting.

designed for one certain norm. There are a total of 570 pairs of evaluations for decision-based black-box attacks and 680 pairs of evaluations for score-based black-box attacks. Each method’s performance in attacking a target model is assessed using three metrics: AQN, MQN, and ASR. A better attacker should report a higher ASR and a lower AQN and MQN simultaneously. In transfer-based attacks, we evaluate 30 methods mentioned in Sec. III-B on datasets and models listed in Sec. IV-A under all four attack settings, leading to 13,132 evaluations in total. The efficacy of adversarial perturbations crafted on a surrogate model by each method are measured by averaging ASR on all targeted models listed in Tab. III. A superior attack method is expected to yield a higher average ASR. For the context of transfer-based attacks, unless explicitly specified otherwise, "ASR" refers to the averaged ASR herein.

Due to space limitations, in Fig. 6 and Fig. 5, we exclusively offer a condensed summary of results specifically for the ImageNet dataset alongside one model architecture—ResNet-50, *i.e.*, we only exhibit results where ResNet50 acts as surrogate model in transfer-based attacks and as target model in query-based attacks. For comprehensive tables including additional models and CIFAR-10 dataset, please refer to BlackboxBench LeaderBoard. Based on the results in Fig. 6 and Fig. 5, our analysis in this section mainly focuses on three aspects: 1) the evolution of black-box adversarial attacks over the years and across the categories; 3) the comparison between targeted and untargeted attacks.

1) *Evolution over time and across categories:* The overview of decision-based attack performance is depicted in the top

row of Fig. 5. At the early stage of this field, represented by Boundary attack [92] and OPT [97], a prominent characteristic is the low ASR coupled with a relatively high AQN. However, a turning point occurred post-2020, where emerging targeted attacks marked a shift with both improved ASR and decreased AQN, and untargeted attacks demonstrated an improvement in ASR without costing more queries. In the category of gradient estimation, methods rooted in the HSJA [100] framework (beginning with QEBA [4], followed by NonLinear-BA [5], and culminating in PSBA [6]) exhibited significant attack capabilities—a decline in AQN while aiming for peak ASR. Their continuous pursuit of methodological advancements has consequently positioned gradient estimation-based techniques as superior in ℓ_∞ attack performance when compared to random search-based approaches, as observed in Fig. 5 (c). Nevertheless, within ℓ_2 norm attacks, random search-based methods, SFA [95] and Rays [96], have carved a niche for themselves by recording the best of ASR and the lowest of AQN.

The bottom row of Fig. 5 shows the result overview of scorer-based attacks in BlackboxBench. Between 2018 and 2019, methods like ZO-signSGD [13] and SimBA [7] had high AQNs but yielded lower ASRs. However, with time, newly proposed methods showed improvements: ℓ_∞ attacks showcased enhanced ASR alongside reduced AQN, meanwhile ℓ_2 attacks exhibited improved ASR without an increase in query costs. Notably, Square attack [9], along with the recently introduced methods CG-attack [18] and MCG [19], stood out by demonstrating the highest ASRs and the lowest AQNs. Analyzing between categories, despite random search-based

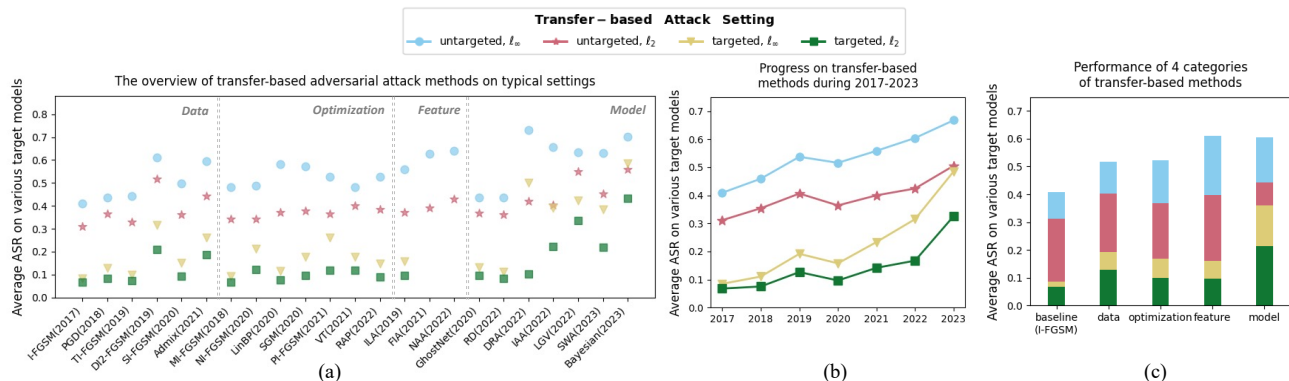


Fig. 6. **Result overview of transfer-based attack.** (a) The performance of various transfer-based black-box adversarial attacks implemented in BlackboxBench. For in-depth analysis, the overview is further summarized according to (b) years and (c) categories. Each color-mark pattern represents an attack setting.

methods and gradient estimation-based methods performing evenly, we notice the surprising achievement of combination-based methods, achieving a perfect ASR of 1 with fewer queries, highlighting the significant role played by the surrogate model’s assistance. Indeed, numerous contemporary score-based black-box attacks utilize the extra information about adversarial samples offered by the surrogate model. BlackboxBench will include more combination-based methods in the future.

The result overview for transfer-based attacks in BlackboxBench is shown in Fig. 6(a). As depicted in Fig. 6(b), there appears an obvious increasing trend of attackers’ performance during the past seven years, suggesting continuing efforts within the active research community. At the early stage, researchers favor the idea that the transferability of the adversarial examples is similar to the generalization ability of the trained models [26]. Accordingly, attempts are more made from data-transformation and gradient-optimization perspectives. Later, inspired by the fact that different DNN models share similar features, transfer-based attacks from a feature perspective have shown promise in relieving the overfitting to the white-box model and the low transferability to black-box model by performing attacks in the intermediate layers. Fig. 6(c) illustrates that, from both data and optimization perspectives, the methods display nearly equal competitiveness, while feature-based methods exhibit superiority in specific attack settings. Recently, there has been a growing focus on refining surrogate models to enhance transferability. This approach has garnered significant attention and has demonstrated exceptional performance, particularly in targeted scenarios, albeit at the cost of increased computational overhead due to additional training requirements.

2) *Untargeted vs. targeted*: Regarding attacks with different targets, we can see that targeted query-based attacks require more query costs than untargeted attacks while exhibiting a relatively lower ASR. Also achieving transferability in targeted attacks proves more challenging than in untargeted attacks. Despite our efforts to conduct evaluations with additional iterations and a logit loss following [67], along with a higher norm budget ϵ to boost targeted attack transferability, existing literature still shows its inability to fool models into predicting a targeted class, even though they perform well in untargeted attacks. Nevertheless, methods from the model perspective

dramatically narrow the gap between targeted and untargeted tasks, illuminating a promising research direction to overcome the low transferability in targeted attack scenarios.

C. Attack Procedure Analysis

For a more qualitative analysis, we explore what is most salient to the target model when an image is under some attack. Using our analytical tools—FullGrad, we visualize the evolution of model attention maps on the perturbed images along the iteration of white-box attacking in transfer-based attacks, or the path traversed by query-based attackers. We are interested in both *how successful attacks succeed* and *how failed attacks fail*.

In transfer-based attacks, given an image from the category of *carousel*, which is selected to be successfully perturbed by about 80% of all implemented methods, the attention maps on its unsuccessfully perturbed counterparts along the iteration are visualized in Fig. 24, the successful cases are visualized in Fig. 26 and Fig. 27. Among the failed attacks, the target model consistently focuses on the original discriminative regions and recognizes them correctly as the attack runs. While in successful attacks, the adversarial images gradually defocus the models from these regions. Finally, the models are misled to focus on those trivial areas and recognize the adversarial images as the category of *four-poster bed*.

In query-based attacks, we choose an image from the category of *squirrel*, which is also selected to be successfully attacked by about 80% of all methods. Following the similar presentation of FullGrad in transfer-based attacks, we show the attention maps through the attack process of unsuccessful attacks in Fig. 25 and successful attacks of both decision-based attacks and score-based attacks in Fig. 28 and Fig. 29. We can also observe that in these samples where attacks did not succeed, the target model continuously concentrated on the critical regions or nearby regions, which failed to mislead the target model and thus the target model can correctly identify them throughout the attack process. Conversely, during successful attacks, the adversarial images incrementally shift the model’s attention away from these critical regions (from the central part to another part). Eventually, the models are deceived into concentrating on insignificant areas, leading to

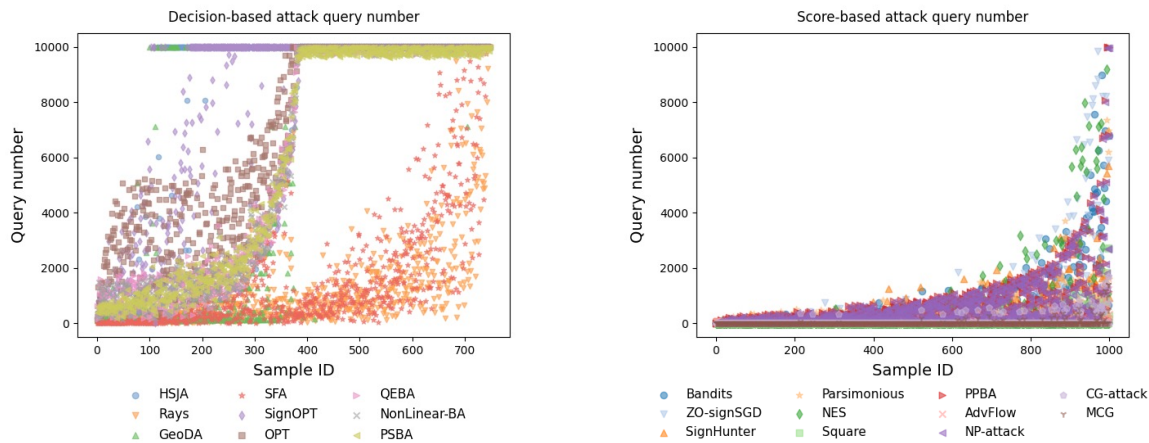


Fig. 7. **Characteristic of hard samples.** Query number of each example for untargeted decision-based black-box attacks (left) and untargeted score-based black-box attacks (right). We test all query-based attack methods on ResNet-50. Note that we only recorded the query numbers of those samples which are successfully initialized at the beginning of decision-based attacks. As for score-based attacks, we recorded the query numbers of the samples which failed to be initialized to be 0 and therefore the number of recorded samples in score-based attacks is 1,000.

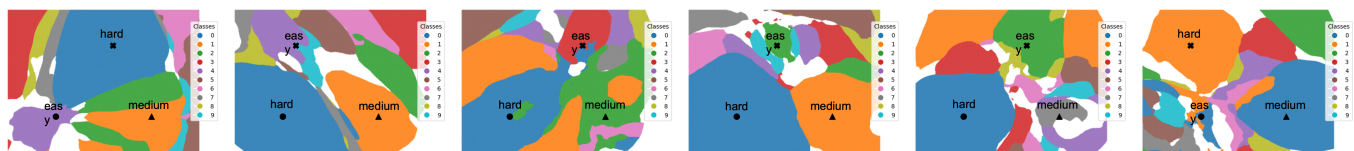


Fig. 8. For the ImageNet dataset on which we deploy our attacks, we select images that are difficult to attack (*i.e.*, those requiring a large number of queries or reaching the query limit) and those that are easy to attack, and visualize the decision boundaries around them. The difficulty level is categorized as “hard”, “medium”, “easy”, corresponding to top 30%, 30%-60%, 60%-90% in terms of the required query numbers. Considering the 1,000 categories of ImageNet, in the figure above, we only display the decision boundaries for the top 10 categories with the highest confidence for the model. Each point in the figure represents the benign images we select, and the chosen model is ResNet-50.

the misclassification of the adversarial images as the category of a *beaver*.

D. Effect of Data

In this section, we investigate how attributes of data impact the black-box adversarial attack performance from two perspectives: 1) characteristic of hard samples, 2) input dimensionality.

1) *Characteristic of Hard Samples:* Fig. 7 presents the performance of decision-based black-box attacks and score-based black-box attacks on the test dataset. The y-axis represents the number of queries required for a successful attack, while the x-axis indicates the index of clean examples sorted according to the query cost. In the case of decision-based attacks, when the number of queries exceeds 10,000 for untargeted attacks, the attack is considered a failure, leading to a cluster of data points at the top of Fig. 7(left). Firstly, the plot shows two distinct regions corresponding to gradient-estimation-based attacks and random search-based attacks, indicating the superiority of the latter when performing ℓ_∞ untargeted attack. The results also reveal that there exist samples for which all attack algorithms fail or require a substantial number of queries to succeed. A similar phenomenon can be observed in score-based black-box attacks (see Fig. 7 (right)). This discovery motivates the exploration of which samples are more difficult or easier to attack.

Based on the quantitative results, our objective was to explore the reasons behind the resilience exhibited by certain

samples against untargeted attacks. To this end, we conducted extensive experiments using the dbViz visualization tool to analyze the decision boundaries surrounding hard-to-attack and easy-to-attack samples in Fig. 8. Our analysis tool will help verify our hypothesis: we believe that samples vulnerable to untargeted attacks are proximate or surrounded by complex, visually fragmented decision boundaries, while those resilient samples are distanced from these boundaries. Recall the nature of untargeted attacks, where the goal is to introduce adversarial perturbations to a clean sample and misclassify it as a label other than its ground truth. Samples near intricate decision boundaries, featuring multiple categories nearby, are more susceptible to this kind of manipulation. Conversely, upon visualizing the decision boundaries around the hard-to-attack samples, we observed their substantial distance from these boundaries, as presented in Fig. 8. This observation suggests that a longer, more intensive attack process might be necessary to shift these perturbed samples away from their original ground-truth category. Our analysis tool provides a more intuitive comprehension of the quantitative results and can serve as a compass for future endeavors aimed at refining attack and defense strategies.

2) *Input dimensionality:* We now quantify the sensitivity to input dimensionality via conducting untargeted, ℓ_∞ attack on ImageNet [41] dataset with varying image size. It’s important to note that when working with a clean dataset with downsampled images, the clean accuracy naturally decreases, potentially

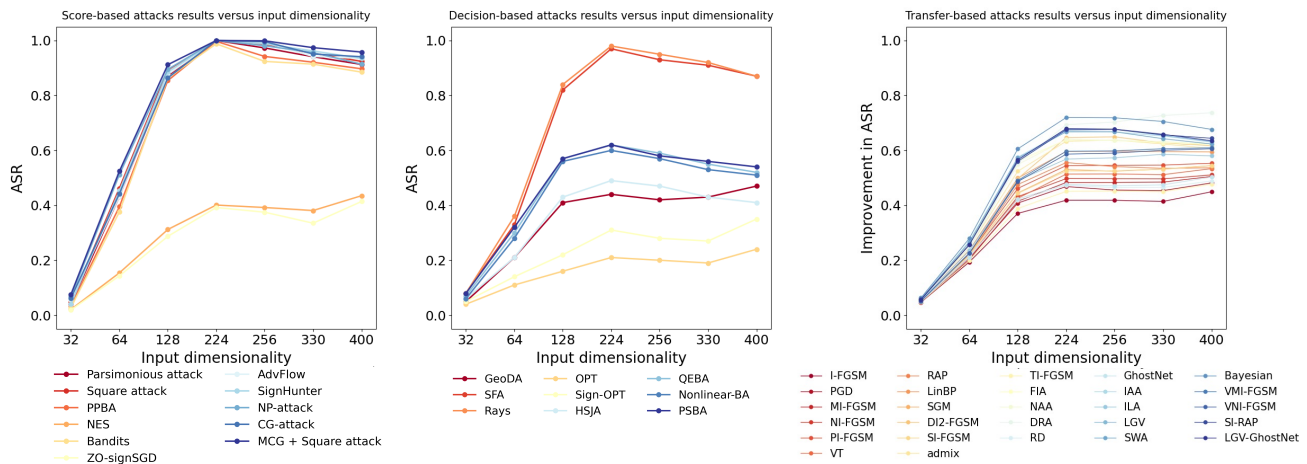


Fig. 9. **Input dimensionality.** The ASR versus input dimensionality of score-based (left) and decision-based (middle). The improvement in ASR versus input dimensionality of transfer-based attacks (right).

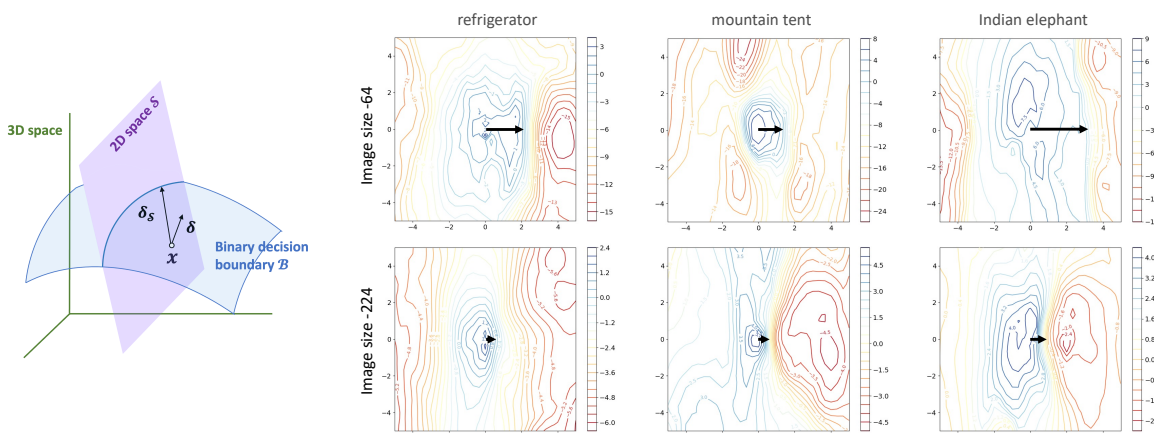


Fig. 10. Pictorial representation (left) of how dimensionality impacts black-box adversarial attacks. Decision boundary visualization (right) with different images of dimensionality 64 and 224.

confusing our analysis. Therefore, we use the *improvement in ASR* after adding adversarial perturbations on benign examples resized to different dimensionalities. This metric only serves as the measure of the transfer-based attack performance. Query-based attacks define the percentage of finally adversarial images in initially non-adversarial images as ASR and thus are not influenced by the dropped clean accuracy. Fig. 9 shows that all adversaries suffer from a considerable failure rate when facing the robustness existing in low dimensional classification tasks. This intuition behind this phenomenon is clearly illustrated in Fig. 10(a). Consider a toy example: \mathcal{B} is the decision boundary of binary classification problem, example x lies in a 2-dimensional subspace \mathcal{S} of a 3-dimensional space \mathbb{R}^3 . δ and $\delta_{\mathcal{S}}$ points in the distance to the nearest decision boundary in 3D space and 2D space respectively. Due to the dimensionality constraint, the attack in lower dimensionality requires a higher perturbation norm budget, as a result, a lower (improvement in) ASR. This intuition could be verified through our analytical tool, Decision Surface, as depicted in Fig. 10(b) where black arrows indicate the distance to cross the decision boundary along the perturbation direction. Notably, inputs in lower dimensionalities require longer distances to traverse the boundary.

E. Effect of Model Architecture

In this section, we are interested in the relationship between attack performances and model architectures. It is well-known that different classification models employ distinct architectural designs as well as different decision boundaries. In query-based attacks, we focus on the vulnerability to input perturbations of different architectures. We specifically compare *the difficulty of crafting successful adversarial samples among various target model architectures from different families*⁴. In transfer-based attacks, our experiment intends to explore *how and what kind of misalignment between surrogate models and target models undermines transferability*. We explore transferability between models within and between different *families*⁴, *i.e.*, intra/cross-family transferability.

1) *Vulnerability of different model architectures:* We choose to implement query-based attacks on model architectures from different families: ResNet-50 from ResNet family [43] which introduces the identity shortcut connection, VGG-19[†] from VGG family [44] which is characterized by its multiple layers of small convolutional filters with consistent receptive fields,

⁴A family contains variants of the same architecture, *e.g.*, ResNet-34/50/152 in ResNet family, Swin-Tiny/Base/Large in Swin family.

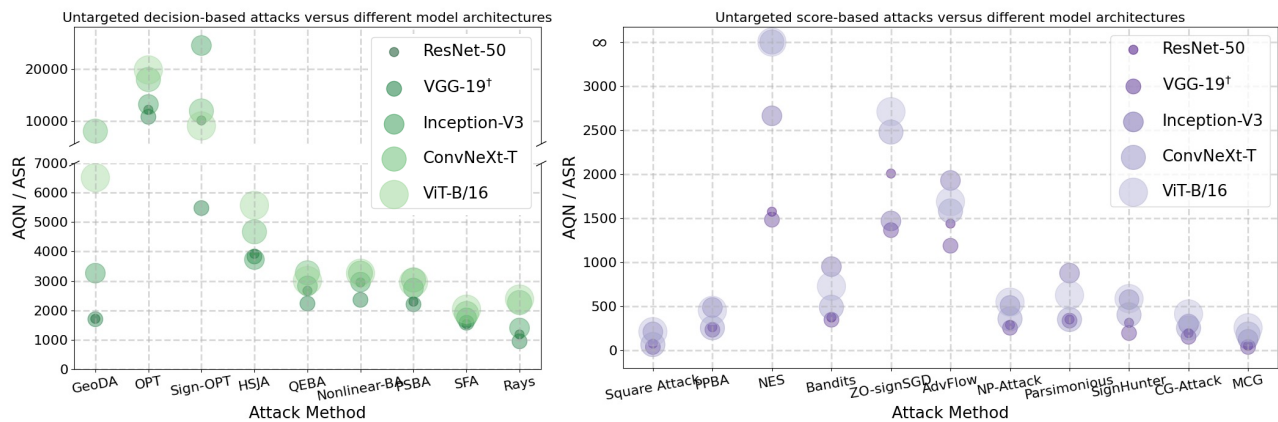


Fig. 11. **Vulnerability of different model architectures.** The ratio of AQN to ASR of decision-based attacks (**left**) and score-based attacks (**right**) versus various target model architectures. An ∞ ratio indicates an ASR of 0, *i.e.*, no image is successfully perturbed, hence implying an extremely hard attacked model.

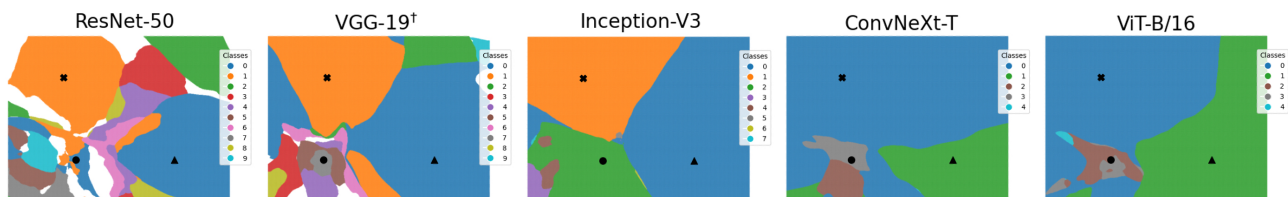


Fig. 12. Visualizations of various models’ decision boundaries. We also utilize the dbViz [121] tools mentioned above to visualize the decision boundaries of these models. Following the plot settings in dbViz [121], we randomly sampled 3 images in ImageNet and constructed an image plane to visualize the decision boundaries. Also, we only present the top 10 categories with the highest confidence scores from target models. More details can be referred to [121].

Inception-V3 [45] which uses "inception modules" to effectively grasp both local and broad image details, ConvNeXt-Tiny (ConvNeXt-T) from ConvNeXt family [57] which merges depth-wise and point-wise convolutions using grouped convolutions to boost its ability to understand local and wide-ranging dependencies, ViT-B/16 from ViT family [55] which adopts self-attention and a Transformer framework to perceive global contexts and manage distant dependencies. We utilize the ratio of AQN to MQN as a metric to measure the difficulty. The higher the ratio is, the harder the model is to be attacked. For both decision-based black-box attacks and score-based black-box attacks, we employ untargeted attacks using ℓ_∞ norm and the ImageNet dataset.

From Fig. 11, we observe that, for the majority of attack methods, attacking SOTA models (ConvNeXt-T and ViT-B/16) tends to yield higher ratio values (*i.e.*, more queries but lower ASR), indicating they are preferable in terms of robustness. Notably, Inception-V3 also demonstrates a comparable or occasionally higher level of resilience against attacks like Sign-OPT, Bandits, AdvFlow and Parsimonious attacks. Conversely, ResNet-50 and VGG-19[†] prove more susceptible to adversarial perturbations, reflected by their lower ratio values.

To investigate the possible hidden reasons, we use our analysis tool, dbViz, to visualize the decision boundaries of various target models. From the visualization results in Fig. 12, we can see that for models with relatively easy architectures like ResNet-50 and VGG-19[†], the decision boundaries on the ImageNet dataset are quite complex and fragmented. Looking at the three samples we took for the graphing, some of these samples are located on the edge of the decision boundaries of

many categories or are surrounded by the decision boundaries of several categories. In comparison, the decision boundaries of the more complex structures, Inception-V3, ConvNeXt-T and ViT-B/16, appear simpler. In other words, the decision boundaries of more complex models are relatively more intact and continuous, without fragmentation. This is bad news for adversarial attacks, as it means that often a larger attack budget is needed to push a clean sample across the decision boundary of the ground-truth category to become an adversarial sample that meets the constraints. In conclusion, our observation and analysis of decision boundary visualizations across various models suggest that the completeness and continuity of decision boundaries in target models constitute a significant factor contributing to the challenge of successful attacks.

2) *Intra/Cross-family transferability:* We investigate intra/cross-family transferability via four families using two *mechanisms*⁵: two CNNs (classic: ResNet [43], SOTA: ConvNeXt [57]) and two SOTA Transformers (ViT [55] and Swin [56]). **ResNet** family are rather simple convolutional models with low capacities. We consider ResNet-34/50/152. **ConvNeXt** family are fully convolutional architectures with designs popularised by Transformers. We consider ConvNeXt-Tiny/Base/Large. **ViT** family modify the original Transformer to make it work with images and induce inductive biases by some training recipes and design choices. We consider ViT-B/16, ViT-B/32 and ViT-L/16. **Swin** families are hierarchical Transformers employing a shifting window

⁵Models with the same mechanism means they share a common foundational block, *e.g.*, both ViT and Swin benefit from self-attention, as well as ResNet and ConvNeXt from convolution.

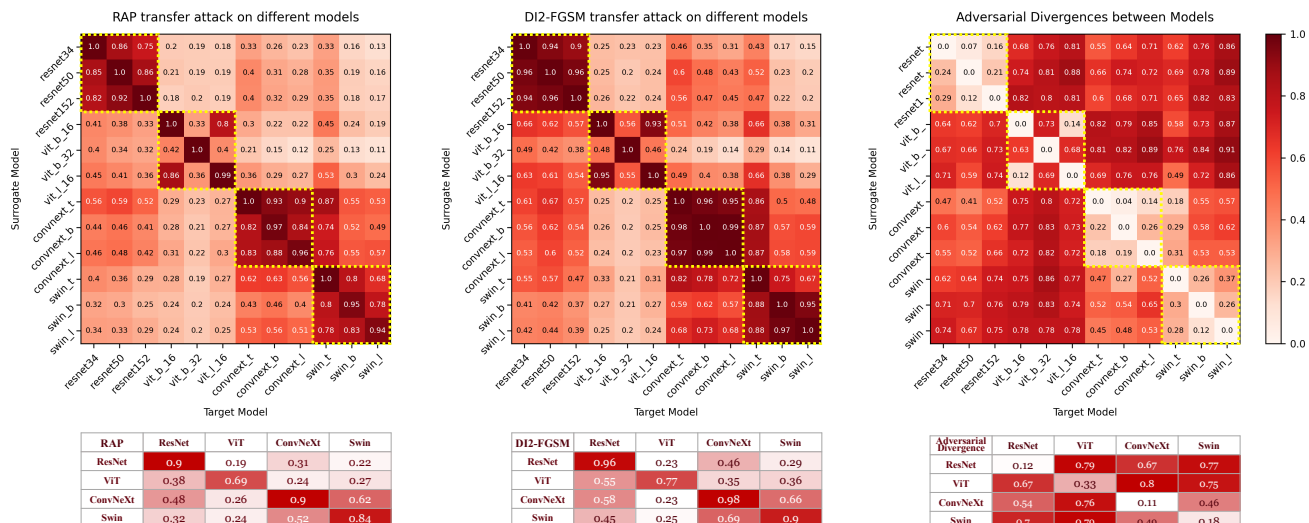


Fig. 13. **Intra/Cross-family transferability.** Matrix of ASR in RAP method [29] (**upper left**), matrix of DI2-FGSM method [25] (**upper middle**), and matrix of Adversarial Divergence (**upper right**), where each entry corresponds to a surrogate-target pair. The y-axis represents surrogate models and the x-axis represents target models. We choose three variants in every model family for our evaluations. Matrices in the second row summarize the first row by averaging entries *w.r.t.* family. Results of more methods which display a similar phenomenon could be found in Appendix G-A.

scheme. We consider Swin-Tiny/Base/Large. We appeal to 12 model architectures in total, leading to $12 \times 12 = 144$ surrogate-target pairs. Fig. 13 reports intra/cross-family transferability rates for various pairs under the untargeted, ℓ_∞ attack on ImageNet.

Rates $(i, j), |i - j| \leq 2$, highlighted by yellow bounding boxes, indicate the proportion of adversarial samples crafted on the white-box model i misclassified by the black-box model j within the same family, representing intra-family transferability. Firstly, the results on the diagonal where surrogates precisely align with targets show that SOTA Transformers and CNNs do not provide additional security than classic CNNs. Therefore, how well an attack would perform is heavily dependent on the surrogate-target alignment rather than the target model architecture. Surprisingly, we observe that all models are vulnerable to intra-family transferability in a non-negligible manner, indicating that surrogates and targets shift with respect to each other but within the same family wouldn't dramatically undermine transferability.

Rates $(i, j), |i - j| > 2$ indicate the proportion of adversarial examples generated to mislead white-box model i that also mislead black-box model j (i, j are from different families), *i.e.*, cross-family transferability. The phenomenon among cross-family transferability is more heterogeneous than intra-family transferability. For the reason behind the heterogeneity, as CNNs induce convolutional inductive biases while Transformers communicate globally via self-attention modules, one intuitive conjecture is that the misalignment that would destroy transferability comes from performing different mechanisms, as previously indicated by [63]. However, the second row in Fig. 13 argues that it's not an absolute rule. For example, the most transferable family to ResNet is intra-mechanism ConvNeXt, but a high cross-mechanism transferability occurs between ConvNeXt and Swin. Thus, the employed mechanism is not

as significant a factor in cross-family transferability as we conjectured.

Instead, we hypothesize that the transferability is implied in the resemblance between adversarial examples generated by the surrogate model and target model, which could be measured by the Adversarial Divergence metric (see Sec. III-C4). Using the analysis tool CAD, we train the conditional adversarial distributions of these models and calculate the Adversarial Divergence of each pair. The results shown in Fig. 13(c) align closely with the transfer success rate illustrated in Fig. 13(a) and (b), *i.e.*, the pair with higher ASR will report a lower Adversarial Divergence value. This alignment verifies our hypothesis that two models with high transferability share a vulnerability to a similar pattern of adversarial perturbation. Additionally, with the effective measurement of misalignment between the surrogates and targets, Adversarial Divergence could guide the search for successful adversarial perturbations and shed light on novel transfer-based attack strategies.

F. Effect of Attack Budget

In this section, we take a closer look at the impact of the attack budgets. We have observed a decrease in the effectiveness or even complete failure of some methods when they attack on a budget that was not fully considered in their original papers. In the following, we provide explanations for these findings. More specifically, we explore attacks with different perturbation norm budgets and query number budgets.

1) *Perturbation norm budget:* We first assess the sensitivity to perturbation norm budget ϵ . The results are summarized in Fig. 14.

In transfer-based attacks, Fig. 14 (middle and right) shows a clear rise in ASR as the perturbation norm budget ϵ increases across all methods. Interestingly, we find the slope in ASR versus budgets remains fairly consistent across most methods, as evidenced by these parallel lines, indicating these attacks

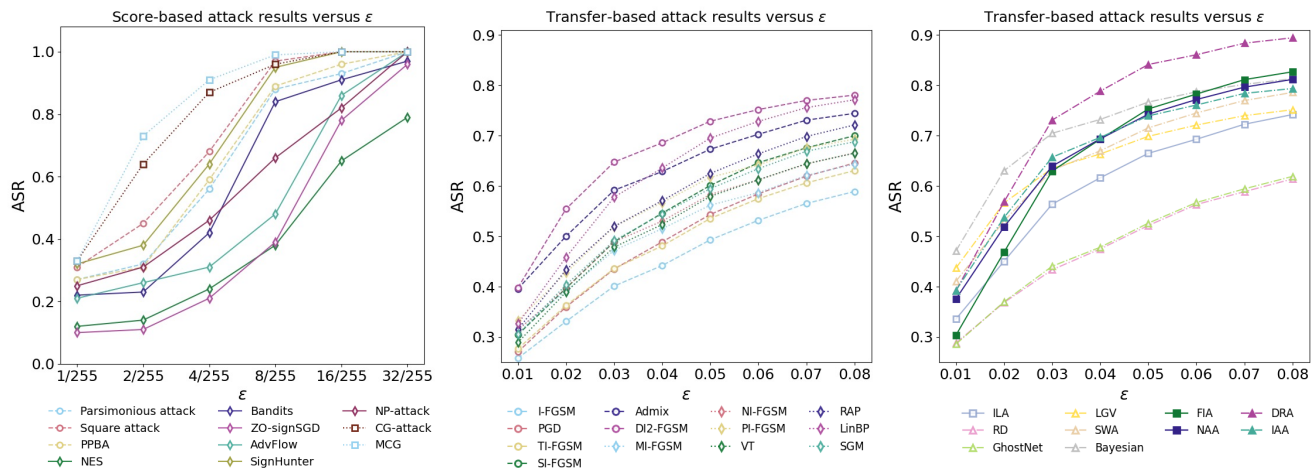


Fig. 14. **Perturbation norm budget.** From left to right: attack results of score-based methods, transfer-based methods from data and optimization perspectives, and transfer-based methods from feature and model perspectives versus the perturbation norm budget ϵ .

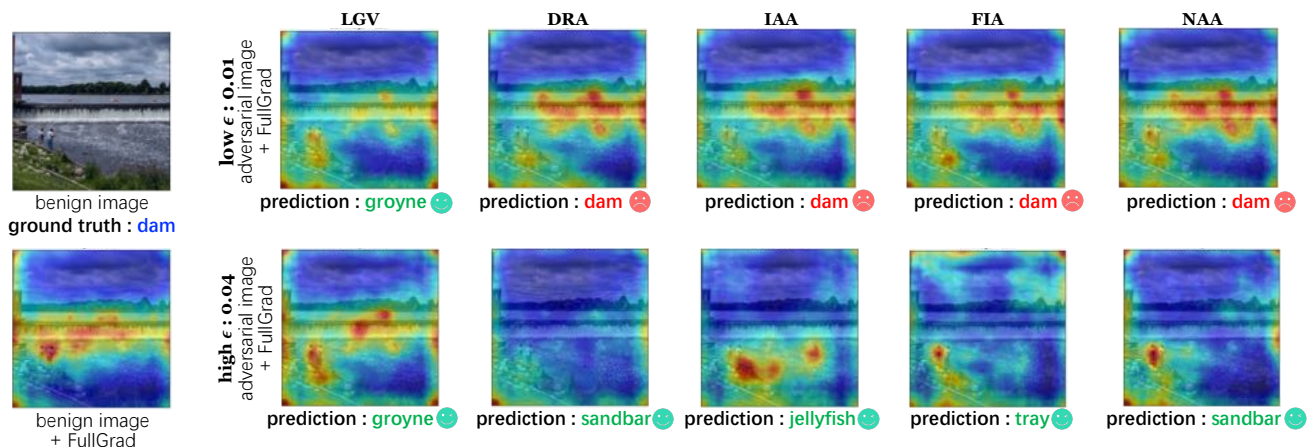


Fig. 15. Comparison between adversarial examples generated by the regular methods (e.g., LGV) and exceptional methods (DRA, IAA, FIA, NAA). The leftmost are a benign image from "dam" category and its FullGrad. The other FullGrad images in the first and second row correspond to adversarial images generated by various methods with a low ϵ (0.01) and a high ϵ (0.04) respectively.

are equally sensitive to the budget. However, exceptions to this consistent pattern are observed in FIA [33], NAA [34], DRA [37] and IAA [38], as their performance drops more significantly in cases of low budgets. Recall that the motivations behind these methods, FIA and NAA both decrease instinct features and increase unimportant features, DRA and IAA both drag images away from the ground-truth data distribution. The common nature implied in these four attacks is to craft *meaningful* noises that make the images *do not "look like"* the ground-truth class. Unlike other attacks that greedily perturb the images to increase the classification loss and generate irregular noises, this nature necessitates a higher norm budget to maintain their superiority. This phenomenon could also be observed from model attention perspective via our analytical tool, FullGrad, as visualized in Fig. 15. For instance, consider an image from the "dam" category. With a low norm budget, LGV easily, greedily misleads the target model into a really closed but different category "groyne". DRA, IAA, FIA, NAA fail to alter the features with this small budget, the target model still focuses on the dam's features and recognizes it correctly. However, when a higher norm budget is applied, these four methods do promote other trivial features. Accordingly, the target model shifts its

focus away from the dam and directs its attention to other features. We use IAA as an illustrative example to substantiate the hypothesis that *the ability to generate semantic adversarial perturbations requires a relatively high norm budget* in Fig. 16. As the budget increases, the perturbation gradually contains more and more obvious features of the "bubble" category. Then this meaningful perturbation overshadows the original features and dominates the classification, as visualized in the attention maps. On the other hand, while this characteristic constrains the attack power in low ϵ cases, it could make attacks stand out when a high budget is available.

In query-based attacks, we only present the experimental results for score-based attacks. This is because the attack process for score-based attacks starts with a clean sample and introduces adversarial perturbations to create an adversarial sample that crosses the decision boundary of the ground-truth category within a specified ℓ_p norm perturbation ball. We believe that the choice of different sizes of perturbation balls will also affect the attack performance of different algorithms, which can be considered as one of the attack budgets for score-based attacks. For decision-based attacks, since the attack mechanism starts with an adversarial sample and gradually

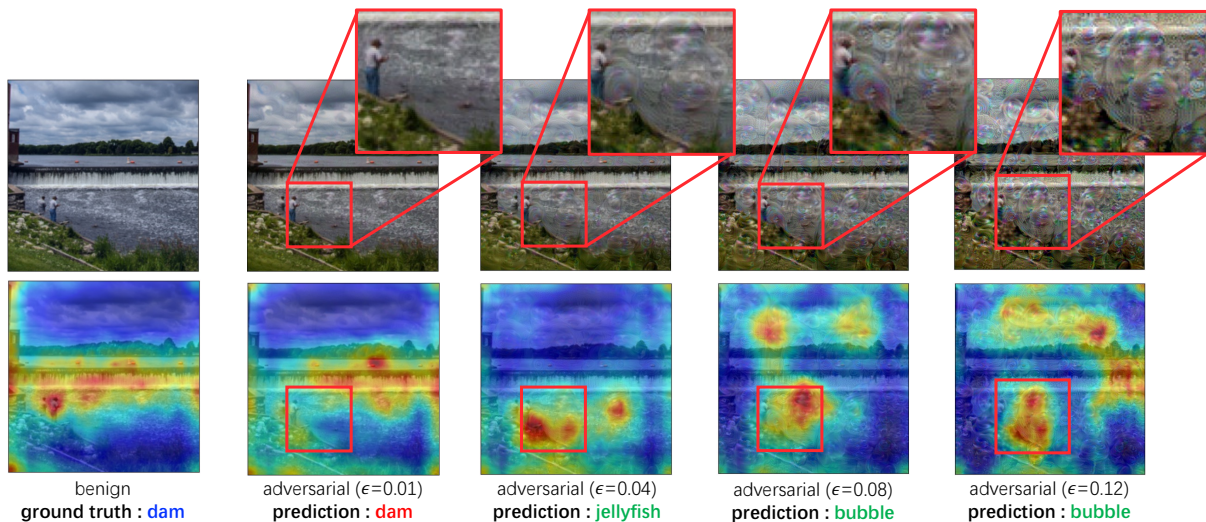


Fig. 16. Adversarial images (**top row**) generated by IAA and target model attention maps (**bottom row**). Each column shows the evolution of adversarial images generated under increasing attack strengths. The red-boxed images amplify the square patches in the adversarial example. We set the maximum norm budget as 0.12 for visibility. IAA could semantically change the "dam" to "jellyfish" and finally to "bubble", but the "bubble"-like perturbations kick in only when they are obvious enough.

narrows the distance to the clean sample, the perturbation ball similar to the attack budget in score-based attacks is no longer applicable. For each method in Fig. 14(left), ASR increases with the perturbation budget. For instance, Parsimonious Attack [8] starts with an ASR of 0.27 at the smallest perturbation budget of 1/255 and reaches an ASR of 1.00 at a budget of 32/255. Similarly, the ASR for Square Attack [9] increases from 0.31 to 1.00 as the perturbation budget grows. PPBA [10], NES [11], and Bandits [12] also show a trend of incrementally higher ASR with larger perturbation budgets. At the lowest budget of 1/255, the highest ASR achieved by any method is 0.31 for MCG [19], and at the highest budget of 32/255, the lowest ASR is 0.79 for NES [11], while all other methods reach ASR of 1.00, indicating that expanding the attack budget indeed improves the performance of the attack methods, aligning with our intuitive judgment. It can be seen that \mathcal{CG} -attack [18] and MCG [19] perform better than other methods across any attack budget, which once again proves that leveraging additional information from a surrogate model can bring significant improvements to the performance of score-based attacks. Even with a lower attack budget, these two methods maintain a high ASR. Furthermore, methods like Square Attack [9], AdvFlow [15], SignHunter [14], and PPBA [10] also maintain good performance, with their unique attack mechanisms (for example, Square Attack [9] explores the perturbation among its L_∞ vertices, and AdvFlow [15] introduces a flow model as the perturbation sampling model, etc.) providing references for the proposal of new methods.

2) *Query number budget*: In query-based attacks, our research focuses on both decision-based black-box attacks and score-based black-box attacks.

For decision-based black-box attacks, we will show the evaluation of Mean Squared Error (MSE) between the optimized adversarial examples and the clean example. We will vary the number of queries while ensuring a 100% attack success rate. This metric represents the magnitude of the adversarial

perturbation. A smaller value indicates that the adversarial example is gradually approaching the clean example to satisfy the adversarial constraint. From the results in Fig. 18, we can see the MSE of the PSBA attack drops most significantly when the query number is still small. Additionally, NonLinear-BA and QEBA, which inherit the HSJA attack framework, also show promising attack performance. These two methods exhibit similar attack behavior, with comparable rates of perturbation magnitude reduction as the number of queries increases. On the other hand, the attack performance of Sign-OPT and OPT is less satisfactory, as the MSE remains high even after a significant number of queries. Furthermore, SFA and Rays rapidly reduce the MSE to lower values at a relatively low query cost.

For score-based black-box attacks, we will show how the ASR changes with an increasing number of queries. We evaluate all decision-based black-box attacks and score-based black-box attacks on ResNet-50 using ℓ_∞ norm untargeted attacks, with the ImageNet dataset as the test set. For score-based black-box attacks, we observe from Fig. 18 that MCG and \mathcal{CG} -attack significantly outperform other methods, achieving the highest ASR levels at the fastest rates. Among the gradient-estimation-based methods, SignHunter is noteworthy as it quickly boosts the ASR to the highest level with minimal query cost. In fact, under untargeted attacks, we can see from the figure that almost all methods achieve a high ASR. It is worth noting that AdvFlow, although it eventually achieves a high ASR, incurs a significant cost as evidenced by its nearly vertical line, indicating a high number of queries for each clean example. Meanwhile, among the random search methods, the Square attack performs exceptionally well, achieving the highest ASR at the fastest rate.

In transfer-based attacks, the term *query number budget* refers to the number of iterations of the white-box attack against the surrogate model. Due to the iterative nature of transfer-based attacks in crafting adversarial examples, it's

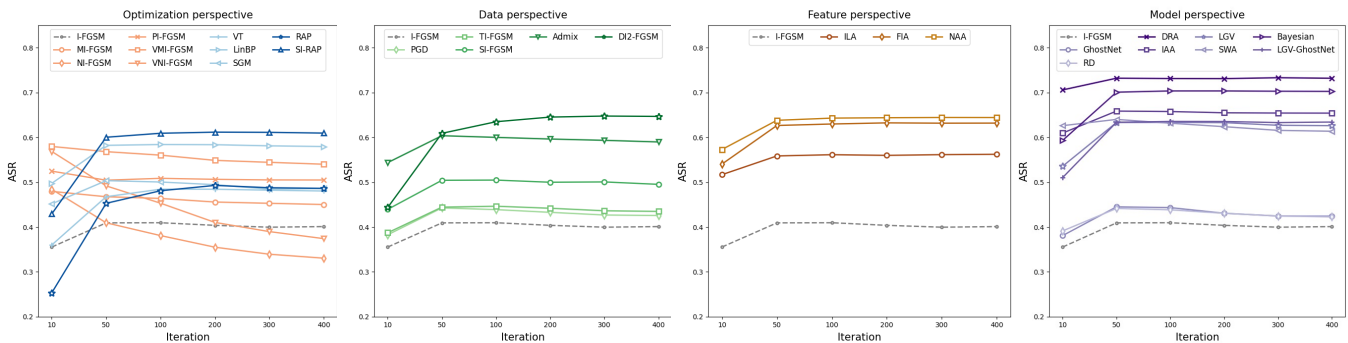


Fig. 17. **Query number budget.** From left to right: attack results of transfer-based attacks from optimization, data, feature and model perspective methods with respect to the number of iteration.

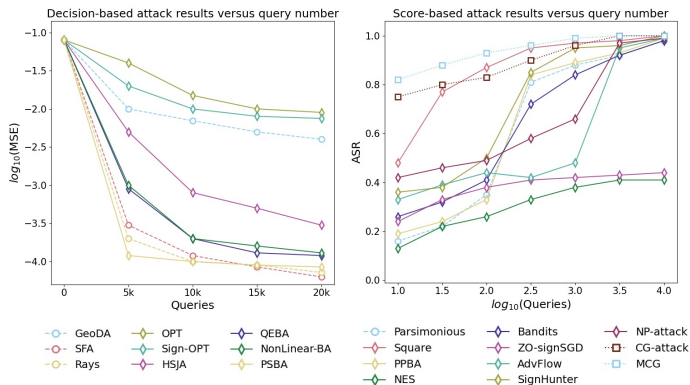


Fig. 18. **Query number budget.** Attack results of decision-based methods (left) and score-based methods (right) versus the query number budget.

therefore necessary to investigate the influence of the number of iterations on the efficacy of these methods. Fig. 17 visualizes the results of untargeted, ℓ_∞ attack on ImageNet, where all method shares a common maximum perturbation ϵ^* and step size α^* . We see that basically optimal performance is attained with 50 iterations, and plateaus with further iterations for data-perspective, feature-perspective, model-perspective, and part of optimization-perspective methods. However, it is worth noting that this stability does not extend to MI [26], NI [23], PI [27], and their corresponding composite attacks (VMI and VNI). They perform best with exactly 10 iterations as suggested in their original papers, however, deteriorate for additional rounds. Recall that the fundamental concept shared by MI, NI and PI is momentum-based gradient optimization. However, inadequate step size will impede the progress of adversarial examples towards the optimal solution. That is to say, over multiple iterations, accumulated momentum may lead to oscillating around the optimal solution or getting stuck in local minima, resulting in a reduction in white-box success rate and, consequently, a decrease in black-box ASR, as shown in Fig. 19(a). Based on this observation, in Fig. 19(b), we propose to adapt the step size of momentum-based attacks. It is evident that even with a suboptimal 50 iterations, a gradual adaptation of step size enables ASR to approach or surpass the optimal results achievable with 10 iterations. These findings boil down to that momentum-based methods’ transferability heavily relies on the early stop, and essentially, appropriate step sizes.

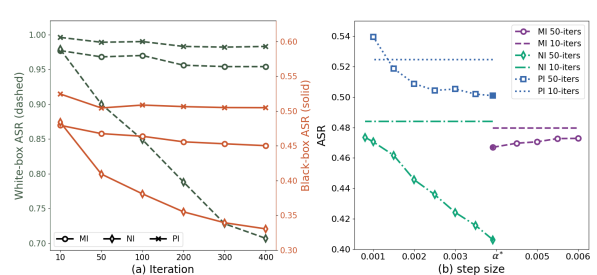


Fig. 19. Momentum-based attack results. (a) White-box(dashed) and black-box(solid) ASR *w.r.t.* iteration numbers. (b) Black-box ASR *w.r.t.* step size. Lines w/ markers plot momentum-based methods ASR versus step size with 50 iterations (more than the recommended 10 iterations), where the solid marker indicates ASR with unadapted step size α^* . Lines w/o markers show ASR with 10 iterations and step size α^* .

G. Effect of Defense

In our previous experimental analyses, we focused on clean models. Now, we shift our focus to attacks on victims involved of defense mechanisms. Here we consider defenses mentioned in Sec. III-B. In the context of query-based attacks, we aim to investigate the evasion capabilities of different attack methods against training-time-based defense and inference-time-based defense and explore the advantages and disadvantages of these two types of defenses. As for transfer-based attacks, in Sec. IV-E we have observed the strong intra-family transferability and heterogeneous cross-family transferability among clean models, we further expand on the previous analyses and now examine the transferability between normally trained models and adversarially trained models, *i.e.*, intra/cross-training-strategy transferability.

1) *Different query-based attacks against defenses:* In this study, we aim to investigate the evasion capabilities of different attack methods against defenses. For our evaluation, we have chosen the ImageNet dataset, which includes two AT models following the ResNet architecture. We specifically evaluate decision-based black-box attacks and score-based black-box attacks using targeted attacks with ℓ_∞ norm. We will present the AQN, MQN and ASR achieved by different attack methods against the defenses in Fig. 20. It is important to note that some defense methods may increase the query numbers of attack methods, but the corresponding increase in ASR indicates that the defense primarily raises the cost of the attack. In decision-based black-box attacks, methods like OPT and Sign-

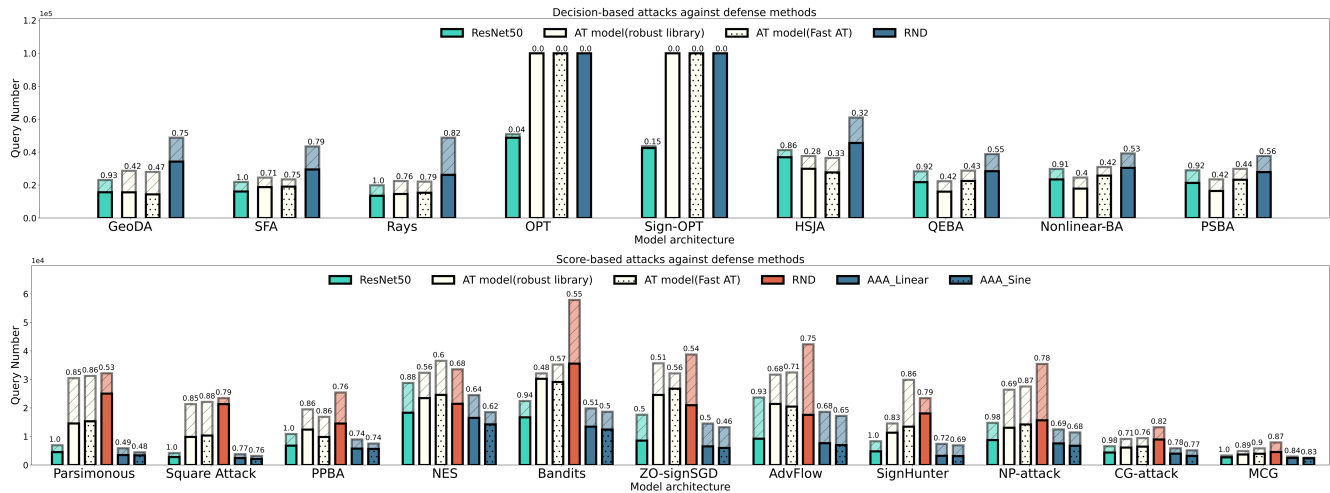


Fig. 20. **Different query-based attacks against defenses.** Each tick on the horizontal axis represents the performance of each method of decision-based attack (**top**) and score-based attack (**bottom**) under different defenses. We use (shaded) bars to represent the MQNs (AQNs) and values above bars to represent ASRs.

OPT face challenges under both training-time and inference-time defenses, often failing to attack even one clean example. However, attacks like QEBA, NonLinear-BA, and PSBA can bypass defenses to some extent, achieving ASRs of around 40%. Remarkably, random search methods such as SFA and Rays consistently outperform, with ASRs exceeding 70% across all defense scenarios, indicating that attacks effective on clean models also perform well against defended models. In score-based black-box attacks, there’s a notable variation in attack performance across different methods, with query numbers ranging from a few thousand to 30,000-40,000. Among all defenses, the combination-based method MCG exhibits the highest ASR and the fewest queries, demonstrating only a 10%-15% reduction in ASR compared to attacking ResNet-50.

2) *Training-time-based defense versus inference-time-based defense:* Defense methods against adversarial attacks fall into two categories: training-time-based and inference-time-based defenses. Assessing their respective pros and cons is essential. Referring to Fig. 20 (top), we compare AT and RND, as AAA exclusively defends against score-based attacks. The results reveal that RND primarily increases the query cost for attackers to achieve performance comparable to, or slightly lower than, those without defense strategies, leading to a trade-off between performance and query cost. Conversely, the query numbers for attacking AT models are similar to those on the clean model (ResNet-50), while the achieved ASR significantly diminishes, indicating a different kind of resistance. In summary, AT could effectively reduce ASR but at the cost of considerable model training overhead. RND provides lightweight and real-time defense while not significantly reducing ASR.

For score-based attacks (see Fig. 20 (bottom)), the comparison between AT models and RND echoes the earlier discussion and is omitted. Particularly, our focus shifts to comparing AAA with AT and RND. Remarkably, AAA markedly reduces ASR within a smaller number of queries, suggesting a more efficient defense strategy by misleading attackers to update adversarial examples in the wrong direction. Compared to AT and RND, AAA represents a more proactive approach, positioning it as

an ideal lightweight defense method.

3) *Intra/Cross-training-strategy transferability:* To comprehensively assess the impact of different training strategies, in addition to normally trained ResNet50, ConvNeXt-B, Swin-B the same as mentioned in Sec. IV-E, we also exploit their adversarially trained counterparts, denoted as ResNet50(AT) [58], ConvNeXt-B(AT) [59] and Swin-B(AT) [59]. This study considers all possible combinations of these models as surrogate-target pairs. For each pair, we subject them to the untargeted, ℓ_∞ attack on the ImageNet and present the transferability between them in Fig. 21. We can see that, in general, the transferability between regular models and AT models is extremely low. For example, in DI2-FGSM, the model with highest transferability to ResNet50(AT) is ConvNeXt-B(AT) instead of ResNet50, the model with highest transferability to ConvNeXt-B is Swin-B instead of ConvNeXt-B(AT). That is to say, strong transferability mostly occurs within the same training strategies, but not between different strategies.

We gain intuition on the cause of this phenomenon by analyzing the spatial frequency features utilized by models to make predictions, via our analysis tool—FSM. The FSMs of these six models are shown in Fig. 21. Firstly, we find that FSMs of normal models consistently display uniform attention distribution across the frequency spectrum, with certain frequency components (e.g., very low frequency) universally disregarded. We also observe the FSM similarity among AT models: their attention spreads over the whole frequency spectrum and predominantly focuses on the frequencies ignored by the normal counterparts. As per Eq. (10), FSM is the Discrete Fourier Transform (DFT) of model gradient *w.r.t* input. Given that adversarial perturbations are largely parallel to the gradient, the magnitude of the Fourier spectrum of adversarial perturbation crafted on a model aligns with the magnitude of the model’s FSM, *i.e.*, the perturbation span frequency ranges which the model is sensitive to. Due to the similarity in frequency attention maps among models with the same training strategy, the crafted perturbations also maintain similarity. The

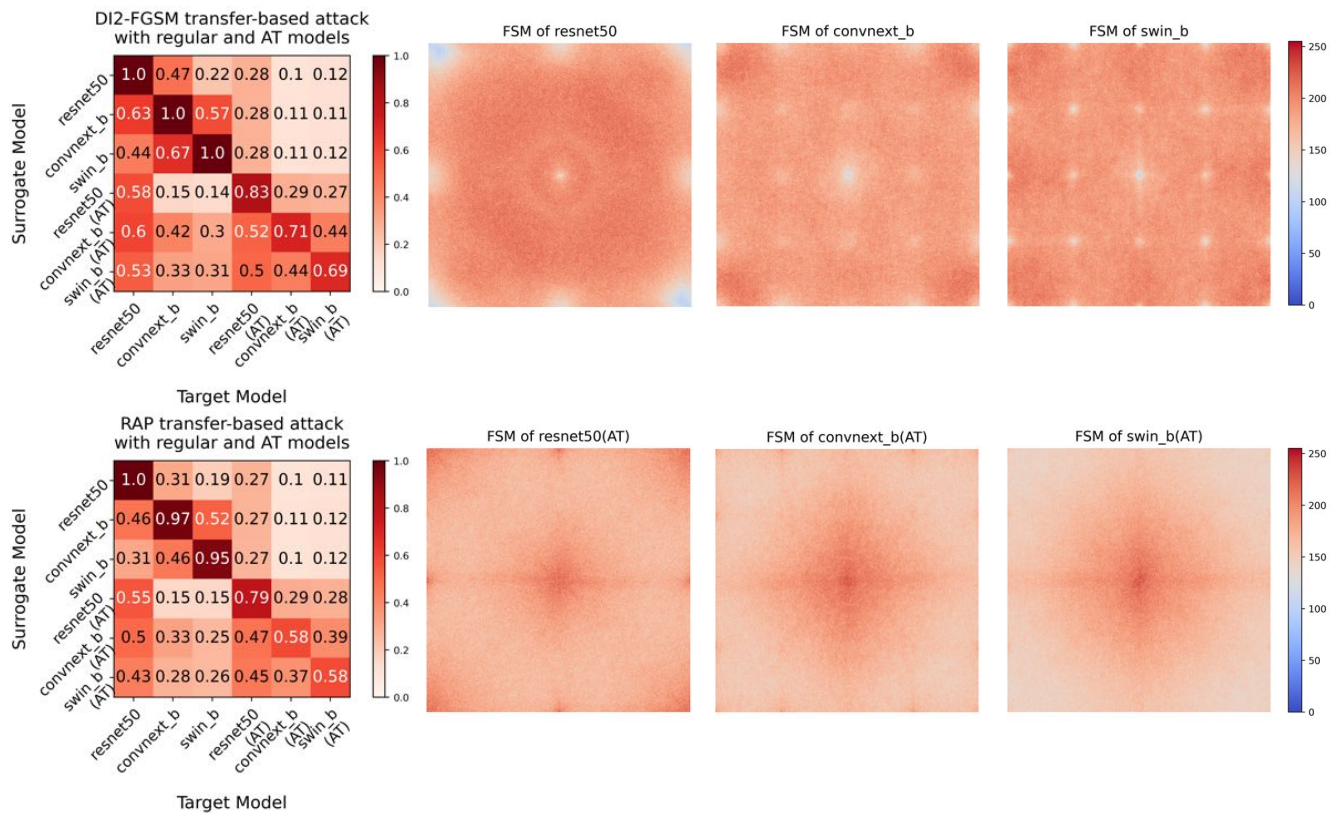


Fig. 21. **Intra/Cross-training-strategy transferability.** The matrices in the first column represent the ASRs for DI2-FGSM (**top**) and RAP (**bottom**) attacks, with each entry corresponding to a surrogate-target pair. The y-axis and x-axis represent surrogate models and target models, respectively. We employ the regular and AT versions of three model architectures for our evaluations. Additional results of more attacks exhibiting similar trends can be found in Appendix G-B. The other columns show the magnitude of the FSM for six models involved in this analysis. Low frequencies are located at the center, and high frequencies at the corners.

transferability of adversarial perturbations between models arises from shared non-robust features. Consequently, perturbations transfer effectively between models with the same training strategy, yet exhibit reduced transferability between models employing different training strategies. Note that all models transfer well to ResNet50 might be attributed to their coverage of a broader frequency spectrum compared to ResNet50.

V. CONCLUSION

The BlackboxBench benchmark, featuring a modular, unified and extensible codebase, can contribute to validating the truly effective ideas within the domain of black-box adversarial attacks. Our implementation encompasses 25 query-based attacks (13 score-based and 12 query-based), along with 30 transfer-based attacks (23 single and 7 composed). These efforts resulted in 14,106 evaluations covering a wide range of attack scenarios. Our aim with BlackboxBench is to facilitate the research community, especially in rapidly comparing with existing literature during the design of new attacks, providing a sound grasp of the progress in black-box adversarial attacks over time, and assessing defenses against adversarial threats at inference time. Furthermore, we demonstrated that our tools are valuable for analyzing various factors related to the vulnerability of DNNs, such as data, model architecture, attack budget, and defense mechanisms. We believe that the research community needs to gain a deeper understanding of how these factors

impact attack effectiveness. In this endeavor, BlackboxBench can play a pivotal role.

APPENDIX A IMPLEMENTATION DETAILS ON EXPERIMENTS

A. Pretrained model download links

For evaluations on CIFAR-10 models, we use the following implementations(embedded links):

- **regular models**
pretrained for query-based black-box attacks: ResNet-50, VGG-19[†], Inception-V3, DenseNet-121
pretrained for transfer-based black-box attacks: ResNet-50, VGG-19[†], Inception-V3, DenseNet-BC, ResNeXt-29, WRN-28-10, PyramidNet[†], GDAS.
- **AT models** AT model(optimization trick), AT model(ddpm), WRN-28-10(AT).

Models for ImageNet dataset are from following implementations:

- **regular models** ResNet-50, VGG-19[†], Inception-V3, DenseNet-121, ViT-B/16, ResNet-152, MobileNet-V2, SENet-154, ResNeXt-101, WRN-101, PNASNet, MNASNet, Swin-B, ConvNeXt-Small ConvNeXt-B.
- **AT models** AT-l_2-ResNet-50, AT-l_inf-ResNet-50, FastAT, ResNet-50(AT), Swin-B(AT), ConvNeXt-B(AT).

B. Experimental setting for Result Overview in Sec. IV-B

In the experiments of query-based attacks, we implemented both untargeted and targeted attacks. For untargeted attacks, we assign the ground-truth label provided by the validation set for each clean example. In this case, one attack is successful if the predicted class of the adversarial example is different from the ground-truth label. The maximum number of queries is set to 10,000 for all untargeted attacks. For targeted attacks, we also assign the ground-truth label as untargeted attacks for each clean example. Besides, we choose the target label for each clean example according to the logit returned by the target model. There are 5 target types of target labels, which are "random", "least likely", "most likely", "median" and "specified label", for users to choose from. In our evaluation, we choose to assign a target label for each clean example by "median", which is the median label of the logit given by the target model. For all targeted attacks, the maximum number of queries is set to 100,000 since if we still set the number to 10,000, which is the same as untargeted attacks, most attacks will fail to craft even one adversarial example. In Sec. IV-B we only select the attack setting with ImageNet as our dataset and ResNet-50 as our target model. We present the performance of both ℓ_2 norm and ℓ_∞ norm attacks.

In the experiments of transfer-based attacks, we test all four attack settings on ImageNet. We employ ResNet50 as the surrogate model and encompass all 17 models listed in Tab. III as target models. The reported performances are averaged ASR over all target models. For untargeted attacks, we utilize Cross Entropy loss. The adversarial perturbation is bounded by $\ell_\infty = 0.03$ with step size $1/255$ and $\ell_2 = 3$ with step size 0.3 for all attacks. The number of iteration is method-specific. For targeted attacks, we utilize the logit loss. The adversarial perturbation is bounded by $\ell_2 = 0.06$ with step size 0.006 and $\ell_2 = 6$ with step size 0.6 for all attacks. The number of iteration varies by method, generally exceeding that of untargeted attacks.

C. Experimental setting for Effect of Data in Sec. IV-D

With regard to character of clean samples, we randomly extracted one image from each class of the ImageNet Large Scale Visual Recognition Challenge 2012 (ILSVRC2012) validation set, totaling 1,000 images, to form the test dataset. Based on this, we perform $\{\text{untargeted}, \ell_\infty\}$ attacks with ℓ_∞ bound to be 0.03 using all attack algorithms on ResNet-50.

Regarding input dimension analysis, to craft adversarial examples of specific sizes, for query-based and transfer-based attacks, we both replace the official pre-processing pipeline of each neural network with resizing transformation. All images are resized to $n \times n$, $n \in \{32, 64, 128, 224, 256, 330, 400\}$. In the experiments of transfer-based attacks, we adopt the same $\{\text{untargeted}, \ell_\infty\}$ attack configuration as discussed in the result overview analysis. Note that the pre-processing for adversarial examples in evaluation module is omitted here due to the potential impact of its resize operation on our analysis. In the experiments of query-based attacks, we also adopt the same $\{\text{untargeted}, \ell_\infty\}$ attack configuration as discussed in Sec. IV-B.

D. Experimental setting for Effect of Model Architecture in Sec. IV-E

For query-based attacks, different model architectures imply different decision boundaries. We specifically compare the difficulty of crafting successful adversarial samples among various target model architectures. We utilize the ratio of AQN to ASR as metrics to measure the difficulty of attacks. For both decision-based black-box attacks and score-based black-box attacks, we employ untargeted attacks using ℓ_∞ norm bounded to be 0.03 and the ImageNet dataset. We specifically set the maximum query number of each evaluation to be 10,000.

For intra/cross-family transferability analysis, we conduct $\{\text{untargeted}, \ell_\infty\}$ attacks on ImageNet dataset. The surrogate model and target model are chosen from twelve model architectures, encompassing four variants within each of three model families. The reported performances are ASR of each surrogate-target pair. We utilize Cross Entropy loss. The adversarial perturbation is bounded by $\ell_\infty = 0.03$ and the step size is set as $1/255$ for all attacks. The number of iteration is method-specific.

E. Implementation details for Effect of Attack budget in Sec. IV-F

In the context of perturbation norm budget analysis, for transfer-based experiments, we adopt the same $\{\text{untargeted}, \ell_\infty\}$ attack configuration as discussed in the result overview analysis. However, the maximum perturbation is defined as $\{0.01, 0.02, 0.03, 0.04, 0.05, 0.06, 0.07, 0.08\}$ with a corresponding step size set at one-tenth of the budget.

In query number budget analysis, for transfer-based attacks, we evaluate the $\{\text{untargeted}, \ell_\infty\}$ attack using the same configuration discussed in the result overview analysis but the iteration number, common across all methods, is drawn from the set $\{10, 50, 100, 200, 300, 400\}$. For decision-based attacks, we vary the query numbers while keeping the sample being successfully attacked to evaluate the distance between original example and adversarial example. A smaller value indicates that the adversarial example is gradually approaching the clean example to satisfy the adversarial constraint. Meanwhile, for score-based black-box attacks, we will show how the attack success rate (ASR) changes with an increasing number of queries. We evaluate all decision-based black-box attacks and score-based black-box attacks on ResNet-50 using ℓ_∞ norm untargeted attacks, with the ImageNet dataset as the test set.

F. Experimental setting for Effect of Defense in Sec. IV-G

Regarding different attacks against defense in query-based attacks, We specifically evaluate decision-based black-box attacks and score-based black-box attacks using targeted attacks with ℓ_∞ norm bounded to be 0.03 and the maximum query number is set to be 100,000.

Regarding training-time-based defense versus inference-time-based defense, we directly add random Gaussian noise on each input to implement RND [64] while deploying the AAA model class to implement AAA-Linear [108] and AAA-Sine [108] respectively according to our configuration in our code.

Regarding intra/cross-training-strategy transferability analysis, we adhere to the configuration specified in the intra/cross-family transferability analysis. However, the models to compose surrogate-target pairs are chosen from the regular and Adversarial Training versions of three distinct model architectures.

APPENDIX B HYPER-PARAMETERS

The hyper-parameters for score-based attacks, decision-based attacks and transfer-based attacks are specified in Tab. V, Tab. IV and Tab. VI. Due to potential variation in effectiveness across the different surrogate model architectures and datasets, hyper-parameter configurations are meticulously detailed for each scenario. One can reproduce all the evaluation results with these configurations. Additionally, we provide our rules to select the hyper-parameters, as follows:

- **Whenever available, we adopt the hyper-parameter configuration recommended in the original paper.**

Generally, the original paper will provide the the values of hyper-parameters specific to one or some scenarios to help reader reproduce their experimental results. For example, the Bayesian Attack [39] outlined their experimentation details: "We tested untargeted ℓ_∞ attacks in the black-box setting, ... On CIFAR-10, ... and used ResNet-18 as source model. While on ImageNet, ... and used ResNet-50 as the source model. ... In possible finetuning, we set $\gamma = 0.1/\|\Delta\mathbf{w}^*\|_2$ and a finetuning learning rate of 0.05 if SWAG was incorporated. ... We use an SGD optimizer with a momentum of 0.9 and a weight decay of 0.0005 and finetune models for 10 epochs on both CIFAR-10 and ImageNet. We set the batch size of 128 and 1024 on CIFAR-10 and ImageNet, respectively. ...". It provides the configuration for $\{\text{untargeted}, L_\infty\}$ white-box attack against ResNet-18 and ResNet-50 on CIFAR-10 and ImageNet datasets. In these instances, we adhere to the prescribed values provided by the authors in the corresponding scenarios.

- **For the scenarios without suggestions, we engage in the search for reasonable, effective hyper-parameter values when datasets and surrogate models architectures vary, then fix the values for different attack types.**

Taking the above Bayesian Attack as an example, maintaining hyper-parameter consistency across different attack settings could guarantee the fairness of our evaluations. However, this set of hyper-parameters for finetuning surrogate models needs to adapt to different surrogate model architectures. Similar considerations apply to methods like DI2-FGSM [25], where image resizing hyper-parameters are irrelevant to attack settings but contingent upon distinct datasets.

APPENDIX C UNIFIED ALGORITHMS

BlackboxBench unifies decision-based attacks, score-based attacks and transfer-based attacks in Alg.1, Alg.2 and Alg.3 respectively. Any attack process in BlackboxBench could be composed of the functional blocks in this algorithm. The algorithms are described in Sec. III-C.

Algorithm 1: Unified Decision-based Black-box Adversarial Attacks

Input: Target model f , a benign example \mathbf{x} , label y ;
Hyper-parameter: Maximum perturbation ϵ , step size α , max query numbers N ;
Function specific to attacks: Adversarial example initialization function \mathcal{I} , perturbation generation function \mathcal{G} ;
1: Initialize: $\mathbf{x}_0^* \leftarrow \mathcal{I}(\mathbf{x})$;
2: **while** $t < N$ and $\|\mathbf{g}_t\|_p > \epsilon$ **do**
3: # Perturbation generation
4: Generate the perturbation \mathbf{g}_{t+1} using $\mathcal{G}(\mathbf{x}_t^*)$;
5: # Acceptance check
6: **if** \mathbf{g}_{t+1} satisfies acceptance check **then**
7: # Update step
8: Generate adversarial example \mathbf{x}_{t+1}^* using an update step based on \mathbf{g}_{t+1} and α ;
9: **end if**
10: **end while**
11: **return** $\mathbf{x}^* = \mathbf{x}_N^*$.

A. Decision-based attack algorithm

B. Score-based attack algorithm

Algorithm 2: Unified Score-based Black-box Adversarial Attacks

Input: Target model f , a benign example \mathbf{x} , label y ;
Hyper-parameter: Maximum perturbation ϵ , step size α , max query numbers N ;
Function specific to attacks: Adversarial example initialization function \mathcal{I} , perturbation generation function \mathcal{G} ;
1: Initialize: $\mathbf{x}_0^* \leftarrow \mathcal{I}(\mathbf{x})$;
2: **while** $t < N$ and \mathbf{x}_0^* is not adversarial **do**
3: # Perturbation generation
4: Generate the perturbation \mathbf{g}_{t+1} using $\mathcal{G}(\mathbf{x}_t^*)$;
5: # Acceptance check
6: **if** \mathbf{g}_{t+1} satisfies acceptance check **then**
7: # Update step
8: Generate adversarial example \mathbf{x}_{t+1}^* using an update step based on $\mathbf{g}_{t+1}, \alpha, \epsilon$
9: **end if**
10: **end while**
11: **return** $\mathbf{x}^* = \mathbf{x}_N^*$.

C. Transfer-based attack algorithm

APPENDIX D

DESCRIPTION OF BLACK-BOX ADVERSARIAL ATTACKS

Here we provide a detailed description of all implemented attacks in BlackboxBench.

A. Description of decision-based attacks

Random search methods

- **Boundary Attack** [92] Boundary attack initializes with an already adversarial example and then gradually reduces the distance to the target image using rejection sampling with a suitable proposal distribution, often a normal distribution. By following a given adversarial criterion, the attack aims to find smaller adversarial perturbations.
- **Evolutionary Attack** [93] Evolutionary attack utilizes the refined covariance matrix adaptation evolution strategy (CMA-ES) [112] to generate adversarial examples. This evolutionary approach improves the efficiency of the attack by employing the Gaussian distribution to example

Algorithm 3: Unified Transfer-based Black-box Adversarial Attacks

Input: A surrogate model f' with parameter θ' , a benign example \mathbf{x} , label y ;
Hyper-parameters: Maximum perturbation ϵ , step size α , iterations T , hyper-parameter set specific to attacks;
Functions specific to attacks: Input transformation function \mathcal{T} , loss function \mathcal{L} , gradient calculation function ∇ , update direction calculation function \mathcal{U} , surrogate model refiner \mathcal{R} ;

- 1: $\mathbf{g}_0 = 0$; $\mathbf{x}_0^* = \mathbf{x}$;
- 2: Obtain auxiliary information \mathbf{I} ; obtain the refined surrogate model $f'' = \mathcal{R}(f')$, parameterized by θ'' ;
- 3: **for** $t = 0$ to $T - 1$ **do**
- 4: # Input transformation block
- 5: Get the transformed images $\mathcal{T}(\mathbf{x}_t^*)$;
- 6: # Gradient calculation block
- 7: Input $\mathcal{T}(\mathbf{x}_t^*)$ to f'' and obtain the loss $\ell = \mathcal{L}(f''(\mathcal{T}(\mathbf{x}_t^*); \theta''), y; \mathbf{I})$;
- 8: Input the loss ℓ to ∇ and calculate the gradient $\nabla_{\mathbf{x}}(\ell)$;
- 9: # Update direction calculation block
- 10: Update perturbation \mathbf{g}_{t+1} as $\mathcal{U}(\nabla_{\mathbf{x}}(\ell))$;
- 11: # Update step
- 12: Update \mathbf{x}_{t+1}^* by one update step specific to different norms:
- 13: $\ell_{\infty} : \mathbf{x}_{t+1}^* = \text{Clip}_{\mathbf{x}}^{\epsilon} \{ \mathbf{x}_t^* + \alpha \cdot \text{sign}(\mathbf{g}_{t+1}) \}$ $L_2 : \mathbf{x}_{t+1}^* = \text{Clip}_{\mathbf{x}}^{\epsilon} \left\{ \mathbf{x}_t^* + \alpha \cdot \frac{\mathbf{g}_{t+1}}{\|\mathbf{g}_{t+1}\|_2} \right\}$
- 14: **end for**
- 15: **return** $\mathbf{x}^* = \mathbf{x}_T^*$.

noises, thereby capturing the local geometries of the search directions.

- **Geometric Decision-based Attack (GeoDA)** [94] GeoDA operates under the intuition that small adversarial perturbations should be sought in directions where the decision boundary of the classifier closely approaches the data examples. By leveraging the low mean curvature of the decision boundary in the vicinity of the data examples, GeoDA effectively estimates the normal vector to the decision boundary, aiding in the search for perturbations.
- **Sign Flip Attack (SFA)** [95] SFA takes a gradient-free iterative approach to craft adversarial perturbations. In each iteration, SFA reduces the distance (usually measured using the ℓ_{∞} norm) through projection and randomly flips the signs of partial entries in the adversarial perturbation, progressively moving closer to an optimal perturbation.
- **Rays** [96] Rays tackles the problem of finding the nearest decision boundary by reformulating it as a discrete optimization problem. It directly searches among a set of ray directions generated from the solutions of the optimization problem, employing the ℓ_{∞} norm as the attack criterion.

Gradient-estimation-based methods

- **OPT** [97] OPT transforms the decision-based black-box attack into a real-valued continuous optimization problem and employs the Random Gradient-Free (RGF) method to locate the stationary point. Notably, OPT guarantees the convergence of decision-based black-box attacks, marking a significant advancement in this field.
- **Sign-OPT** [98] Sign-OPT turns to estimate the sign of the gradient instead of the gradient itself. This approach offers the advantage of requiring only a single query in each iteration.
- **HopSkipJumpAttack (HSJA)** [100] HSJA introduces a novel framework for decision-based black-box attacks. There are mainly 3 modules for attackers to implement in

each iteration. Attackers need to estimate the gradient for the next update first, search for the step size through geometric progression, and finally perform a binary search to project the point onto the decision boundary. HSJA utilizes Monte Carlo estimation to approximate the gradient, and subsequent works have proposed improved strategies for gradient estimation.

- **Query-Efficient Boundary-based black-box Attack (QEBA)** [4] QEBA proposes gradient estimation within a small representative subspace, employing techniques such as spatial transformation, discrete cosine transformation (DCT).
- **NonLinear-BA** [5] NonLinear-BA follows the overall framework of HSJA as well, and leverages popular deep generative models such as AEs, VAEs, and GANs to estimate gradients, which corresponds to the gradient estimation by Monte Carlo method in HSJA.
- **Progressive-Scale based projective Boundary Attack (PSBA)** [6] Based on the research of HSJA, QEBA, and NonLinear-BA, PSBA is proposed. PSBA also follows the attack framework of HSJA and incorporates gradient estimation strategies similar to QEBA and NonLinear-BA. It progressively searches for the optimal scale in a self-adaptive manner across spatial, frequency, and spectrum scales.
- **Triangle Attack** [99] Triangle attack breaks away from the requirement of adversarial points being restricted to the decision boundary or gradient estimation at each iteration. Triangle attack builds triangles iteratively based on the current adversarial example and learned or searched angles. It aims to find an adversarial point by utilizing geometric information in the low-frequency space generated by DCT [69].

B. Description of score-based attacks

Random search methods

- **Simple Black-box Attack (SimBA)** [7] SimBA employs a stochastic approach by randomly selecting a direction, which will be sampled from a set of orthonormal basis vectors, to perform either addition or subtraction for the perturbation at each step.
- **Parsimonious Attack** [8] Parsimonious attack introduces a novel methodology to determine the perturbation among the vertices of the ℓ_{∞} ball denoted as $\mathbb{B}_{\mathbf{x}, \epsilon}$. Consequently, this formulation gives rise to a discrete set maximization problem.
- **Square Attack** [9] Square attack also operates within the ℓ_{∞} ball $\mathbb{B}_{\mathbf{x}, \epsilon}$, exploring the perturbation among its vertices. However, in contrast to SimBA and Parsimonious attacks, the Square attack restricts its search to a randomly exemplified local patch at each step.
- **Projection & Probability-driven Black-box Attack (PPBA)** [10] PPBA pursues perturbation exploration within a low-dimensional and low-frequency subspace, which is constructed through the application of the discrete cosine transform (DCT) [69] and its inverse transform (IDCT).

- **BABIES** [17] BABIES implements ℓ_2 black-box adversarial attack in the frequency domain. BABIES leverages quadratic interpolation to approximate adversarial losses and guide perturbation updates, resulting in improved query efficiency for constraint optimization on an ℓ_2 sphere.

Gradient-estimation-based methods

- **Natural Evolution Strategy (NES)** [11] NES employs the natural evolution strategy [102] to estimate gradients by sampling perturbations from Gaussian distribution and adjust the attack direction according to the feedback from the targeted model.
- **Bandits** [12] Bandits formulates the score-based attack into a bandit optimization problem. By considering different priors, such as time-dependent and data-dependent priors, Bandits can carry over latent vectors to improve gradient estimation.
- **AdvFlow** [15] AdvFlow further expands upon the NES attack by replacing the Gaussian distribution with a complex distribution modeled by a pre-trained normalizing flow model [103].
- **Neural Process based black-box attack (NP-attack)** [16] NP-attack incorporates the structure information of the image using Neural Process(NP) [104], an efficient autoencoder method, to model a distribution over regression functions, allowing for reduced query counts and more efficient reconstruction of adversarial examples.
- **Zeroth-Order sign-based Stochastic Gradient Descent (ZO-signSGD)** [13] ZO-signSGD proposes updating the perturbations based on the idea of signSGD by incorporating zeroth-order optimization. The sign operation in ZO-signSGD can mitigate the negative effect of gradient noise.
- **SignHunter** [14] SignHunter introduces a divide-and-conquer strategy to expedite gradient sign direction estimation. Instead of sequentially flipping the gradient sign of each pixel, SignHunter performs group-wise flipping operations on specific regions of the image.

Combination-based methods

- **\mathcal{CG} -Attack** [18] \mathcal{CG} -Attack leverages the evolution strategy (ES) [105] and a Conditional Glow (c-Glow, \mathcal{CG}) model as the search distribution. By utilizing the information of a surrogate model, \mathcal{CG} -Attack learned the parameters of the c-Glow model. When attacking the target model, \mathcal{CG} -Attack refers to partial parameters learned from the c-Glow model while updating the other parameters based on feedback from the target model in the attacking process. This partial transfer mechanism addresses the issue of surrogate biases and allows for flexible adjustment of the conditional adversarial distribution (CAD) for the target model.
- **Meta Conditional Generator (MCG)** [19] MCG utilizes the information from surrogate models to boost the attack performance. MCG involves three steps: (a) fine-tuning the meta generator using inner optimization with adversarial loss function, (b) fine-tuning the surrogate model using historical information and the current task to mimic the

behavior of the target model, and (c) attacking the target black-box model using the adapted generator combined with off-the-shelf attack methods, where the generated adversarial examples are used to refine the surrogate model.

C. Description of transfer-based attacks

- **Iterative Fast Gradient Sign Method (I-FGSM)** [20] I-FGSM is the first work to optimize function5 multiple times with a small step size and iteratively update adversarial examples. Compared with the one-step attack FGSM [107], I-FGSM performs better in the white-box setting and worse in the black-box setting.

Optimization perspective

- **Projected Gradient Descent (PGD)** [21] PGD is an iterative version of FGSM [107] but starts at a random perturbation in the ℓ_p -ball at each run.
- **Momentum Iterative Fast Gradient Sign Method (MI-FGSM)** [26] To mitigate the overfitting to white-box models, MI-FGSM integrates the idea of momentum to the gradient ascent of I-FGSM to escape from poor local maxima.
- **Nesterov Iterative Fast Gradient Sign Method (NI-FGSM)** [23] Beyond the stability from MI-FGSM, NI-FGSM further leverages the looking ahead property of Nesterov Accelerated Gradient to escape from poor local maxima easier and faster.
- **Pre-gradient guided momentum Iterative Fast Gradient Sign Method (PI-FGSM)** [27] Given that the accumulated momentum in NI-FGSM does not serve as an optimal look ahead direction, PI-FGSM instead looks ahead by relying on the gradient of last iteration.
- **Variance Tuning (VT)** [28] VT tunes the gradient of the adversarial example at each iteration with the gradient variance from last iteration, thereby enhancing the stability of the update direction.
- **Reverse Adversarial Perturbation (RAP)** [29] When adversarial examples are located at a sharply local maximum, even a minor misalignment between the surrogate and the target results in a large decrease in adversarial loss. Thus, RAP encourages adversarial examples not only of high adversarial loss but also within local flat regions.
- **Linear BackPropagation (LinBP)** [30] Motivated by Goodfellow et al.'s interpretation of adversarial examples as a result of linearity of DNNs [107], LinBP enhances linearity by backpropagating the loss as if no non-linear activation function is encountered in the forward pass.
- **Skip Gradient Method (SGM)** [31] Observed that gradients flowing through skip connections are more transferable, SGM crafts adversarial examples by utilizing more gradients from skip connections rather than residual modules.

Data perspective

- **Diverse Inputs Iterative Fast Gradient Sign Method (DI2-FGSM)** [25] Inspired by applying data augmentation to prevent networks from overfitting, DI2-FGSM adds inputs transformed by random resizing and random

padding with probability p into the attack process for the sake of transferability.

- **Scale-invariant Iterative Fast Gradient Sign Method (SI-FGSM)** [23] SI-FGSM augments models via the loss-preserving input transformation, scaling, to alleviate overfitting on white-box models.
- **Admix** [24] To improve the attack transferability, admix adopts information from images in other classes by admixing two images in a master and slave manner for the gradient calculation.
- **Translation-invariant Fast Gradient Sign Method (TI-FGSM)** [22]: As adversarial examples generated against a white-box model are highly correlated with the discriminative region of the white-box model at the given input point, the transferability to models with different discriminative regions is reduced. TI-FGSM shifts images by translation operation to generate adversarial examples less sensitive to the discriminative regions of the white-box model.

Feature perspective

- **Feature Importance-aware Attack (FIA)** [33] FIA generates adversarial examples by only distorting “important” (object-related) features, where the feature importance is defined as how the features contribute to the final decision, intuitively, gradient. FIA aggregates gradients from the randomly masked input to highlight object-aware gradients and neutralize model-specific gradients.
- **Neuron Attribution-based Attack (NAA)** [34] Beyond FIA, NAA provides more accurate neuron importance measures that not only completely attribute a model’s output to each neuron but also reflect the polarity and magnitude of neuron importance.
- **Intermediate Level Attack (ILA)** [32] ILA expects to use the suboptimal perturbation found by the basic attack as a proxy and stray from it in exchange for increasing the norm. Considering increasing the norm of perturbation in image space is perceptible, FIA increases the norm in feature space.

Model perspective

- **Random Directions (RD)** [35] RD adds random directions in the weight space to a regularly trained DNN to increase its transferability. The success is sensitive to the magnitude of noise but demonstrates the feasibility of exploiting variations in the weight space.
- **Ghost Networks (GhostNet)** [36] GhostNet generates a vast number of ghost networks on the fly by imposing erosion on certain intermediate structures of the base network and performs longitudinal ensemble attack on this a huge candidate pool.
- **Distribution-Relevant Attack (DRA)** [37] The main intention is dragging the adversarial image into the target distribution to mislead classifiers to classify the image as the target class. DRA achieves this by approximating the gradient of the target class data distribution through score matching and subsequently moving the initial image towards it using Langevin Dynamics.

- **Intrinsic Adversarial Attack (IAA)** [38] Similar to DRA, IAA also boosts the alignment between adversarial attack and intrinsic attack but further replaces activation function ReLU with Softplus to make the classifier smoother and decrease the weight for certain residual modules to reduce those impact.
- **Large Geometric Vicinity (LGV)** [35] LGV collects weights in a single run along the SGD trajectory with a high constant learning rate and iteratively attacks the collected models. The high constant learning rate is key to sample much wider models with better generalization and consequently produce flatter adversarial examples same as RAP.
- **Stochastic Weight Averaging (SWA)** [39] SWA samples models in a sufficiently large vicinity via SGD with a high constant learning rate and averages the weights to move into a broader space. SWA needs to update the batch-normalization statistics of the averaged model before attacks against it.
- **Bayesian Attack** [39] To consider model diversity as well as low time complexity, Bayesian Attack models the Bayesian posterior of the surrogate model, obtaining an ensemble of infinitely many DNNs from a single run of training. Adversarial examples are subsequently generated on this Bayesian model.

Composite Attack

- BlackboxBench provides 7 composite attacks. MI-DI is the composition of MI and DI. MI-DI-TI is the composition of MI, DI and TI. MI-DI-TI-SI is the composition of MI, DI, TI, and SI. VMI is the composition of VT and MI. VNI is the composition of VT and NI. SI-RAP is the composition of SI and RAP. LGV-GhostNet is the composition of LGV and GhostNet.

APPENDIX E

DESCRIPTION OF BLACK-BOX ADVERSARIAL DEFENSES

A. Description of static defenses

Static defenses refer to defense strategies that are established during or before the training phase of the model and do not change in response to varying attacks. The most widely-used static defense method is **Adversarial Training (AT)**

- **Adversarial Training (AT)** AT is a method in machine learning designed to improve the robustness of models against adversarial examples—inputs crafted to deceive models into making mistakes. This method is particularly relevant in the field of deep learning where neural networks can be surprisingly vulnerable to slight, often imperceptible, perturbations of their inputs. During the training phase, the model is exposed not only to the original training data but also to adversarial examples. These adversarial examples are typically generated by applying small but strategically chosen perturbations to the training data, intended to mislead the model. By training on both regular and adversarial examples, the model learns to generalize better and become more resistant to adversarial manipulation.

B. Description of dynamic defenses

Dynamic defenses refer to defense strategies that can dynamically adjust in response to changes in adversarial attacks. Dynamic defense is particularly important in this field because attackers often change their attack strategies to circumvent existing defense mechanisms. Besides, dynamic defenses are often lightweight since there is no cost for training.

- **Random Noise Defense (RND) [64]** RND is to add random noise to the responses of machine learning models during the inference stage for each query, which adds uncertainty for attackers attempting to make queries. This uncertainty makes it difficult for attackers to accurately discern the model’s behavior or extract sensitive information from the model. RND also aims to find a balance between maintaining model accuracy and enhancing defense performance, which is achieved by adjusting the magnitude of the noise to ensure effective defense without overly compromising accuracy.
- **Adversarial Attack on Attackers (AAA) [108]** AAA introduces a defense mechanism to particularly counteract score-based query attacks (SQAs) on target models. The AAA approach aims to mitigate SQAs by manipulating the output logits of the model. This manipulation is designed to confuse the SQAs, leading them towards incorrect attack directions. Specifically, AAA-sine utilizes a sine function or a similar periodic function to adjust or perturb the model’s outputs (logits). This perturbation aims to confuse and mislead score-based query attacks (SQAs), making it difficult for attackers to accurately estimate how to modify inputs to create adversarial samples. AAA-line adopts linear functions or adjustments in the model’s output logits. This could apply a straightforward, possibly constant or proportional change to the logits to disrupt the attack patterns.

APPENDIX F

DESCRIPTION OF ANALYTICAL TOOLS

In this section, we provide implementation details of our analytical tools mentioned in Sec. III-C.

Attack-component effect visualization tool In BlackboxBench, we expand the scopes of the three components of the attack scenario to include values under-explored in existing literature. This strategic expansion serves a twofold purpose: from the perspective of methods, they could be tested more rigorously. From the perspective of components, their effects on attack performance could be thoroughly investigated. During the assessment of each component across its extended range, the other two components are fixed. The outcomes are graphically summarized through line charts, scatter charts, bar charts, bubble charts, and heatmaps.

Model attention visualization tool BlackboxBench visualizes model attention by means of saliency map-based interpretability methods. Saliency methods are useful tools to comprehend neural networks by assigning each input feature a score to measure its distribution. Specifically, we employ *Full-Gradient Saliency Maps* (FullGrad) [118] and *Frequency*

Saliency Map (FSM) [117] to achieve interpretability in pixel and frequency domains respectively.

FullGrad is a variant of a saliency map that not only captures the importance of each pixel but also provides that of groups of pixels, which correspond to structures. Consider a neural network function $f : \mathbb{R}^D \rightarrow \mathbb{R}$ with inputs $\mathbf{x} \in \mathbb{R}^D$. Let c_l be the channel of layer l in a neural network. Let $\psi(\cdot)$ be the post-processing operations. The FullGrad saliency map is given by

$$S_f(\mathbf{x}) = \psi(\nabla_{\mathbf{x}}f(\mathbf{x}) \odot \mathbf{x}) + \sum_{l \in L} \sum_{c \in c_l} \psi(f^b(\mathbf{x})_c), \quad (8)$$

where $\nabla_{\mathbf{x}}f(\mathbf{x})$ is the input-gradient, $f^b(\mathbf{x})$, short-hand notation for $\nabla_b f(\mathbf{x}, \mathbf{b}) \odot \mathbf{b}$, is the bias-gradient. Together, they constitute full-gradients.

FSM further measures the importance of each frequency feature. Consider a neural network function $f : \mathbb{R}^{H \times W \times C} \rightarrow \mathbb{R}$ with inputs $\mathbf{x} \in \mathbb{R}^{H \times W \times C}$. Let \mathcal{F} be the the channel-wise Discrete Fourier Transform (DFT) and \mathcal{F}^{-1} be the Inverse Discrete Fourier Transform (IDFT). We define the frequency counterpart of f , which is the classifier for spectrum $\tilde{\mathbf{x}} = \mathcal{F}(\mathbf{x})$, as follows:

$$F(\tilde{\mathbf{x}}) = f(\mathbf{x}) = f(\mathcal{F}^{-1}(\tilde{\mathbf{x}})). \quad (9)$$

Inspired by the saliency map in the pixel domain, FSM is given by

$$\begin{aligned} S_F(\tilde{\mathbf{x}}) &= \frac{\partial F(\tilde{\mathbf{x}})}{\partial \tilde{\mathbf{x}}(u, v, c)} \\ &= \sum_{c=1}^C \sum_{h=0}^{H-1} \sum_{w=0}^{W-1} \sum_{c'=0}^C \frac{\partial f(\mathbf{x})}{\partial \mathbf{x}(h, w, c')} \cdot \frac{\partial \mathbf{x}(h, w, c')}{\partial \tilde{\mathbf{x}}(u, v, c)} \\ &= \sum_{c=1}^C \sum_{h=0}^{H-1} \sum_{w=0}^{W-1} \frac{\partial f_s(\mathbf{x})}{\partial \mathbf{x}(h, w, c)} e^{2\pi i(\frac{uh}{H} + \frac{vw}{W})}. \end{aligned} \quad (10)$$

As we can see, FSM is exactly the DFT of the model gradient.

Adversarial divergence measurement tool When harnessing adversarial transferability from transfer-based attacks, the performance is notably destroyed by the misalignment between surrogate model f_s with parameter θ_s and target models f_t with parameter θ_t . To properly measure this misalignment, we consider conditional adversarial distribution (CAD), denoted as $\mathcal{P}(\delta_{\mathbf{x}}|\mathbf{x}, \theta)$. As CAD models the distribution of perturbations $\delta_{\mathbf{x}}$ conditioned on clean examples \mathbf{x} for each model with parameter θ , minimal divergence between CADs ensures a high transferability between models. The rationale behind is that if $\mathcal{P}(\delta_{\mathbf{x}}|\mathbf{x}, \theta_s)$ and $\mathcal{P}(\delta_{\mathbf{x}}|\mathbf{x}, \theta_t)$ yield similar probabilities for perturbation $\delta_{\mathbf{x}}$, then the perturbation crafted by f_s can effectively substitute the authentic perturbation crafted by f_t , thus misleading f_t . Building on this premise, BlackboxBench quantifies this divergence between $\mathcal{P}(\delta_{\mathbf{x}}|\mathbf{x}, \theta_t)$ and $\mathcal{P}(\delta_{\mathbf{x}}|\mathbf{x}, \theta_s)$ as Adversarial Divergence (AD):

$$\text{AD} = 1 - \frac{1}{\log_2 \left[\mathbb{E}_{\mathcal{P}(\delta_{\mathbf{x}}|\mathbf{x}, \theta_s)} \left[\log \frac{\mathcal{P}(\delta_{\mathbf{x}}|\mathbf{x}, \theta_s)}{\mathcal{P}(\delta_{\mathbf{x}}|\mathbf{x}, \theta_t)} \right] \right]}, \quad (11)$$

where $\left[\mathbb{E}_{\mathcal{P}(\delta_{\mathbf{x}}|\mathbf{x}, \theta_s)} \left[\log \frac{\mathcal{P}(\delta_{\mathbf{x}}|\mathbf{x}, \theta_s)}{\mathcal{P}(\delta_{\mathbf{x}}|\mathbf{x}, \theta_t)} \right] \right]$ denotes the KL divergence between $\mathcal{P}(\delta_{\mathbf{x}}|\mathbf{x}, \theta_t)$ and $\mathcal{P}(\delta_{\mathbf{x}}|\mathbf{x}, \theta_s)$. Adversarial

Divergence normalizes the KL divergence to be bounded within $[0, 1]$.

Following [18], we learned the conditional generative flow model (c-Glow) for each classifier f to approximate its CAD. The training details can be found in the supplementary materials in [18]. With two CADs, we compute the KL divergence between them as follows:

- 1) *Sampling*: Sample a set of values $\{\delta_x^{(i)}\}$ from the distribution $\mathcal{P}(\delta_x | \mathbf{x}, \theta_s)$.
- 2) *Compute the Log Ratio for Each Sample*: For each sampled $\delta_x^{(i)}$, compute:

$$\log \frac{\mathcal{P}(\delta_x^{(i)} | \mathbf{x}, \theta_s)}{\mathcal{P}(\delta_x^{(i)} | \mathbf{x}, \theta_t)}. \quad (12)$$

- 3) *Average Over Samples*: Compute the average of the computed log ratios:

$$\begin{aligned} & \left[\mathbb{E}_{\mathcal{P}(\delta_x | \mathbf{x}, \theta_s)} \left[\log \frac{\mathcal{P}(\delta_x | \mathbf{x}, \theta_s)}{\mathcal{P}(\delta_x | \mathbf{x}, \theta_t)} \right] \right] \\ & \approx \frac{1}{N} \sum_{i=1}^N \log \frac{\mathcal{P}(\delta_x^{(i)} | \mathbf{x}, \theta_s)}{\mathcal{P}(\delta_x^{(i)} | \mathbf{x}, \theta_t)} \end{aligned}, \quad (13)$$

where N is the number of samples. Note that The accuracy of this approximation depends on the number of samples. We randomly sampled 100,000 examples in our evaluation. More samples generally provide a better approximation to the true expectation.

A lower metric value indicates a lower divergence between models. With this metric, misalignment can be quantified, negative transfer can be understood, and more effective attack strategies can be devised.

Decision boundary visualization tool Decision Surface [120] measures the network’s loss variations concerning the input perturbations and contains the explicit decision boundary, naturally aligning with our analytical requirements of measuring the distance between the benign images and decision boundary.

Let $F(\cdot)$ be the loss function. To visualize the loss $F(x)$ w.r.t the high-dimensional inputs in a 2D hyper-plane, Decision Surface [120] selects two normalized basis vectors for $x - y$ hyper-plane and interpolates the start point o with them, then the loss is calculated as :

$$V(i, j, \alpha, \beta) = F(o + i \cdot \alpha + j \cdot \beta). \quad (14)$$

For our purpose of assessing the network’s loss variations w.r.t perturbations, α represents an attack-specific perturbation direction, β stands for a random direction vector, and o denotes the benign image. The variables i and j quantify the degree of deviation from point o along the α and β directions, respectively.

Regarding the form the loss function $F(\cdot)$, [120] replaces the cross-entropy loss with a novel decision surface:

$$S(x) = Z(x)_t - \max \{Z(x)_i, i \neq t\}. \quad (15)$$

Here, $Z(x)_t$ is the logit output w.r.t the ground truth label t . For correct predictions, $S(x) > 0$, while for incorrect ones, $S(x) < 0$. The contour where $S(x) = 0$ indicates an explicit decision boundary, which significantly aids our goal of visualizing the proximity of benign images to this boundary.

As shown in Fig. 10, with the loss for clean images serving as the central point, the decision surface show the loss variation w.r.t the perturbation density (shown in x-axis) and the noise density along (shown in y-axis). Evidently, it requires a shorter distance to traverse the decision boundary in the adversarial direction compared to the random direction. This observation indicates that adversarial attacks can identify directions toward the decision boundary within the immediate vicinity of clean images.

BlackboxBench also utilizes dbViz [121] to visualize the decision boundaries of various DNN models. The authors propose plotting decision boundaries on the convex hull between data samples. This proposed method is simple, controllable, and capable of capturing significant portions of the decision space that are close to the data manifold. The following are some key mathematical concepts and formulas:

- 1) *Plotting Decision Boundaries*: To plot decision boundaries, dbViz first defines a plane spanned by three randomly chosen image samples x_1, x_2, x_3 and then constructs two vectors $\tilde{v}_1 = x_2 - x_1$ and $\tilde{v}_2 = x_3 - x_1$, which defines a plane. The decision boundaries are then plotted on this plane.
- 2) *Sampling Points on the Plane*: To plot the decision boundaries on this plane, it is necessary to sample inputs to the network. The coordinates of the sampling points can be expressed as $\beta \tilde{v}_1 + \phi(\tilde{v}_2 - \text{proj}_{\tilde{v}_1} \tilde{v}_2)$, where $0 \leq \beta, \phi \leq 1$, and $\text{proj}_{\tilde{v}_1} \tilde{v}_2$ is the projection of \tilde{v}_2 onto \tilde{v}_1 .
- 3) *Proof of Off-Manifold Behavior*: dbViz also mentions a lemma (Lemma 2.1) about off-manifold behavior. This lemma suggests that any neural network that varies smoothly as a function of its input will have nearly constant outputs over most of the input space. The mathematical statement of this lemma is: Let $f : [0, 1]^n \rightarrow [0, 1]$ be a neural network satisfying $|f(x) - f(y)| \leq L\|x - y\|$, where L is a constant. Then, for a uniformly random image x in the unit hypercube, the probability that $|f(x) - \tilde{f}| \leq t$ is at least $1 - Le^{-\frac{2nt^2}{L^2}}$, where \tilde{f} is the median value of f on the unit hypercube.

These mathematical methods and formulas above conduct a detailed analysis of decision boundaries under different neural network architectures and training conditions. Through this approach, they are able to gain a deeper understanding and explanation of model behavior, especially in terms of the formation and changes of decision boundaries. More details can be found in [121].

APPENDIX G

ADDITIONAL EVALUATION RESULTS

A. Intra/Cross-family transferability

In Sec. IV-E, we explore the transferability between models from four families employing two mechanisms. With the help of DI-FGSM [25] and RAP [29] to generate adversarial examples, we observed a strong intra-family transferability as well as a heterogeneous cross-family transferability which is demonstrated to be irrelevant to involved mechanisms but the distance between models. Here we provide the transferability

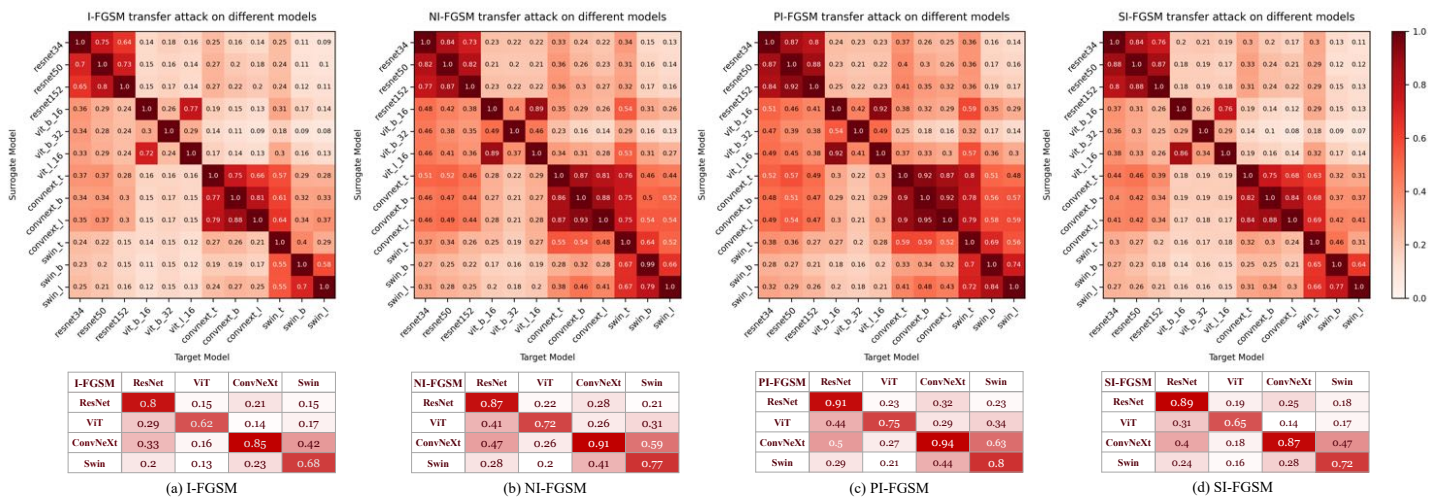


Fig. 22. Matrices of ASR in (a) I-FGSM [20], (b) NI-FGSM [23], (c) PI-FGSM [27] and (d) SI-FGSM [23] attacks, where each entry correspond to a surrogate-target pair. The y-axis represents surrogate models and the x-axis represents target models. We choose three variants in every model family for our evaluations. Matrices in the second row summarizes the first row by averaging ASR *w.r.t.* family.

matrices from more methods to confirm our findings. In Fig. 22, we can observe a similar phenomenon as in Fig. 13.

B. Intra/Cross-training-strategy transferability

In Fig. 23, we expand the set of adversarial example generation candidates for evaluating intra/cross-training-strategy transferability, as discussed in Sec. IV-G, to include NI-FGSM [23], PI-FGSM [27], VT [28], and SI-FGSM [23]. A similar phenomenon is observed: all target models are found more vulnerable to intra-training-strategy transferability—misclassification of examples generated by surrogate models using the same training strategy.

REFERENCES

- [1] H. Salman, A. Ilyas, L. Engstrom, A. Kapoor, and A. Madry, “Do adversarially robust imagenet models transfer better?” in *Advances in Neural Information Processing Systems*, 2020.
- [2] S. Goyal, C. Qin, J. Uesato, T. Mann, and P. Kohli, “Uncovering the limits of adversarial training against norm-bounded adversarial examples,” *arXiv e-prints*, 2020.
- [3] S. Goyal, S.-A. Rebuffi, O. Wiles, F. Stimberg, D. A. Calian, and T. A. Mann, “Improving robustness using generated data,” in *Advances in Neural Information Processing Systems*, 2021.
- [4] H. Li, X. Xu, X. Zhang, S. Yang, and B. Li, “Qeba: Query-efficient boundary-based blackbox attack,” in *Conference on Computer Vision and Pattern Recognition*, 2020.
- [5] H. Li, L. Li, X. Xu, X. Zhang, S. Yang, and B. Li, “Nonlinear projection based gradient estimation for query efficient blackbox attacks,” in *International conference on artificial intelligence and statistics*, 2021.
- [6] J. Zhang, L. Li, H. Li, X. Zhang, S. Yang, and B. Li, “Progressive-scale boundary blackbox attack via projective gradient estimation,” in *International Conference on Machine Learning*, 2021.
- [7] C. Guo, J. Gardner, Y. You, A. G. Wilson, and K. Weinberger, “Simple black-box adversarial attacks,” in *International Conference on Machine Learning*, 2019.
- [8] S. Moon, G. An, and H. O. Song, “Parsimonious black-box adversarial attacks via efficient combinatorial optimization,” in *International Conference on Machine Learning*, 2019.
- [9] M. Andriushchenko, F. Croce, N. Flammarion, and M. Hein, “Square attack: a query-efficient black-box adversarial attack via random search,” in *European Conference on Computer Vision*, 2020.
- [10] J. Li, R. Ji, H. Liu, J. Liu, B. Zhong, C. Deng, and Q. Tian, “Projection & probability-driven black-box attack,” in *Conference on Computer Vision and Pattern Recognition*, 2020.
- [11] A. Ilyas, L. Engstrom, A. Athalye, and J. Lin, “Black-box adversarial attacks with limited queries and information,” in *International Conference on Machine Learning*, 2018.
- [12] A. Ilyas, L. Engstrom, and A. Madry, “Prior convictions: Black-box adversarial attacks with bandits and priors,” *arXiv e-prints*, 2018.
- [13] S. Liu, P.-Y. Chen, X. Chen, and M. Hong, “signsgd via zeroth-order oracle,” in *International Conference on Learning Representations*, 2019.
- [14] A. Al-Dujaili and U.-M. O’Reilly, “Sign bits are all you need for black-box attacks,” in *International Conference on Learning Representations*, 2020.
- [15] H. Mohaghegh Dolatabadi, S. Erfani, and C. Leckie, “Advflow: Inconspicuous black-box adversarial attacks using normalizing flows,” in *Advances in Neural Information Processing Systems*, 2020.
- [16] Y. Bai, Y. Zeng, Y. Jiang, Y. Wang, S.-T. Xia, and W. Guo, “Improving query efficiency of black-box adversarial attack,” in *European Conference on Computer Vision*, 2020.

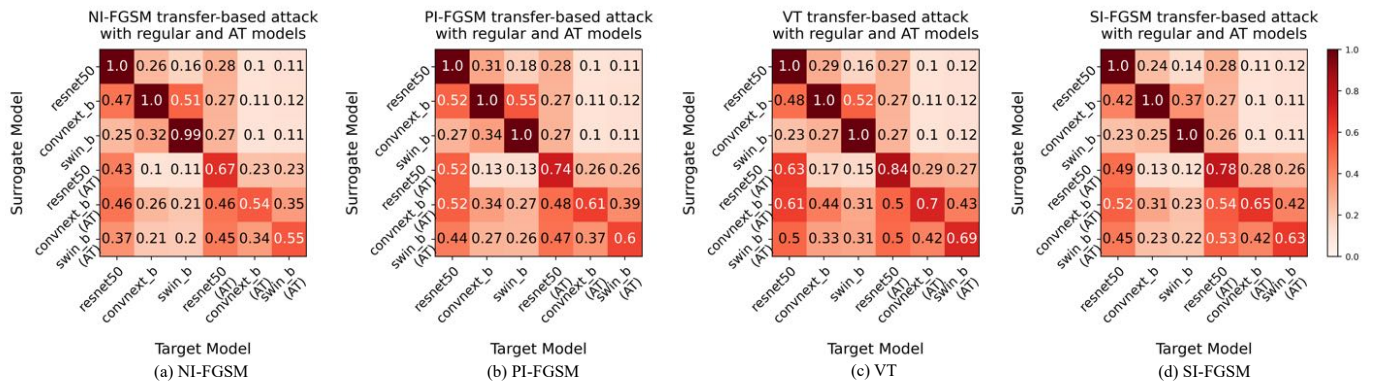


Fig. 23. The matrices representing the ASR for (a) NI-FGSM [23], (b) PI-FGSM [27], (c) VT [28], (d) SI-FGSM [23] attacks, with each entry corresponding to a surrogate-target pair. The y-axis and x-axis represent surrogate models and target models, respectively. We employ the regular and AT versions of three model architectures for our evaluations.

- [17] H. Tran, D. Lu, and G. Zhang, “Exploiting the local parabolic landscapes of adversarial losses to accelerate black-box adversarial attack,” in *European Conference on Computer Vision*, 2022.
- [18] Y. Feng, B. Wu, Y. Fan, L. Liu, Z. Li, and S.-T. Xia, “Boosting black-box attack with partially transferred conditional adversarial distribution,” in *Conference on Computer Vision and Pattern Recognition*, 2022.
- [19] F. Yin, Y. Zhang, B. Wu, Y. Feng, J. Zhang, Y. Fan, and Y. Yang, “Generalizable black-box adversarial attack with meta learning,” *Transactions on Pattern Analysis and Machine Intelligence*, 2023.
- [20] A. Kurakin, I. Goodfellow, and S. Bengio, “Adversarial examples in the physical world,” 2017.
- [21] A. Madry, A. Makelov, L. Schmidt, D. Tsipras, and A. Vladu, “Towards deep learning models resistant to adversarial attacks,” in *International Conference on Learning Representations*, 2018.
- [22] Y. Dong, T. Pang, H. Su, and J. Zhu, “Evading defenses to transferable adversarial examples by translation-invariant attacks,” in *Conference on Computer Vision and Pattern Recognition*, 2019.
- [23] J. Lin, C. Song, K. He, L. Wang, and J. E. Hopcroft, “Nesterov accelerated gradient and scale invariance for adversarial attacks,” in *International Conference on Learning Representations*, 2019.
- [24] X. Wang, X. He, J. Wang, and K. He, “Admix: Enhancing the transferability of adversarial attacks,” in *International Conference on Computer Vision*, 2021.
- [25] C. Xie, Z. Zhang, Y. Zhou, S. Bai, J. Wang, Z. Ren, and A. L. Yuille, “Improving transferability of adversarial examples with input diversity,” in *Conference on Computer Vision and Pattern Recognition*, 2019.
- [26] Y. Dong, F. Liao, T. Pang, H. Su, J. Zhu, X. Hu, and J. Li, “Boosting adversarial attacks with momentum,” in *Conference on Computer Vision and Pattern Recognition*, 2018.
- [27] X. Wang, J. Lin, H. Hu, J. Wang, and K. He, “Boosting adversarial transferability through enhanced momentum,” *arXiv e-prints*, 2021.
- [28] X. Wang and K. He, “Enhancing the transferability of adversarial attacks through variance tuning,” in *Conference on Computer Vision and Pattern Recognition*, 2021.
- [29] Z. Qin, Y. Fan, Y. Liu, L. Shen, Y. Zhang, J. Wang, and B. Wu, “Boosting the transferability of adversarial attacks with reverse adversarial perturbation,” in *Advances in Neural Information Processing Systems*, 2022.
- [30] Y. Guo, Q. Li, and H. Chen, “Backpropagating linearly improves transferability of adversarial examples,” in *Advances in Neural Information Processing Systems*, 2020.
- [31] D. Wu, Y. Wang, S.-T. Xia, J. Bailey, and X. Ma, “Skip connections matter: On the transferability of adversarial examples generated with resnets,” in *International Conference on Learning Representations*, 2019.
- [32] Q. Huang, I. Katsman, H. He, Z. Gu, S. Belongie, and S.-N. Lim, “Enhancing adversarial example transferability with an intermediate level attack,” in *International Conference on Computer Vision*, 2019.
- [33] Z. Wang, H. Guo, Z. Zhang, W. Liu, Z. Qin, and K. Ren, “Feature importance-aware transferable adversarial attacks,” in *International Conference on Computer Vision*, 2021.
- [34] J. Zhang, W. Wu, J.-t. Huang, Y. Huang, W. Wang, Y. Su, and M. R. Lyu, “Improving adversarial transferability via neuron attribution-based attacks,” in *Conference on Computer Vision and Pattern Recognition*, 2022.
- [35] M. Gubri, M. Cordy, M. Papadakis, Y. L. Traon, and K. Sen, “Lgv: Boosting adversarial example transferability from large geometric vicinity,” in *European Conference on Computer Vision*, 2022.
- [36] Y. Li, S. Bai, Y. Zhou, C. Xie, Z. Zhang, and A. Yuille, “Learning transferable adversarial examples via ghost networks,” in *Association for the Advancement of Artificial Intelligence*, 2020.
- [37] Y. Zhu, Y. Chen, X. Li, K. Chen, Y. He, X. Tian, B. Zheng, Y. Chen, and Q. Huang, “Toward understanding and boosting adversarial transferability from a distribution perspective,” *Transactions on Image Processing*, vol. 31, pp. 6487–6501, 2022.
- [38] Y. Zhu, J. Sun, and Z. Li, “Rethinking adversarial transferability from a data distribution perspective,” in *International Conference on Learning Representations*, 2022.
- [39] Q. Li, Y. Guo, W. Zuo, and H. Chen, “Making substitute models more bayesian can enhance transferability of adversarial examples,” in *International Conference on Learning Representations*, 2023.
- [40] A. Krizhevsky, “Learning multiple layers of features from tiny images,” *University of Toronto*, 2009.
- [41] O. Russakovsky, J. Deng, H. Su, J. Krause, S. Satheesh, S. Ma, Z. Huang, A. Karpathy, A. Khosla, M. Bernstein *et al.*, “Imagenet large scale visual recognition challenge,” *International Journal of Computer Vision*, vol. 115, pp. 211–252, 2015.
- [42] F. Croce, M. Andriushchenko, V. Schwag, E. Debenedetti, N. Flammarion, M. Chiang, P. Mittal, and M. Hein, “Robustbench: a standardized adversarial robustness benchmark,” in *Conference on Neural Information Processing Systems Datasets and Benchmarks Track*, 2021.
- [43] K. He, X. Zhang, S. Ren, and J. Sun, “Deep residual learning for image recognition,” in *Conference on Computer Vision and Pattern Recognition*, 2016.
- [44] K. Simonyan and A. Zisserman, “Very deep convolutional networks for large-scale image recognition,” in *International Conference on Learning Representations*, 2015.
- [45] C. Szegedy, V. Vanhoucke, S. Ioffe, J. Shlens, and Z. Wojna, “Rethinking the inception architecture for computer vision,” in *Conference on Computer Vision and Pattern Recognition*, 2016.
- [46] G. Huang, Z. Liu, L. Van Der Maaten, and K. Q. Weinberger, “Densely connected convolutional networks,” in *Conference on Computer Vision and Pattern Recognition*, 2017.
- [47] M. Sandler, A. Howard, M. Zhu, A. Zhmoginov, and L.-C. Chen, “Mobilenetv2: Inverted residuals and linear bottlenecks,” in *Conference on Computer Vision and Pattern Recognition*, 2018.
- [48] J. Hu, L. Shen, and G. Sun, “Squeeze-and-excitation networks,” in *Conference on Computer Vision and Pattern Recognition*, 2018.
- [49] S. Xie, R. Girshick, P. Dollár, Z. Tu, and K. He, “Aggregated residual transformations for deep neural networks,” in *Conference on Computer Vision and Pattern Recognition*, 2017.
- [50] S. Zagoruyko and N. Komodakis, “Wide residual networks,” in *British Machine Vision Conference 2016*, 2016.
- [51] C. Liu, B. Zoph, M. Neumann, J. Shlens, W. Hua, L.-J. Li, L. Fei-Fei, A. Yuille, J. Huang, and K. Murphy, “Progressive neural architecture search,” in *European Conference on Computer Vision*, 2018.
- [52] M. Tan, B. Chen, R. Pang, V. Vasudevan, M. Sandler, A. Howard, and Q. V. Le, “Mnasnet: Platform-aware neural architecture search for mobile,” in *Conference on Computer Vision and Pattern Recognition*, 2019.

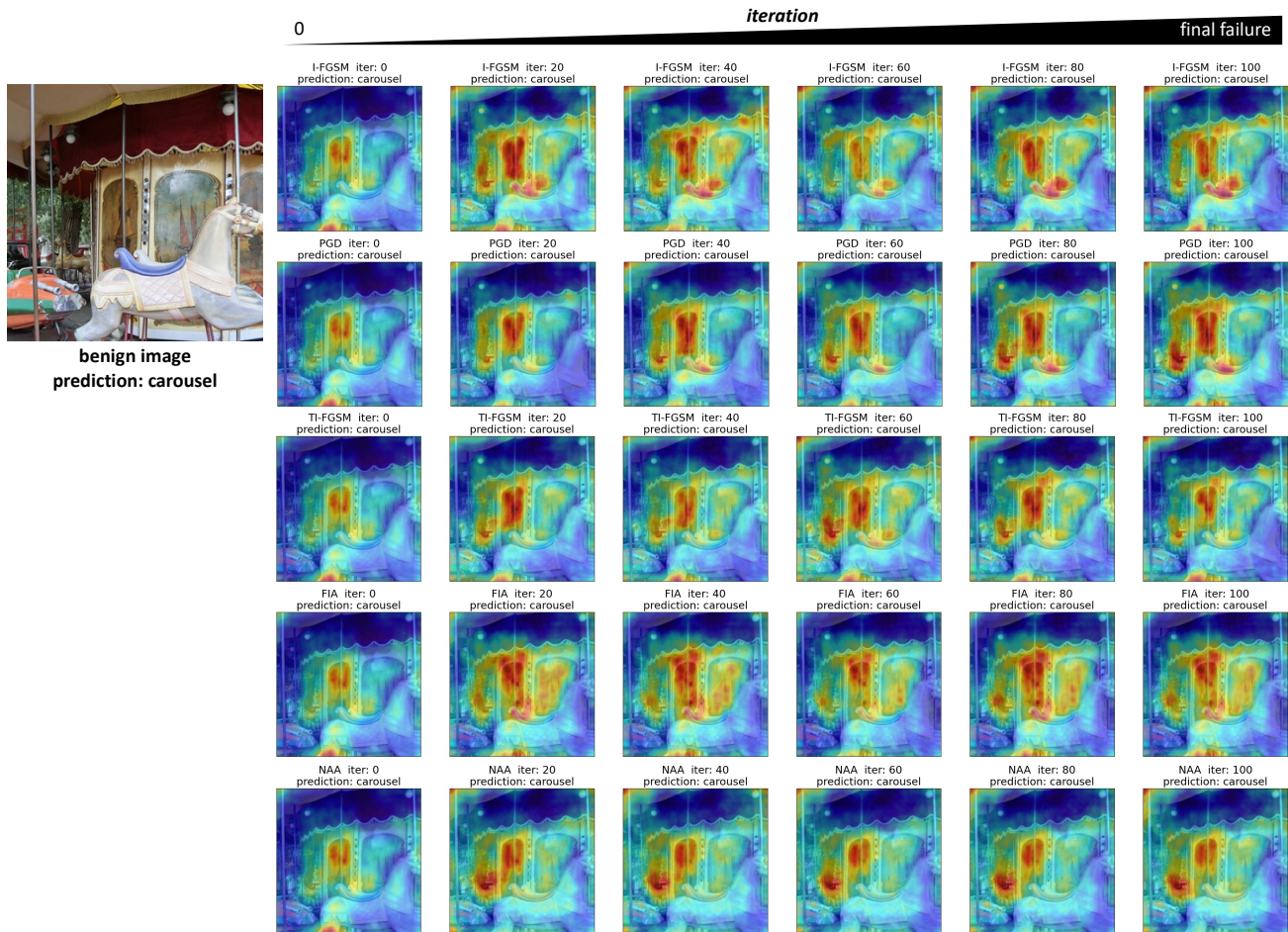


Fig. 24. The benign image from the category of carousel (**first up**), and the attention maps on its perturbed counterparts generated by failed transfer-based attacks (**others**). Each row plots the evolution of adversarial images crafted by a certain attack. For these failed attacks, we plot the adversarial images at regular intervals between the first iteration and the final iteration. The title of each image indicates the method, current iteration number and target model prediction. It's observed that when attacks fail, the discriminative regions remain unchanged.

- [53] D. Han, J. Kim, and J. Kim, "Deep pyramidal residual networks," in *Conference on Computer Vision and Pattern Recognition*, 2017.
- [54] X. Dong and Y. Yang, "Searching for a robust neural architecture in four gpu hours," in *Conference on Computer Vision and Pattern Recognition*, 2019.
- [55] A. Dosovitskiy, L. Beyer, A. Kolesnikov, D. Weissenborn, X. Zhai, T. Unterthiner, M. Dehghani, M. Minderer, G. Heigold, S. Gelly *et al.*, "An image is worth 16x16 words: Transformers for image recognition at scale," in *International Conference on Learning Representations*, 2020.
- [56] Z. Liu, Y. Lin, Y. Cao, H. Hu, Y. Wei, Z. Zhang, S. Lin, and B. Guo, "Swin transformer: Hierarchical vision transformer using shifted windows," in *International Conference on Computer Vision*, 2021.
- [57] Z. Liu, H. Mao, C.-Y. Wu, C. Feichtenhofer, T. Darrell, and S. Xie, "A convnet for the 2020s," in *Conference on Computer Vision and Pattern Recognition*, 2022.
- [58] H. Salman, A. Ilyas, L. Engstrom, A. Kapoor, and A. Madry, "Do adversarially robust imagenet models transfer better?" in *Advances in Neural Information Processing Systems*, 2020.
- [59] C. Liu, Y. Dong, W. Xiang, X. Yang, H. Su, J. Zhu, Y. Chen, Y. He, H. Xue, and S. Zheng, "A comprehensive study on robustness of image classification models: Benchmarking and rethinking," *arXiv e-prints*, 2023.
- [60] Y. Carmon, A. Raghunathan, L. Schmidt, J. C. Duchi, and P. S. Liang, "Unlabeled data improves adversarial robustness," in *Advances in Neural Information Processing Systems*, 2019.
- [61] Y. Yamada, M. Iwamura, T. Akiba, and K. Kise, "Shakedrop regularization for deep residual learning," *IEEE Access*, vol. 7, pp. 186 126–186 136, 2019.
- [62] E. D. Cubuk, B. Zoph, D. Mane, V. Vasudevan, and Q. V. Le, "Autoaugment: Learning augmentation policies from data," *arXiv e-prints*, 2018.
- [63] K. Mahmood, R. Mahmood, and M. Van Dijk, "On the robustness of vision transformers to adversarial examples," in *International Conference on Computer Vision*, 2021.
- [64] Z. Qin, Y. Fan, H. Zha, and B. Wu, "Random noise defense against query-based black-box attacks," in *Advances in Neural Information Processing Systems*, 2021.
- [65] S.-A. Rebuffi, S. Gowal, D. A. Calian, F. Stimberg, O. Wiles, and T. Mann, "Fixing data augmentation to improve adversarial robustness," *arXiv e-prints*, 2021.
- [66] N. Papernot, P. McDaniel, and I. Goodfellow, "Transferability in machine learning: from phenomena to black-box attacks using adversarial samples," *arXiv e-prints*, 2016.
- [67] Z. Zhao, Z. Liu, and M. Larson, "On success and simplicity: A second look at transferable targeted attacks," in *Advances in Neural Information Processing Systems*, 2021.
- [68] H. Abdi and L. J. Williams, "Principal component analysis," *Wiley interdisciplinary reviews: computational statistics*, 2010.
- [69] N. Ahmed, T. Natarajan, and K. R. Rao, "Discrete cosine transform," *IEEE transactions on Computers*, 1974.
- [70] N. Carlini, A. Athalye, N. Papernot, W. Brendel, J. Rauber, D. Tsipras, I. Goodfellow, A. Madry, and A. Kurakin, "On evaluating adversarial robustness," *arXiv e-prints*, 2019.
- [71] F. Croce and M. Hein, "Reliable evaluation of adversarial robustness with an ensemble of diverse parameter-free attacks," in *International Conference on Machine Learning*, 2020.
- [72] D. Hendrycks and T. Dietterich, "Benchmarking neural network robustness to common corruptions and perturbations," *arXiv e-prints*, 2019.
- [73] G. Katz, C. Barrett, D. L. Dill, K. Julian, and M. J. Kochenderfer,

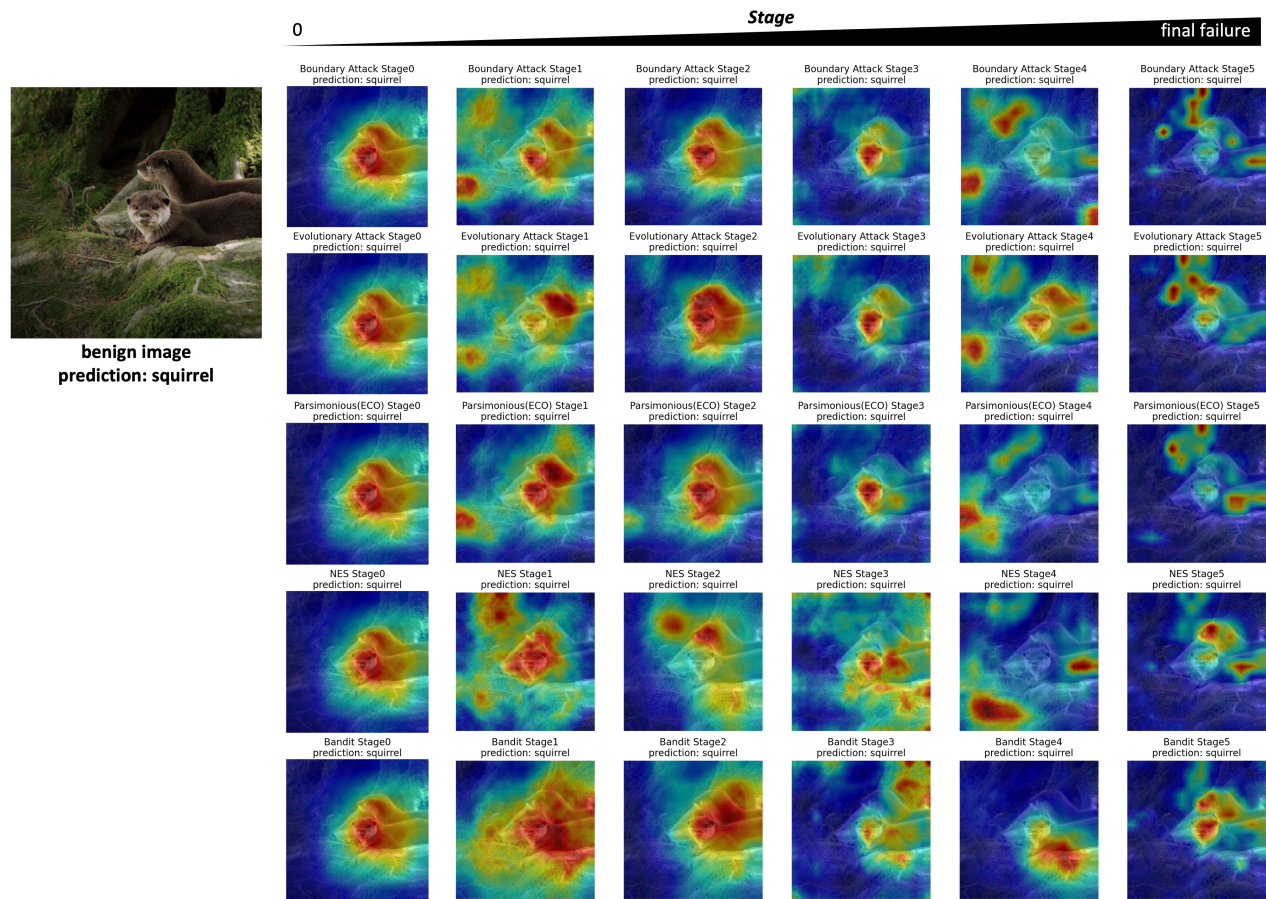


Fig. 25. The benign image from the category of squirrel (**first up**), and the attention maps on its perturbed counterparts generated by failed decision-based attacks (**the first 2 rows**) and failed score-based attacks (**the following 3 rows**). Each row plots the evolution of adversarial images crafted by a certain attack. For these failed attacks, we plot the adversarial images at each stage, where we divide the entire attack process into 6 stages (from the beginning to the end, no matter fails or succeeds). The title of each image indicates the method, current stage period, and target model prediction. It's observed that when attacks fail, the prediction label provided by the target model remains unchanged.

- “Reluplex: An efficient smt solver for verifying deep neural networks,” in *International Conference on Computer Aided Verification*, 2017.
- [74] L. Engstrom, A. Ilyas, and A. Athalye, “Evaluating and understanding the robustness of adversarial logit pairing,” *arXiv e-prints*, 2018.
- [75] A. Athalye, N. Carlini, and D. Wagner, “Obfuscated gradients give a false sense of security: Circumventing defenses to adversarial examples,” in *International Conference on Machine Learning*, 2018.
- [76] C. Szegedy, W. Zaremba, I. Sutskever, J. Bruna, D. Erhan, I. Goodfellow, and R. Fergus, “Intriguing properties of neural networks,” *arXiv e-prints*, 2013.
- [77] J. Gilmer, R. P. Adams, I. Goodfellow, D. Andersen, and G. E. Dahl, “Motivating the rules of the game for adversarial example research,” *arXiv e-prints*, 2018.
- [78] A. Fawzi and P. Frossard, “Manitest: Are classifiers really invariant?” *arXiv e-prints*, 2015.
- [79] E. Wong, F. Schmidt, and Z. Kolter, “Wasserstein adversarial examples via projected sinkhorn iterations,” in *International Conference on Machine Learning*, 2019.
- [80] C. Laidlaw and S. Feizi, “Functional adversarial attacks,” in *Advances in Neural Information Processing Systems*, 2019.
- [81] J. Rauber, W. Brendel, and M. Bethge, “Foolbox: A python toolbox to benchmark the robustness of machine learning models,” *arXiv e-prints*, 2017.
- [82] N. Papernot, F. Faghri, N. Carlini, I. Goodfellow, R. Feinman, A. Kurakin, C. Xie, Y. Sharma, T. Brown, A. Roy *et al.*, “Technical report on the clevehans v2. 1.0 adversarial examples library,” *arXiv e-prints*, 2016.
- [83] G. W. Ding, L. Wang, and X. Jin, “Advertorch v0. 1: An adversarial robustness toolbox based on pytorch,” *arXiv e-prints*, 2019.
- [84] D. Goodman, H. Xin, W. Yang, W. Yuesheng, X. Junfeng, and Z. Huan, “Advbox: a toolbox to generate adversarial examples that fool neural networks,” *arXiv e-prints*, 2020.
- [85] M.-I. Nicolae, M. Sinn, M. N. Tran, B. Buesser, A. Rawat, M. Wistuba, V. Zantedeschi, N. Baracaldo, B. Chen, H. Ludwig *et al.*, “Adversarial robustness toolbox v1. 0.0,” *arXiv e-prints*, 2018.
- [86] M. Pintor, L. Demetrio, A. Sotgiu, M. Melis, A. Demontis, and B. Biggio, “secml: A python library for secure and explainable machine learning,” *arXiv e-prints*, 2019.
- [87] Y. Li, W. Jin, H. Xu, and J. Tang, “Deeprobust: A pytorch library for adversarial attacks and defenses,” *arXiv e-prints*, 2020.
- [88] A. Mađry, A. Athalye, D. Tsipras, and L. Engstrom, “Robustml,” <https://www.robust-ml.org/>, 2019.
- [89] A. Mađry, A. Makelov, L. Schmidt, D. Tsipras, and A. Vladu, “Towards deep learning models resistant to adversarial attacks,” *arXiv e-prints*, 2017.
- [90] H. Zhang, Y. Yu, J. Jiao, E. Xing, L. El Ghaoui, and M. Jordan, “Theoretically principled trade-off between robustness and accuracy,” in *International Conference on Machine Learning*, 2019.
- [91] E. Wong, L. Rice, and J. Z. Kolter, “Fast is better than free: Revisiting adversarial training,” *arXiv e-prints*, 2020.
- [92] W. Brendel, J. Rauber, and M. Bethge, “Decision-based adversarial attacks: Reliable attacks against black-box machine learning models,” *arXiv e-prints*, 2017.
- [93] Y. Dong, H. Su, B. Wu, Z. Li, W. Liu, T. Zhang, and J. Zhu, “Efficient decision-based black-box adversarial attacks on face recognition,” in *Conference on Computer Vision and Pattern Recognition*, 2019.
- [94] A. Rahmati, S.-M. Moosavi-Dezfooli, P. Frossard, and H. Dai, “Geoda: a geometric framework for black-box adversarial attacks,” in *Conference on Computer Vision and Pattern Recognition*, 2020.
- [95] W. Chen, Z. Zhang, X. Hu, and B. Wu, “Boosting decision-based black-

TABLE IV
HYPER-PARAMETERS OF DECISION-BASED ATTACKS.

Decision-based attacks	Hyperparameters	L_inf, untargeted attack		L_2, untargeted attack		L_inf, targeted attack		L_2, targeted attack	
		ImageNet	CIFAR-10	ImageNet	CIFAR-10	ImageNet	CIFAR-10	ImageNet	CIFAR-10
General hyperparameters	maximum perturbation	0.05	0.05	5	1	0.05	0.05	5	1
	maximum queries	10000	10000	10000	10000	100000	100000	100000	100000
	batch size	1	1	1	1	1	1	1	1
Boundary Attack [92]	steps	25000	25000	25000	25000	25000	25000	25000	25000
	spherical_step	0.01	0.01	0.01	0.01	0.01	0.01	0.01	0.01
	source_step	0.01	0.01	0.01	0.01	0.01	0.01	0.01	0.01
	source_step_convergence	1e-7	1e-7	1e-7	1e-7	1e-7	1e-7	1e-7	1e-7
	step_adaptation	1.5	1.5	1.5	1.5	1.5	1.5	1.5	1.5
	update_stats_every_k	10	10	10	10	10	10	10	10
Evolutionray Attack [93]	sub	2	2	2	2	2	2	2	2
GeoDA [94]	sub_dim	10	10	10	10	10	10	10	10
	tol	0.001	0.001	0.001	0.001	0.001	0.001	0.001	0.001
	alpha	0.002	0.002	0.002	0.002	0.002	0.002	0.002	0.002
	mu	0.6	0.6	0.6	0.6	0.6	0.6	0.6	0.6
	search_space	"sub"	"sub"	"sub"	"sub"	"sub"	"sub"	"sub"	"sub"
	grad_estimator_batch_size	40	40	40	40	40	40	40	40
	sigma	0	0	0	0	0	0	0	0
SFA [95]	resize_factor	1.0	1.0	1.0	1.0	1.0	1.0	1.0	1.0
Rays [96]	No other hyperparameters	/	/	/	/	/	/	/	/
OPT [97]	alpha	0.2	0.2	0.2	0.2	0.2	0.2	0.2	0.2
	beta	0.001	0.001	0.001	0.001	0.001	0.001	0.001	0.001
Sign-OPT [98]	alpha	0.2	0.2	0.2	0.2	0.2	0.2	0.2	0.2
	beta	0.001	0.001	0.001	0.001	0.001	0.001	0.001	0.001
	svm	FALSE	FALSE	FALSE	FALSE	FALSE	0.001	FALSE	FALSE
	momentum	0	0	0	0	0	0	0	0
	k	200	200	200	200	200	200	200	200
	sigma	0	0	0	0	0	0	0	0
HSJA [100]	gamma	1	1	1	1	1	1	1	1
	stepsize_search	"geometric_	"geometric_	"geometric_	"geometric_	"geometric_	"geometric_	"geometric_	"geometric_
	max_num_evals	10000	10000	10000	10000	10000	10000	10000	10000
	init_num_evals	100	100	100	100	100	100	100	100
	EOT	1	1	1	1	1	1	1	1
	sigma	0	0	0	0	0	0	0	0
QEBA [4]	pgen	DCT	DCT	"DCT"	"DCT"	"DCT"	"DCT"	"DCT"	"DCT"
Nonlinear-BA [5]	pgen	AE9408	AE9408	AE9408	AE9408	AE9408	AE9408	AE9408	AE9408
PSBA [6]	pgen	AE9408	AE9408	AE9408	AE9408	AE9408	AE9408	AE9408	AE9408
Triangle Attack [99]	ratio_mask	0.1	0.1	0.1	0.1	0.1	0.1	0.1	0.1
	dim_num	1	1	1	1	1	1	1	1
	max_iter_num_in_2d	2	2	2	2	2	2	2	2
	init_theta	2	2	2	2	2	2	2	2
	init_alpha	np.pi/2	2	np.pi/2	np.pi/2	np.pi/2	np.pi/2	np.pi/2	np.pi/2
	plus_learning_rate	0.1	0.1	0.1	0.1	0.1	0.1	0.1	0.1
	minus_learning_rate	0.005	0.005	0.005	0.005	0.005	0.005	0.005	0.005
	half_range	0.1	0.1	0.1	0.1	0.1	0.1	0.1	0.1

- box adversarial attacks with random sign flip," in *European Conference on Computer Vision*, 2020.
- [96] J. Chen and Q. Gu, "Rays: A ray searching method for hard-label adversarial attack," in *ACM SIGKDD Conference on Knowledge Discovery and Data Mining*, 2020.
- [97] M. Cheng, T. Le, P.-Y. Chen, J. Yi, H. Zhang, and C.-J. Hsieh, "Query-efficient hard-label black-box attack: An optimization-based approach," *arXiv e-prints*, 2018.
- [98] M. Cheng, S. Singh, P. Chen, P.-Y. Chen, S. Liu, and C.-J. Hsieh, "Sign-opt: A query-efficient hard-label adversarial attack," *arXiv e-prints*, 2019.
- [99] X. Wang, Z. Zhang, K. Tong, D. Gong, K. He, Z. Li, and W. Liu, "Triangle attack: A query-efficient decision-based adversarial attack," in *European Conference on Computer Vision*, 2022.
- [100] J. Chen, M. I. Jordan, and M. J. Wainwright, "Hopskipjumpattack: A query-efficient decision-based attack," in *Symposium on Security and Privacy*, 2020.
- [101] U. Feige, V. S. Mirrokni, and J. Vondrák, "Maximizing non-monotone submodular functions," *SIAM Journal on Computing*, 2011.
- [102] D. Wierstra, T. Schaul, T. Glasmachers, Y. Sun, J. Peters, and J. Schmidhuber, "Natural evolution strategies," *Journal of Machine Learning Research*, vol. 15, no. 1, pp. 949–980, 2014.
- [103] E. G. Tabak and C. V. Turner, "A family of nonparametric density estimation algorithms," *Communications on Pure and Applied Mathematics*, 2013.
- [104] M. Garnelo, J. Schwarz, D. Rosenbaum, F. Viola, D. J. Rezende, S. Eslami, and Y. W. Teh, "Neural processes," *arXiv e-prints*, 2018.
- [105] H.-G. Beyer and H.-P. Schwefel, "Evolution strategies—a comprehensive introduction," *Natural computing*, 2002.
- [106] Y. Lu and B. Huang, "Structured output learning with conditional generative flows," in *Association for the Advancement of Artificial Intelligence*, 2020.
- [107] I. J. Goodfellow, J. Shlens, and C. Szegedy, "Explaining and harnessing adversarial examples," *arXiv e-prints*, 2014.
- [108] S. Chen, Z. Huang, Q. Tao, Y. Wu, C. Xie, and X. Huang, "Adversarial attack on attackers: Post-process to mitigate black-box score-based query attacks," *arXiv e-prints*, 2022.
- [109] R. R. Selvaraju, M. Cogswell, A. Das, R. Vedantam, D. Parikh, and D. Batra, "Grad-cam: Visual explanations from deep networks via gradient-based localization," in *International Conference on Computer Vision*, 2017.
- [110] S. M. Lundberg and S.-I. Lee, "A unified approach to interpreting model predictions," in *Advances in Neural Information Processing Systems*, 2017.
- [111] O. Russakovsky, J. Deng, H. Su, J. Krause, S. Satheesh, S. Ma, Z. Huang, A. Karpathy, A. Khosla, M. Bernstein *et al.*, "Imagenet large scale visual recognition challenge," *International Journal of Computer Vision*, vol. 115, pp. 211–252, 2015.
- [112] N. Hansen and A. Ostermeier, "Completely derandomized self-adaptation in evolution strategies," *Evolutionary computation*, 2001.
- [113] X. Ling, S. Ji, J. Zou, J. Wang, C. Wu, B. Li, and T. Wang, "Deepsec: A uniform platform for security analysis of deep learning model," in *Symposium on Security and Privacy*, 2019.
- [114] Y. Dong, Q.-A. Fu, X. Yang, T. Pang, H. Su, Z. Xiao, and J. Zhu, "Benchmarking adversarial robustness on image classification," in *Conference on Computer Vision and Pattern Recognition*, 2020.
- [115] F. Croce, M. Andriushchenko, V. Schwag, E. Debenedetti, N. Flammarion, M. Chiang, P. Mittal, and M. Hein, "Robustbench: a standardized adversarial robustness benchmark," *arXiv e-prints*, 2020.
- [116] R. R. Selvaraju, M. Cogswell, A. Das, R. Vedantam, D. Parikh, and

- D. Batra, "Grad-cam: Visual explanations from deep networks via gradient-based localization," in *International Conference on Computer Vision*, 2017.
- [117] B. Wu, H. Chen, M. Zhang, Z. Zhu, S. Wei, D. Yuan, and C. Shen, "Backdoorbench: A comprehensive benchmark of backdoor learning," in *Advances in Neural Information Processing Systems*, 2022.
- [118] S. Srinivas and F. Fleuret, "Full-gradient representation for neural network visualization," in *Advances in Neural Information Processing Systems*, 2019.
- [119] N. Carlini, "A critique of the deepsec platform for security analysis of deep learning models," *arXiv e-prints*, 2019.
- [120] F. Yu, Z. Qin, C. Liu, L. Zhao, Y. Wang, and X. Chen, "Interpreting and evaluating neural network robustness," in *International Joint Conference on Artificial Intelligence*, 2019.
- [121] G. Somepalli, L. Fowl, A. Bansal, P. Yeh-Chiang, Y. Dar, R. Baraniuk, M. Goldblum, and T. Goldstein, "Can neural nets learn the same model twice? investigating reproducibility and double descent from the decision boundary perspective," *arXiv e-prints*, 2022.
- [122] B. Wu, L. Liu, Z. Zhu, Q. Liu, Z. He, and S. Lyu, "Adversarial machine learning: A systematic survey of backdoor attack, weight attack and adversarial example," *arXiv e-prints*, 2023.
- [123] A. Goel, A. Singh, A. Agarwal, M. Vatsa, and R. Singh, "Smartbox: Benchmarking adversarial detection and mitigation algorithms for face recognition," in *2018 IEEE 9th international conference on biometrics theory, applications and systems (BTAS)*, 2018.
- [124] N. Hingun, C. Sitawarin, J. Li, and D. Wagner, "Reap: A large-scale realistic adversarial patch benchmark," in *International Conference on Computer Vision*, 2023.
- [125] Q. Zheng, X. Zou, Y. Dong, Y. Cen, D. Yin, J. Xu, Y. Yang, and J. Tang, "Graph robustness benchmark: Benchmarking the adversarial robustness of graph machine learning," *arXiv e-prints*, 2021.
- [126] B. Wang, C. Xu, S. Wang, Z. Gan, Y. Cheng, J. Gao, A. H. Awadallah, and B. Li, "Adversarial glue: A multi-task benchmark for robustness evaluation of language models," *arXiv e-prints*, 2021.
- [127] L. Hsiung, Y.-Y. Tsai, P.-Y. Chen, and T.-Y. Ho, "Carben: Composite adversarial robustness benchmark," *arXiv e-prints*, 2022.
- [128] S. Dai, S. Mahloujifar, C. Xiang, V. Sehwag, P.-Y. Chen, and P. Mittal, "Multirobustbench: Benchmarking robustness against multiple attacks," *arXiv e-prints*, 2023.
- [129] Z. Zhao, H. Zhang, R. Li, R. Sicre, L. Amsaleg, M. Backes, Q. Li, and C. Shen, "Revisiting transferable adversarial image examples: Attack categorization, evaluation guidelines, and new insights," *arXiv e-prints*, 2023.
- [130] X. Ling, S. Ji, J. Zou, J. Wang, C. Wu, B. Li, and T. Wang, "Deepsec: A uniform platform for security analysis of deep learning model," in *Symposium on Security and Privacy*, 2019.
- [131] Y. Dong, Q.-A. Fu, X. Yang, T. Pang, H. Su, Z. Xiao, and J. Zhu, "Benchmarking adversarial robustness on image classification," in *Conference on Computer Vision and Pattern Recognition*, 2020.
- [132] S. Chen, Z. He, C. Sun, J. Yang, and X. Huang, "Universal adversarial attack on attention and the resulting dataset damagenet," *Transactions on Pattern Analysis and Machine Intelligence*, vol. 44, no. 4, pp. 2188–2197, 2022.
- [133] Y. Shi, Y. Han, Q. Hu, Y. Yang, and Q. Tian, "Query-efficient black-box adversarial attack with customized iteration and sampling," *Transactions on Pattern Analysis and Machine Intelligence*, vol. 45, no. 2, pp. 2226–2245, 2023.
- [134] Y. Dong, S. Cheng, T. Pang, H. Su, and J. Zhu, "Query-efficient black-box adversarial attacks guided by a transfer-based prior," *Transactions on Pattern Analysis and Machine Intelligence*, vol. 44, no. 12, pp. 9536–9548, 2022.
- [135] A. Mustafa, S. H. Khan, M. Hayat, R. Goecke, J. Shen, and L. Shao, "Deeply supervised discriminative learning for adversarial defense," *Transactions on Pattern Analysis and Machine Intelligence*, vol. 43, no. 9, pp. 3154–3166, 2021.
- [136] C. Zhao, S. Mei, B. Ni, S. Yuan, Z. Yu, and J. Wang, "Variational adversarial defense : A bayes perspective for adversarial training," *Transactions on Pattern Analysis and Machine Intelligence*, pp. 1–17, 2023.
- [137] S. Lee, H. Kim, and J. Lee, "Graddiv: Adversarial robustness of randomized neural networks via gradient diversity regularization," *Transactions on Pattern Analysis and Machine Intelligence*, vol. 45, no. 2, pp. 2645–2651, 2023.
- [138] C. P. Lau, J. Liu, H. Souri, W.-A. Lin, S. Feizi, and R. Chellappa, "Interpolated joint space adversarial training for robust and generalizable defenses," *IEEE Transactions on Pattern Analysis and Machine Intelligence*, vol. 45, no. 11, pp. 13 054–13 067, 2023.
- [139] B. Wu, S. Wei, M. Zhu, M. Zheng, Z. Zhu, M. Zhang, H. Chen, D. Yuan, L. Liu, and Q. Liu, "Defenses in adversarial machine learning: A survey," 2023.
- [140] X. Wei, B. Pu, J. Lu, and B. Wu, "Physically adversarial attacks and defenses in computer vision: A survey," *arXiv e-prints*, 2022.

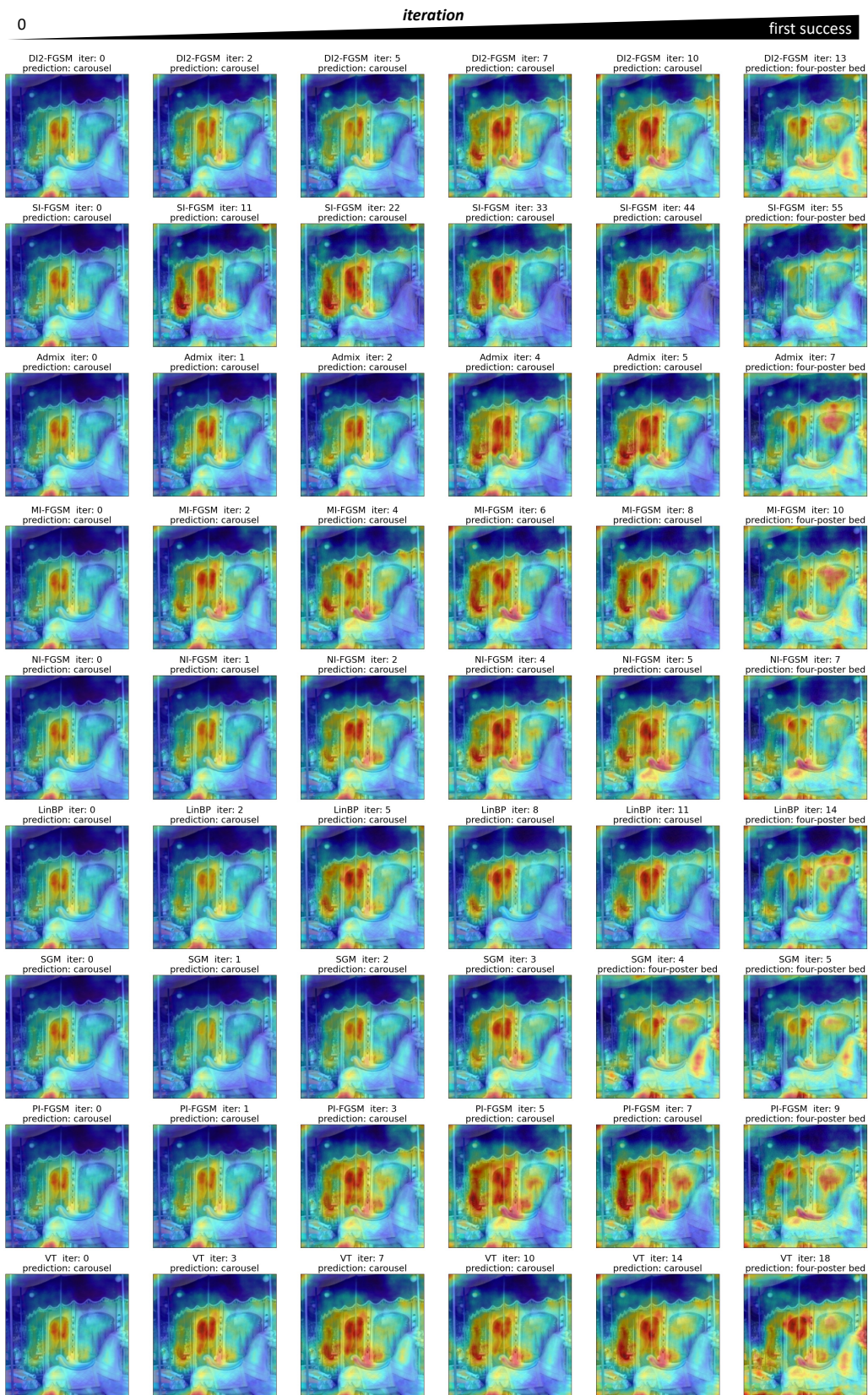


Fig. 26. Given a benign image from the category of *carousel* (same as the benign image in Fig. 24), the attention maps on its perturbed counterparts generated by successful transfer-based attacks. Each row plots the evolution of adversarial images crafted by a certain attack. For these successful attacks, we plot the adversarial images at regular intervals between the first iteration and the first successfully attacked iteration. The title of each image indicates the method, current iteration number and target model prediction. It's observed that when attacks succeed, the discriminative regions change to trivial features, and the important features are not captured.

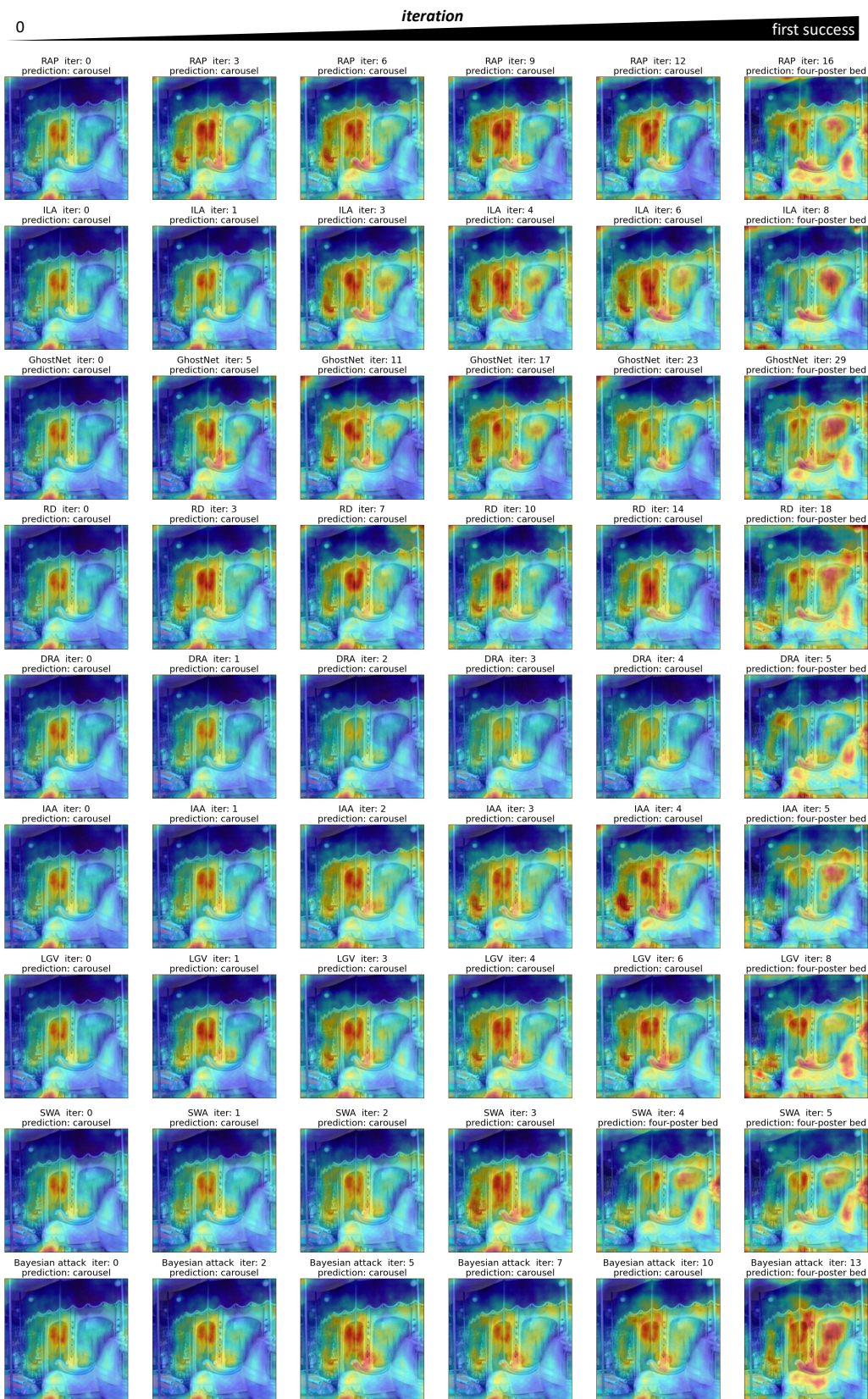


Fig. 27. The rest part of Fig. 26

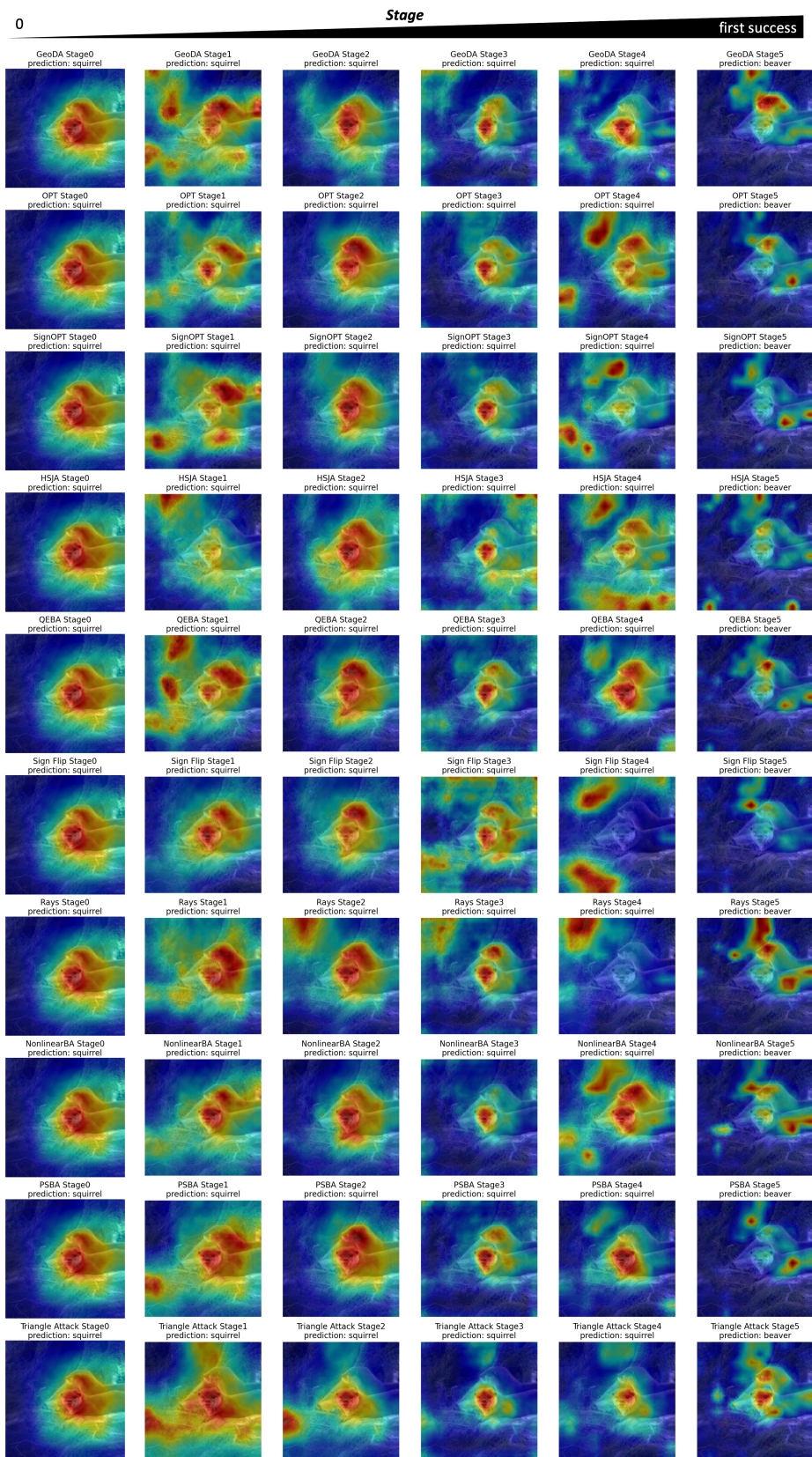


Fig. 28. Given a benign image from the category of *squirrel* (same as the benign image in Fig. 25), the attention maps on its perturbed counterparts generated by successful decision-based attacks. Each row plots the evolution of adversarial images crafted by a certain attack. For these successful attacks, we also plot the adversarial images at each stage, where we divide the entire attack process into 6 stages (from the beginning to the end, no matter fails or succeeds). The title of each image indicates the method, current stage period, and target model prediction. It's observed that when attacks succeed, the prediction label provided by the target model will be changed to *beaver*.

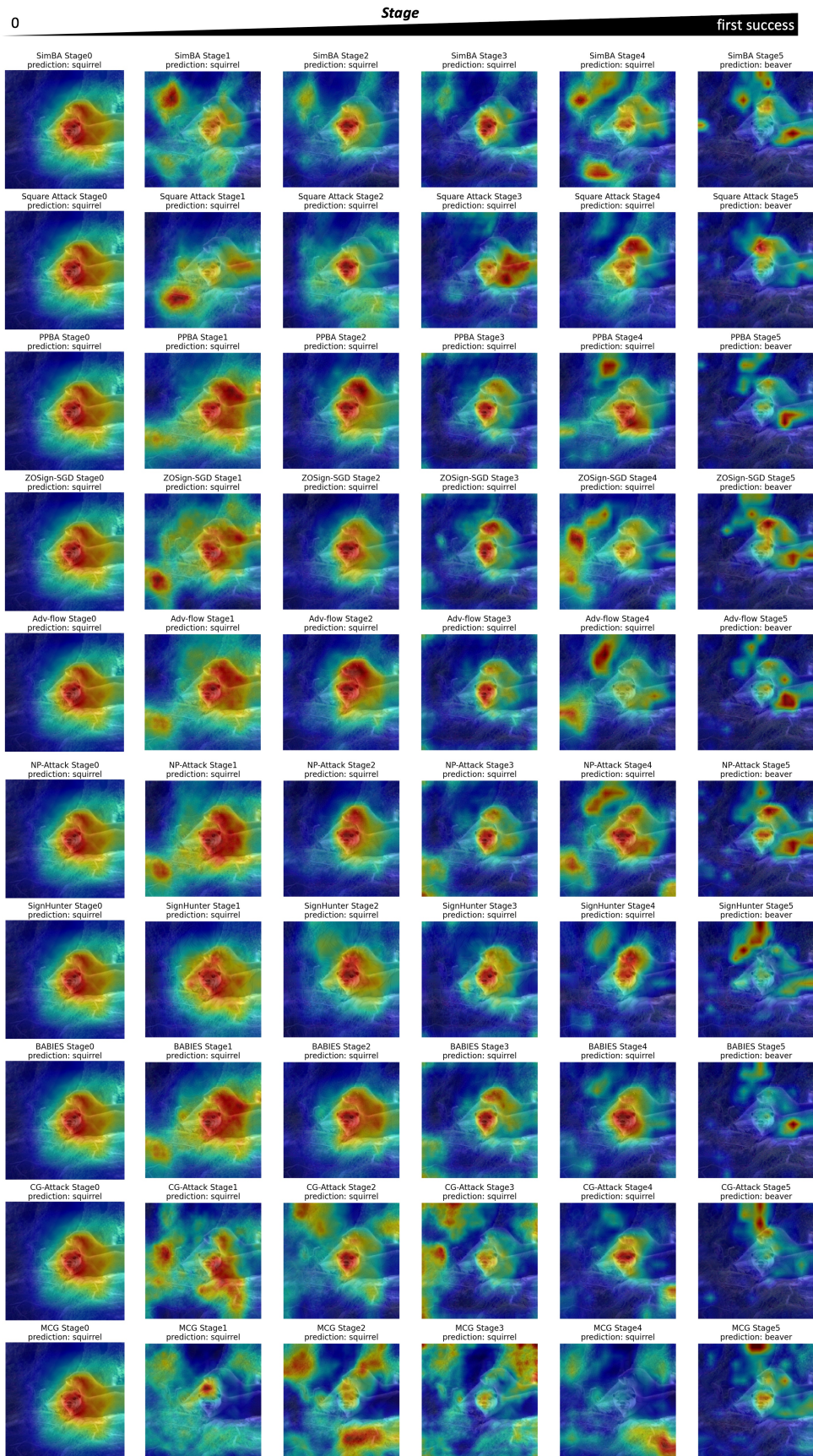


Fig. 29. The attention maps of successful score-based attacks which follows the setting as Fig. 28

TABLE VI
HYPER-PARAMETERS OF TRANSFER-BASED ATTACKS.

Transfer-based attacks	Hyper-parameters	ImageNet				CIFAR-10			
		untargeted		targeted		untargeted		targeted	
		ℓ_∞	ℓ_2	ℓ_∞	ℓ_2	ℓ_∞	ℓ_2	ℓ_∞	ℓ_2
General hyper-parameters	maximum perturbation step size	0.03 0.003	3 0.3	0.06 0.006	6 0.6	0.03 0.003	1 0.1	0.03 0.003	1 0.1
I-FGSM [20]	iterations	100		300		100		300	
PGD [21]	iterations bound of random start of perturbation	100		300		100		300	
MI-FGSM [26]	iterations decay factor	10		300		100		300	
NI-FGSM [23]	iterations decay factor / step size of looking ahead	10		300		100		300	
PI-FGSM [27]	iterations decay factor / step size of looking ahead	100		300		100		300	
VT [28]	iterations number of samples to calculate variance	100		300		100		300	
RAP [29]	iterations late start / iteration number of inner maximization	400 100 / 10				400 100 / 5			
LinBP [30]	iterations position to perform linear backpropagation	100		300		100		300	
SGM [31]	iterations decay parameter	ResNet-50: 0.2; DenseNet-121: 0.5; ViT-B/16: 0.6		300		ResNet-50: 0.5; DenseNet-BC: 0.6		300	
D12-FGSM [25]	iterations resized dimension / transformation probability	100		299 / 0.5		100		40 / 0.5	
SI-FGSM [23]	iterations number of the scale copies / scale factor	100		5 / 2		100		3 / 1.5	
Admix [24]	iterations strength of sampled image / number of sampled images number of admixed copies / scale factor	100		0.2 / 3 5 / 2		100		0.2 / 3 3 / 1.5	
TI-FGSM [22]	iterations kernel size	100		5		100		3	
FIA [33]	iterations intermediate layer to extract feature maps ensemble number in aggregate gradient / drop probability	100 ResNet-50: the 2nd stage; VGG-19 [†] : the conv layer at the 10th VGG block; Inception-V3: the 2nd Inception module in the 2nd Inception block; DenseNet-121: the 3rd dense block; ViT-B/16: the 3rd transformer encoder layer;		FIA could't perform targeted attack.		100 ResNet-50: the 2nd stage; VGG-19 [†] : the conv layer at the 7th VGG block; Inception-V3: the 3rd Inception module in the 2nd Inception block; DenseNet-BC: the 2nd transition layer;		FIA could't perform targeted attack.	
NAA [34]	iterations target layer integrated step	100 ResNet-50: the 2nd stage; VGG-19 [†] : the conv layer at the 10th VGG block; Inception-V3: the 2nd Inception module in the 2nd Inception block; DenseNet-121: the 3rd dense block; ViT-B/16: the 3rd transformer encoder layer;		NAA could't perform targeted attack.		100 ResNet-50: the 2nd stage; VGG-19 [†] : the conv layer at the 7th VGG block; Inception-V3: the 3rd Inception module in the 2nd Inception block; DenseNet-BC: the 2nd transition layer;		NAA could't perform targeted attack.	
IIA [32]	iterations of attack / baseline attack intermediate layer	100 / 10		300 / 30		100 / 10		300 / 30	
RD [35]	iterations scale of noise added on DNN weights number of ensemble models	100		300		100		300	
GhostNet [36]	iterations dropout probability parameter of uniform distribution that modulating scalars are drawn from	100		300		100		300	
DRA [37]	iterations batch size / epochs / learning rate / regularization constant learning rate schedule	100		300				No officially released code.	
IAA [38]	iterations shape-related hyper-parameter of Softplus decay factor on residual module	100		300				No officially released code.	
LGV [35]	iterations batch size / epochs / learning rate schedule learning rate/weight decay/momentum	100		300		100		300	
SWA [39]	iterations batch size / epochs / learning rate schedule / momentum / σ learning rate / weight decay / $\lambda_{\epsilon, \sigma} / \gamma$	100		300		100		300	
Bayesian Attack [39]	iterations batch size / epochs / learning rate schedule / momentum / σ learning rate / weight decay / $\lambda_{\epsilon, \sigma} / \gamma$ number of sampled models rescaling factor of the covariance matrix	100		300		100		300	